WILEY ONLINE LIBRARY

Early View publication on wileyonlinelibrary.com
(issue and page numbers not yet assigned;
citable using Digital Object Identifier – DOI)

LASER & PHOTONICS REVIEWS

Laser Photonics Rev., 1–41 (2011) / **DOI** 10.1002/lpor.201000046

Abstract This review focuses on the optical properties and device applications of deterministic aperiodic media generated by mathematical rules with spectral features that interpolate in a tunable fashion between periodic crystals and disordered random media. These structures are called Deterministic Aperiodic Nano Structures (DANS) and can be implemented in different materials (linear and nonlinear) and physical systems as diverse as dielectric multilayers, optical gratings, photonic waveguides and nanoparticle arrays. Among their distinctive optical properties are the formation of multi-fractal bandgaps and characteristic optical resonances, called critical modes, with unusual localization, scaling and transport properties. The goal of the paper is to provide a detailed review of the conceptual foundation and the physical mechanisms governing the complex optical response of DANS in relation to the engineering of novel devices and functionalities. The discussion will mostly focus on passive and active planar structures with enhanced light-matter coupling for photonics and plasmonics technologies.

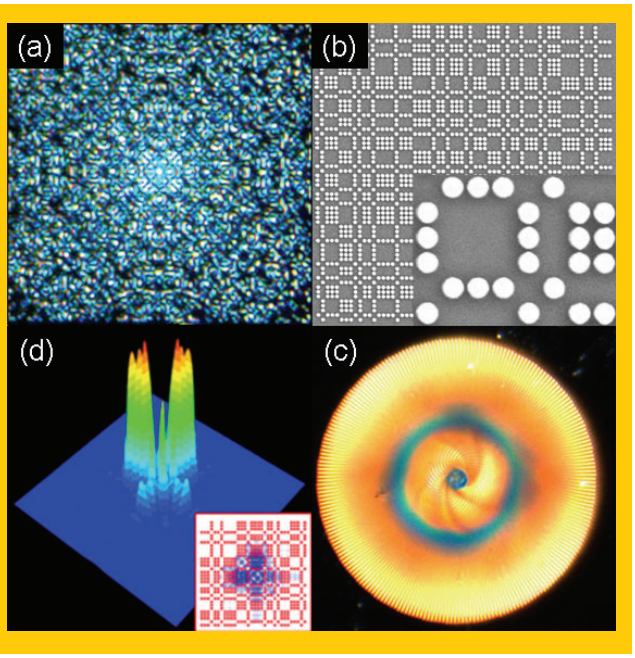

Deterministic aperiodic nanostructures for photonics and plasmonics applications

Luca Dal Negro* **and Svetlana V. Boriskina**

Introduction

Understanding optical interactions in aperiodic deterministic arrays of resonant nanostructures offers an almost unexplored potential for the manipulation of localized electromagnetic fields and light scattering phenomena on planar optical chips.

Periodic scattering media support extended Bloch eigenmodes and feature continuous energy spectra corresponding to allowed transmission bands. On the other hand, in the absence of inelastic interactions, random media sustain exponentially localized eigenmodes with discrete (i. e., pure-point) energy spectra characterized by isolated δ-peaks. A substantial amount of work has been devoted in the past few years to understand transport, localization and wave scattering phenomena in disordered random media [1–5]. These activities have unveiled fascinating analogies between the behavior of electronic and optical waves, such as disorder-induced Anderson light localization [5,6], the photonic Hall effect [7], optical magnetoresistance [8], universal conductance fluctuations of light waves [9], and optical negative temperature coefficient resistance [10]. However, the technological and engineering appeal of multiple light scattering and disorder-induced phenomena in random systems, such as the celebrated Anderson-light localization, are still very limited. Random structures, while in fact providing a convenient path to field localization, are irreproducible and lack predictive models and *specific engineering design rules* for deterministic optimization. These difficulties have strongly limited our ability to conceive, explore, and manipulate optical resonances and photon transport in systems devoid of spatial periodicity. On the other hand, aperiodic optical media generated by deterministic mathematical rules have recently attracted significant attention in the optics and electronics communities due to their simplicity of design, fabrication, and full compatibility with current materials deposition and device technologies [11–14]. Initial work, mostly confined to theoretical investigations of one-dimensional (1D) aperiodic systems [15–22], have succeeded in stimulating broader experimental/theoretical studies on photonic-plasmonic structures that fully leverage on deterministic aperiodicity as a novel strategy to engineer optical modes, devices, and functionalities. Beyond the emerging technological implications, the study of aperiodic structures in nanophotonics is a highly interdisciplinary and fascinating research field whose conceptual underpinning is deeply rooted in three highly interconnected research areas: mathematical crystallography [23–25], dynamical sys-

Department of Electrical and Computing Engineering & Photonics Center, Boston University, 8 Saint Mary's street, Room 825, Boston, MA 02215-2421, USA
* e-mail: dalnegro@bu.edu

tems (i. e., specifically, symbolic dynamics and automatic sequences) [26–28], and number theory [29–31].

The scope of this review is to discuss the foundation along with the optical properties and the current device applications of Deterministic Aperiodic Nano Structures (DANS). DANS are optical structures in which the refractive index varies over length scales comparable or smaller than the wavelength of light. They include dielectric and metallic structures, metallo-dielectric nanostructures and metamaterials. In all cases, DANS are designed by mathematical algorithms that interpolate in a tunable fashion between periodicity and randomness, thus providing novel opportunities to explore and manipulate light-matter interactions at the nanoscale. DANS can be conveniently fabricated using conventional nanolithographic techniques while displaying unique transport and localization properties akin to random systems. Differently from well-investigated fractal structures, DANS may not possess self-similarity in direct space although they exhibit a far richer complexity in Fourier space resulting in distinctive diffraction patterns. Most importantly, the Fourier space of DANS can be simply designed to range from a pure-point discrete spectrum, such as for periodic and quasiperiodic crystals, to a diffused spectrum with short-range correlations, as for disordered amorphous systems. In addition, DANS diffraction patterns can display non-crystallographic point symmetries of arbitrary order as well as more abstract mathematical symmetries [12].

The structural complexity of DANS profoundly influences the character of photon transport in the multiple scattering regime, and results in a high density of discrete resonances, known as *critical modes*, with multi-fractal spatial patterns and large fluctuations of their photonic mode density (LDOS). As we will discuss, these are key attributes *to boost the frequency bandwidth and the strength of light-matter coupling in photonic-plasmonic structures*, offering yet unexplored avenues to advance fundamental optical sciences and device technology.

This review is organized as follows: Sect. 1 covers the conceptual foundation and the different notions of aperiodic order, generation techniques and classification schemes based on Fourier spectral properties. In Sect. 2 we review the main achievements in the engineering of dielectric DANS in one spatial dimension, such as photonic multilayers, and their device applications. Section 3 focuses on the optical properties of two-dimensional (2D) DANS in the linear and nonlinear optical regime and surveys their primary device applications. In Sect. 4 we introduce the emerging field of Complex Aperiodic Nanoplasmonics (CAN) and its engineering applications. Theoretical and computational methods for photonic and plasmonic DANS are briefly reviewed in Sect. 5. The summary in Sect. 6 offers our thoughts on the outlook for this technological platform based on the engineering of aperiodic order. Finally, a word has to be added about our list of cited papers. Given the enormous amount of references in this diversified and fast-growing field, we have chosen to cite only a few representative articles rather than to attempt to be exhaustive. We apologize in advance for those cases where our selection was defective.

1. Deterministic aperiodic order

1.1. Order with periodicity

Structural order is often exclusively associated with the concept of *spatial periodicity*. Humans can easily recognize periodic patterns even in the presence of substantial noise or perturbations, and many of the beautiful regularity of natural phenomena are manifestations of periodic systems. In his book "An introduction to mathematics", published in 1911, the English mathematician Alfred North Whitehead remarked that [32]: "*The whole life of nature is dominated by the existence of periodic events... The presupposition of periodicity is fundamental to our very conception of life*". The rotation of the Earth, the yearly recurrence of seasons, the phases of the moon, the cycles of our bodily life, are all familiar examples of periodic events. Periodic patterns repeat a basic motif or building block in three-dimensional space. In general, any vector function of position vector $\mathbf{r}$ satisfying the condition $\Phi(\mathbf{r}+\mathbf{R}_0)=\Phi(\mathbf{r})$ describes spatially periodic patterns because it is invariant under the set of translations generated by the vector $\mathbf{R}_0$. As a result, we say that periodic structures display *a specific kind of long-range order* characterized by *translational invariance symmetry* along certain spatial directions. The beautiful regularity of inorganic crystals best exemplifies periodically ordered patterns where a certain atomic configuration, known as the *base,* repeats in space according to an underlying periodic lattice, thus defining *a crystal structure.* In three-dimensional (3D) space, crystal structures are mathematically described by their 32 point-group symmetries[1], which are combinations of pure rotation, mirror, and roto-inversion operations fully compatible with the translational symmetry of the 14 Bravais lattices. The addition of translation operations defines the crystallographic space-groups, which have been completely enumerated in 230 different types by Fedorov and Schoenflies in 1890 [23–25]. One of the most fundamental results of classical crystallography states that the combination of translation and rotation operations restricts the total number of rotational symmetries to only the ones compatible with the periodicity of the lattice. This important result is known as the *crystallographic restriction*. We say that a structure possesses an *n-fold* rotational symmetry if it is left unchanged when rotated by an angle $2\pi/n$, and the integer n is called the *order* of the rotational symmetry (or the order of the symmetry axis). It can be shown that only rotational symmetries of order $n=2,3,4$ and 6 can match the translational symmetry of 2D and 3D periodic lattices in Euclidean space [23–25]. As a result, the pentagonal symmetry, which is often encountered in the world of living structures as the

[1] A point group is a group of geometric symmetries (i. e., isometries) leaving a point fixed. Point groups can exist in a Euclidean space of any dimension. The discrete point groups in two dimensions, also called rosette groups, are used to describe the symmetries of an ornament. There are infinitely many discrete point groups in each number of dimensions. However, the crystallographic restriction theorem demonstrates that only a finite number are compatible with translational symmetry.

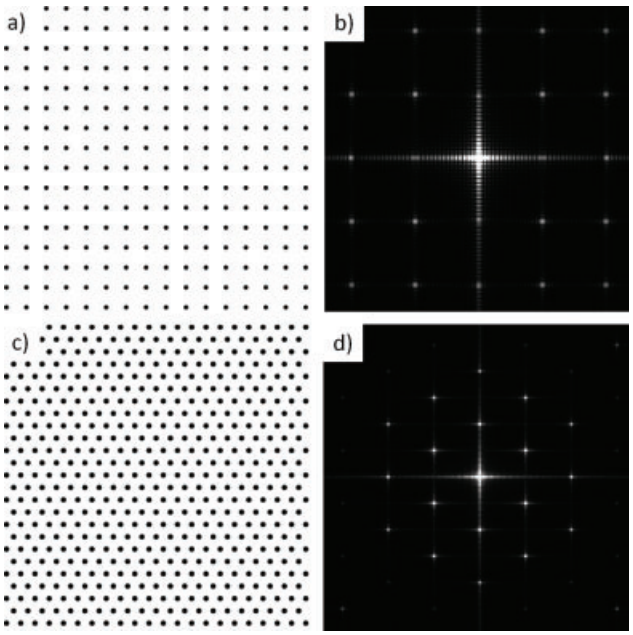

Figure 1 (a) Periodic square lattice. (b) Reciprocal space of the square lattice calculated via its Fourier transform amplitude. (c) Periodic hexagonal lattice. (d) Reciprocal space of the hexagonal lattice calculated via its Fourier transform amplitude.

pentamerism of viruses, micro-organisms such as *radiolarians*, plants, and marine animals (i. e., sea stars, urchins, crinoids, etc.) was traditionally excluded from the mineral kingdom until the revolutionary discovery of quasiperiodic order.

A fundamental feature of the diffraction patterns of all types of periodic lattices is the presence of well defined and sharp (i. e., δ-like) peaks corresponding to the presence of periodic long-range order. As a result, the reciprocal Fourier space of periodic and multi-periodic lattices is discrete (i. e., pure-point), with Bragg peaks positioned at rational multiples of primitive reciprocal vectors. As an example, we show in Fig. 1 the square and hexagonal lattices (Fig. 1a,c) with their corresponding diffraction spectra (Fig. 1b,d), or reciprocal spaces, obtained by calculating the amplitudes of the lattice Fourier transforms (i. e., the Fraunhofer regime). Bright diffraction spots arranged in patterns with square and hexagonal symmetries are clearly visible in Figs. 1(b,d). Their intensities progressively decrease away from the centers of the diffraction diagrams due to the contributions of the circular shape of finite-size particles, which filter the diffraction pattern according to the envelope of a Bessel function, and the size of the entire arrays, which determines the shape/size of individual diffraction spots.

This picture best exemplifies the notion of periodic arrangement of atoms which is at the origin of the traditional classification scheme of materials into the two broad categories of *crystalline* and *amorphous* structures. According to this simple classification scheme, *long-range structural order* and *periodicity* are considered identical, leading to the widespread conception of crystalline materials as the *paradigm of order* in solid state electronics and optics (e. g., photonic crystals). We will see in the next section that this simple picture proved to be inadequate after the discovery that certain metallic structures exhibit long-range orientational order without translational symmetry, forcing a complete redefinition of our notion of crystalline materials.

1.2. Order without periodicity: quasicrystals

One of the great intellectual triumphs of the twentieth century is the discovery of *aperiodic order* in the mathematical and physical sciences. In a series of lectures on the applicability of physical methods in biology, the physicist Erwin Schrödinger envisioned an *aperiodic crystal* storing genetic information in the geometric configuration of its covalent bonds. Schrödinger noticed that information storage could be more efficiently achieved [33] "*... without the dull device of repetition. That is the case of the more and more complicated organic molecule in which every atom, and every groups of atoms, plays an individual role, not entirely equivalent to that of every others (as it is the case in a periodic structure). We might quite properly call that an aperiodic crystal or solid and express our hypothesis by saying: we believe a gene, of perhaps the whole chromosome fiber, to be an aperiodic solid*".

In mathematics, quasiperiodic order was originally investigated by Harald Bohr who developed in 1933 a general theory of *almost periodic functions*, including *quasiperiodic functions* strictly as a subset [12, 23]. However, it was the mathematical study of symmetry, planar tilings, and discrete point sets (i. e., Delone sets) that paved the way to the discovery of aperiodic order in geometry, leading to the first application of quasiperiodic functions.

The study of tilings and the associated point sets, which is among the oldest branches of geometry, has only recently been formalized using the advanced group-theoretic methods of modern mathematical crystallography and provides the most general framework to understand quasiperiodic and aperiodic structures [23, 24, 34]. Tilings or *tessellations* are a collection of plane figures (i. e., *tiles*) that fill the plane without leaving any empty space. Early attempts to tile planar regions of *finite size* using a combinations of pentagonal and decagonal tiles were already explored by Johannes Kepler, arguably the founder of the mathematical theory of tilings, in his book *Harmonices Mundi* published in 1619 [35].

However, it was not until 1974 when the mathematician Roger Penrose discovered the existence of two simple polygonal shapes capable of tiling the *infinite* Euclidean plane *without spatial periodicity* [36]. Three dimensional generalizations of Penrose tilings were demonstrated in 1976 by Robert Ammann, who produced a pair of stretched and squashed building blocks (i. e., Ammann rhombohedra) filling the 3D space aperiodically [37].

It was realized in the early 1980s that the diffraction patterns of aperiodic point sets consist of *sharp diffraction peaks* with icosahedral point-group symmetry, which includes the "forbidden" pentagonal symmetry. In Fig. 2a we show a particle array displaying ten-fold rotational symmetry in the arrangement of its interior Bragg peaks. This array

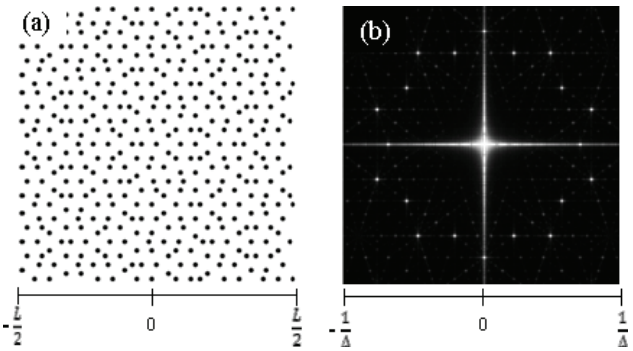

Figure 2 (a) Penrose particle array, $L = 11.9\,\mu$m, generation 12; (b) Reciprocal space sampled within a pseudo-Brillouin zone. Δ is the minimum center to center particle distance ($\Delta = 400$ nm); The tenfold rotational symmetry of the diffraction spots is clearly observable.

is simply obtained by positioning particles at the vertices of a Penrose tiling. In general, the symmetry of particle arrays is best displayed by the corresponding diffraction diagrams, obtained by calculating the amplitudes of their Fourier transforms. However, while for periodic arrays all the information contained in their reciprocal space can be compressed into periodic Brillouin zones, aperiodic arrays have non-periodic diffraction diagrams and therefore Brillouin zones cannot uniquely be defined. As a result, when comparing diffraction patterns of different types of aperiodic arrays, it is important to adopt an approach that guarantees a homogeneous sampling of their aperiodic spectral features. This can be done by restricting their reciprocal spaces to the so-called pseudo-Brillouin zones, which contain spatial frequencies in the compact interval $\pm 1/\Delta$, where Δ is the minimum or the average inter-particle separation for the specific type of aperiodic array. By using this convention, in Fig. 2b we display the pseudo-Brillouin zone of the Penrose particle array shown in Fig. 2a. Throughout this review, we will always compare pseudo-Brillouin zones of aperiodic particle arrays of comparable interparticle separations. One of the main features of aperiodic arrays is their ability to encode rotational symmetries in either discrete or continuous Fourier spectra. It was recently discovered that aperiodic tilings can be constructed with an arbitrary degree of rotational symmetry using an algebraic approach [38]. In addition, deterministic tilings with full rotational symmetry of infinite order (i. e., circular symmetry) have also been demonstrated [39] by a simple procedure that iteratively decomposes a triangle into five congruent copies. The resulting tiling, called Pinwheel tiling, has triangular elements (i. e., tiles) which appear in infinitely many orientations, and in the infinite-size limit, its diffraction pattern displays continuous ("infinity-fold") rotational symmetry. Radin has shown that there is no discrete component in the Pinwheel diffraction spectrum, but it is still unknown if the spectrum is continuous [23]. In Figs. 3 we compare a particle array with seven-fold symmetry (i. e., Danzer arrays [40]) and the Pinwheel array along with their corresponding diffraction spectra (i.e., pseudo-Brillouin zones). We will see in Sect. 3.2 that finite-size particle arrays with full circular

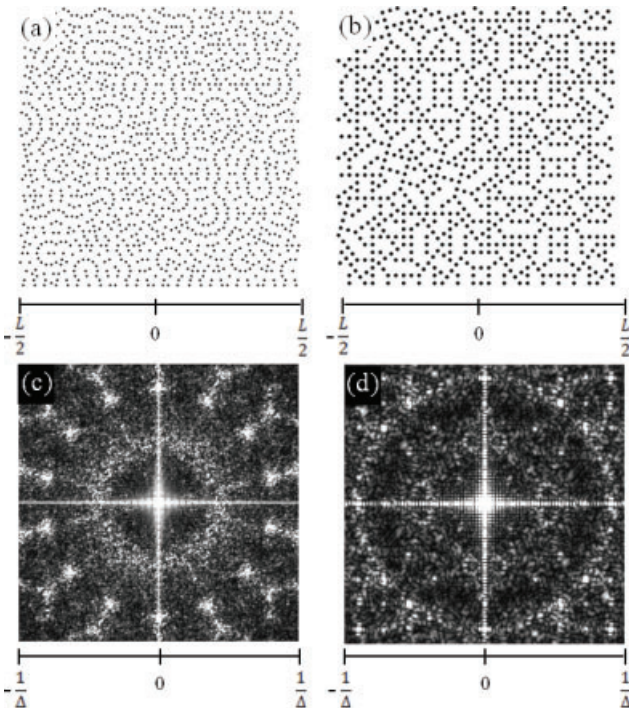

Figure 3 (a) Danzer array, $L = 26.6\,\mu$m, generation 4; (b) Pinwheel array, $L = 16.1\,\mu$m, generation 5; (c) Danzer reciprocal space where Δ is the minimum center to center particle distance ($\Delta = 400$ nm); (d) Pinwheel reciprocal space where Δ is the minimum center to center particle distance ($\Delta = 400$ nm);

symmetry in Fourier space can also be obtained by engineering aperiodic spiral order in the form of Vogel's spirals. Despite no rigorous results exist on the spectral nature of aperiodic spirals, they appear to best exemplify the concept of a "turbulent crystals" discussed by Ruelle [41].

It is clear from our discussion that aperiodic structures possess a *rich and novel type of long-range order*, described by more abstract symmetries than simple translational invariance. A simple example of abstract symmetry in quasicrystals was given by John Horton Conway for the case of Penrose tilings. Conways' theorem states that, despite the global aperiodicity of Penrose tilings, if we select a local pattern of any given size, an identical pattern can be found within a distance of twice that size [42].

In 1984, Dan Shechtman et al [43] were the first to experimentally demonstrate the existence of physical structures with non-crystallographic rotational symmetries. When studying the electron diffraction spectra from certain metallic alloys (Al_6Mn), they discovered sharp diffraction peaks arranged according to the icosahedral point group symmetry (i. e., consisting of 2-, 3-, 5-, and 10-fold rotation axes for a total of 120 symmetry elements). The sharpness of the measured diffraction peaks, which is related to the coherence of the spatial interference, turned out to be comparable with the one of ordinary periodic crystals. Stimulated by these findings, Dov Levine and Paul Steinhardt promptly formulated the notion of *quasicrystals* in a seminal paper titled [44]: "Quasicrystals: a new class of ordered structures". It was

subsequently discovered that three-dimensional icosahedral structures can be obtained by projecting *periodic crystals* from an abstract six-dimensional *superspace*, starting the fascinating field of *quasi-crystallography* [23, 24]. In response to these breakthrough discoveries, the International Union of Crystallography (IUCr) established in 1991 a special commission with the goal of redefining the concept of crystal structures According to the IUCr report, the term "crystal" should be associated to "*any solid having an essentially discrete diffraction diagram"* [45], irrespective of spatial periodicity. The essential attribute of crystalline order (both periodic and quasiperiodic) is to display an essentially discrete spectrum of Bragg peaks. As observed in [12], this definition has shifted the main attribute of crystalline structures from real space to reciprocal Fourier space. This shift directly affects the engineering of aperiodic systems, which is best achieved in reciprocal Fourier space for structures of low to intermediate refractive index contrast, as we will later detail.

In the next two sections, we will significantly broaden the notion of aperiodic order by discussing more general approaches and methods for the generation of deterministic systems with non-periodic spatio-temporal complexity beyond quasicrystals.

1.3. Aperiodic order beyond quasicrystals

Deterministic aperiodic order plays today an important role in several fields of mathematics, biology, chemistry, physics, economics, finance, and engineering. Nonlinear dynamical systems, continuous or discrete, often manifest an extreme sensitivity to their initial conditions, rendering long-term prediction impossible in general [45, 46]. This feature was fully recognized by the mathematician Poincaré in the context of celestial mechanics in 1890 [47, 48]. In his research on the three-body problem, Poincaré discovered an Hamiltonian dynamical system with *sensitive dependence on initial conditions.* This phenomenon was brought to worldwide attention by the meteorologist Edward Lorenz who showed in 1963 that a simple system of three coupled differential equations, used to model atmospheric convection, can give rise to chaotic behavior with extreme dependence on initial conditions (i. e., the *butterfly effect)*, laying the foundations of the theory of *chaotic dynamical systems* [49]. Spatio-temporal *chaotic behavior* has since then been discovered in a large number of deterministic physical systems, including coupled nonlinear oscillators, hydrodynamic turbulence, chemical reactions, nonlinear optical devices (i. e., lasers) and even low-dimensional conservative systems such as geometric billiards [45, 46, 50, 51][2]. The long-term behavior of deterministic chaotic systems is *unpredictable,* though not random, due to the sensitive dependence on initial conditions, which cannot be specified with enough precision.

The theory of chaotic dynamical systems has recently found direct application to problems of condensed matter physics, including the study of the excitation spectra of 1D and 2D aperiodic optical systems [52–54] such as the ones discussed in Sects. 2–4.

Numeric sequences and geometric patterns with deterministic, though unpredictable behavior, are deeply rooted in discrete mathematics and number theory. Number theory is primarily concerned with the properties of integer numbers [30, 31], and provides algorithms for the generation of various types of *pseudo-random* point sets and aperiodic tilings. The connection between *deterministic aperiodicity* and *unpredictability*[3] [55] is central to number theory and it has motivated many engineering applications in fields such as cryptography and coding theory [56–58]. The origin of this type of unpredictability can be traced back to the difficulty (i. e., algorithmic complexity) of certain arithmetic problems, such as factoring, the invertibility of one-way functions (e. g., the discrete logarithm problem) [29, 56], or to open number-theoretic questions related to the distribution of prime numbers and primitive roots. Number-theoretic methods are ideally suited to generate aperiodic point sets with different degrees of structural correlations and geometrical complexity [29]. Moreover, these methods provide simple algorithms, defined on finite number fields, to construct aperiodic binary sequences with well-defined Fourier spectral properties [29, 31]. These properties have been utilized to engineer pseudo-random number generators, mostly based on the behavior of polynomial congruencies or more advanced methods that have even been shown to be cryptographically secure (i. e., Blum-Blum-Shub algorithms) [56–58].

Deterministic pseudo-random generators (DPRG) produce numerical sequences and spatial patterns displaying *statistical randomness* (i. e., no recognizable patterns or regularities) and Fourier spectra approaching uncorrelated white noise. Deterministic structures generated by number-theoretic numerical sequences with flat-Fourier spectra have recently found technological applications in different research areas ranging from the engineering of acoustic diffusers to radar abatement (stealth surfaces), spread spectrum communication (jamming countermeasures, secure channel sharing), and the design of minimum redundancy antenna arrays (surveillance) in the RF regime [29]. However, these techniques are still largely unexplored in the domain of optical technologies.

In Fig. 4 we show two interesting examples of aperiodic particle arrays constructed on Gaussian primes (Fig. 4a) and finite Galois fields[4] (Fig. 4b). The corresponding pseudo-

[2] Chaotic dynamics is also displayed by elastic collision problems involving only few particles, such as the scattering of a small mass by three disks [45]. Additional examples of deterministic chaotic behavior can be found in the iterations of simple nonlinear maps, such as one-dimensional quadratic functions (i. e., the logistic map) and their generalizations in the complex domain [45, 46].

[3] The role of *randomness in number theory* and its relation with *computability*, *non-decidability* and *algorithmic complexity* lies at the core of the fascinating and highly interdisciplinary research field, pioneered by G. Chaitin, R. Solomonoff, and A. N. Kolmogorov, known as *Algorithmic Information Theory* (AIT) [55].

[4] Galois fields are finite number fields of prime order p, denoted as GF(p). They consist, for example, of the elements

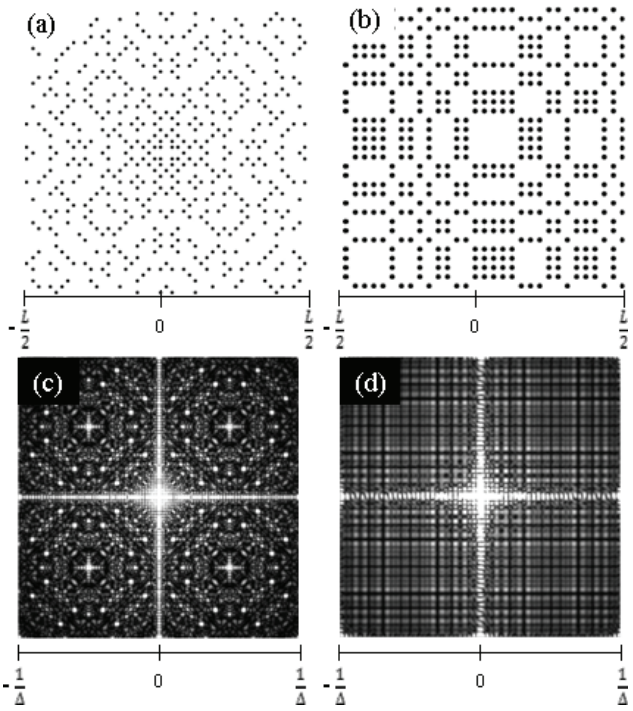

Figure 4 (a) Gaussian Prime Array, $L = 19.4\,\mu$m, generation 6; (b) Galois Array, $L = 12.2\,\mu$m, generation 5; (c) Gaussian Prime reciprocal space where Δ is the minimum center to center particle distance ($\Delta = 400$ nm); (d) Galois reciprocal space where Δ is the minimum center to center particle distance ($\Delta = 400$ nm)

Brillouin zones are shown in Figs. 4 (c-d). Gaussian primes are integers that are prime in the complex field, and are defined by $n + im$, where n and m are integers and i is the imaginary unit [29]. We notice that primes of the form $4k-1$ in the field of integers are still primes in the complex field, but 2 and primes of the form $4k+1$ can be factored in the complex field [29]. By plotting the Gaussian primes with (n, m) integer coordinates in the plane we obtain the highly symmetric pattern shown in Fig. 4a. Patterns with different degree of rotational symmetries can be obtained by considering primes defined by $n + \alpha m$, where α is a complex algebraic root of unity. When considering the complex cube root of unity, which is the solution of the algebraic equation $1 + \alpha + \alpha^2 = 0$, we obtain the two-dimensional pattern of Eisenstein primes, which displays hexagonal symmetry [29]. Finite Galois fields can also be utilized to generate binary-valued periodic sequences with pseudo-random properties, and particle arrays in two spatial dimensions [29], as shown in Fig. 4b. Sequences with elements from GF(p) and with coefficients determined by primitive polynomials in GF(p^m) have unique correlation and flat Fourier transform properties which found important applications in error-correcting codes, speech recognition, and cryptography [29, 56–58]. Moreover, in contrast to other number-theoretic sequences (e. g., Legendre sequences) with flat Fourier spectra, Galois sequences can be generated by simple linear recursions [29, 56–58]. Two-dimensional Galois arrays display diffraction spectra with a high density of spatial frequencies, theoretically a flat measure for infinite-size arrays. This property has been used to improve the image resolution of X-ray sources in astronomy [29]. Only recently, aperiodic arrays of metal nanoparticles generated according to Gaussian primes, and other number-theoretic functions have been explored in the context of plasmon scattering and optical sensing [59–61]. These structures are: (i) coprime arrays, which are 2D distributions of particles with coprime coordinates[5], (ii) the prime number arrays, which are 2D arrays of particles representing prime numbers in reading order; and (iii) Ulam spirals, which consist of prime numbers arranged on a square spiral. The direct and reciprocal Fourier spaces of the prime number arrays are shown in Fig. 5.

1.4. Aperiodic substitutions

In optics and electronics, an alternative approach to generate deterministic aperiodic structures with controlled Fourier spectral properties relies on symbolic substitutions [12, 26, 27, 62]. Not surprisingly, profound connections exist between the theory of substitutional sequences, dynamical systems, and number theory [26, 27]. Substitutions are an essential component of every recursive *symbolic dynamical system* formally defined on a finite symbolic alphabet $\vec{G} = \{\mathrm{A}, \mathrm{B}, \mathrm{C}, \ldots\}$. In physical realizations, each letter corresponds to a different type of building block (e. g., nanoparticle, dielectric layer, etc). A specific substitution rule ω replaces each letter in the alphabet by a finite word, starting from a given letter called an *axiom* or *initiator.* An aperiodic (deterministic) sequence is then obtained by iterating the substitution rule ω, resulting in a symbolic string of arbitrary length. For instance, the Fibonacci sequence is simply obtained by the iteration of the rule ω_F: A $\rightarrow$ AB, B $\rightarrow$ A with axiom A, as exemplified in the process: A $\rightarrow$ AB $\rightarrow$ ABA $\rightarrow$ ABAAB $\rightarrow$ ABAABABA $\rightarrow$ ABAABABAABAAB $\rightarrow \ldots$. Symbolic dynamical systems are examples of *L-systems* or Lindenmayer systems [63]. L-systems were introduced and developed in 1968 by the Hungarian theoretical biologist and botanist Aristid Lindenmayer (1925–1989). L-systems are used to model the growth processes of plant development, but also the morphology of a variety of organisms [63]. In addition, L-systems can be used to generate self-similar fractals and certain classes of aperiodic tilings such as the Penrose lattice.

A large variety of substitutions have been explored in the study of deterministic aperiodic optical multi-layered systems [12–14]. It is possible to associate to each substitution rule a *substitution matrix* $S_{ij} = N_i[\omega(j)]$ whose elements

$0, 1, 2, \ldots p-1$, for which addition, subtraction, multiplication and division (except by 0) are defined, and obey the usual commutative, distributive and associative laws. For every power p^n of a prime, there is exactly one finite field with p^n elements, and these are the only finite fields. The field with p^n elements is called GF(p^n) where GF stands for Galois field.

[5] Two numbers n and m that have no common factors are called relatively prime, mutually prime or *coprime.* Their greatest common divisor (gcd) is equal to 1.

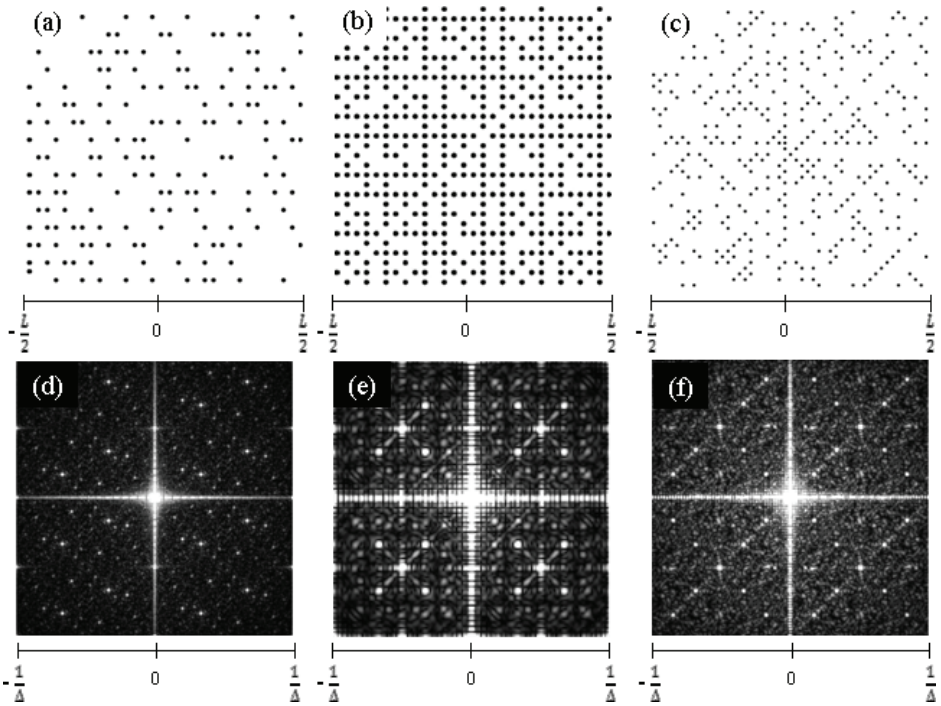

Figure 5 (a) Prime Array, $L = 12.6\,\mu$m, generation 5; (b) Co-Prime Array, $L = 11.4\,\mu$m, generation 5; (c) Ulam Spiral Array, $L = 19.2\,\mu$m, generation 50; (d) Prime reciprocal space where Δ is the minimum center to center particle distance ($\Delta = 400$ nm); (e) Co-Prime reciprocal space where Δ is the minimum center to center particle distance ($\Delta = 400$ nm); (f) Ulam Spiral reciprocal space where Δ is the minimum center to center particle distance ($\Delta = 400$ nm).

indicate the number of times a given letter $i = A, B$ appears in the substitution rule $\omega(j)$, irrespective of the order in which it occurs. The dimension of the matrix S_{ij} is determined by the size of the letter alphabet **G**. For instance, the substitution matrix of the Fibonacci sequence is: $\left(\begin{smallmatrix}1 & 1\\ 1 & 0\end{smallmatrix}\right)$. The advantage of this substitutional approach over purely geometrical or number-theoretic methods is that relevant information on the characteristics of the diffraction spectra can be directly obtained from the *substitution matrix.* As discovered by Bombieri and Taylor, there is a fundamental connection between the arithmetical nature of substitutions and the presence/absence of Bragg peaks in the corresponding Fourier transforms [64–68]. According to the Bombieri-Taylor theorem [69, 70], if the spectrum of the substitution matrix S contains a so-called Pisot-Vijayvaraghavan (PV) number as an eigenvalue, then the sequence is quasiperiodic and its spectrum can be expressed as a finite sum of weighted Dirac δ-functions, corresponding to Bragg peaks that are indexed by integer numbers, otherwise it is not.[6] A very relevant result, know as the *gap-labeling theorem,* relates the positions of the diffraction Bragg peaks of substitutional sequences with the locations of the gaps in the energy spectra of elementary excitations supported by the structures (e. g., optical modes, electronic states, etc) [64, 65, 71]. More specifically, a perturbative analysis of the integrated density of states of aperiodic structures generated by Pisot-type substitutions shows that both the positions and the widths of the gaps in their energy or transmission spectra can be "labeled" by the singularities of the Fourier transform associated to the sequence of scattering potentials (optical or electronic) [64, 71]. This approach, first introduced for the 1D Schrödinger equation [54], is valid beyond perturbation theory for quasiperiodic and almost-periodic structures, and it has been recently extended in two dimensions for sequences with more complex Fourier spectra [64, 71], such as the Thue-Morse and Rudin-Shapiro sequences, which we will discuss in the next section.

[6] A PV number is a positive algebraic number larger than one and such that all of its conjugate elements (i. e., the other solutions of its defining algebraic equation) have absolute value less than one. For instance, the golden mean, satisfying the algebraic equation $x^2 - x - 1 = 0$is a PV number.

1.5. Classification of aperiodic structures

Until recently, patterns were simply classified as either periodic or non-periodic, without the need of further distinctions. However, it should now be sufficiently clear that the word "non-periodic" encompasses a very broad range of different structures with varying degrees of order and spatial correlations, ranging from quasiperiodic crystals to more disordered "amorphous" materials with diffuse diffraction spectra. Moreover, mixed spectra with both discrete peaks and diffuse backgrounds can also frequently occur, as demonstrated in Figs. 3–7. One of the most fascinating questions in quasicrystals theory is whether there exist tilings with absolutely continuous diffraction spectra, as opposed to mixed ones [23]. The pinwheel tiling is a plausible candidate, and we will now introduce others that can be obtained by 2D generalizations of 1D substitution rules. Finally, we will review important ideas and results that motivate a general classification of deterministic structures, significantly expanding our definition of aperiodic order.

Aperiodic structures can be rigorously distinguished according to the nature of their diffraction patterns and energy spectra, which correspond to mathematical spectral measures [12, 27]. In optics and electronics, these spectral

measures are often identified with the characteristics of the transmission/energy spectra of the structures. A spectral measure is also associated with the Fourier transforms of the structures, or *lattice spectrum,* providing information on the nature of the corresponding diffraction patterns.

According to the *Lebesgue's decomposition theorem*, any measure can be uniquely decomposed in terms of three kinds of primitive spectral components (or mixtures of them), namely: pure-point (μ_P), singular continuous (μ_{SC}), and absolutely continuous spectra (μ_{AC}), such that:$\mu = \mu_P \cup \mu_{SC} \cup \mu_{AC}$. For example, the diffraction spectrum of a Fibonacci lattice is pure-point, featuring a countable set of δ-like Bragg peaks at incommensurate intervals. More complex structures display singular continuous spectra, meaning that the support of their Fourier transforms can be covered by an ensemble of open intervals with arbitrarily small total length [12]. For these structures, and in the limit of systems with infinite size, individual Bragg peaks are not separated by well-defined intervals, but tend to cluster forming "broad bands" in the reciprocal space. As a result, the corresponding eigenmodes (e. g., optical modes, electronic wavefunctions, acoustic modes, etc) are generally more localized in space compared to structures with pure-point spectra.

The chief example of a deterministic sequence with singular continuous diffraction and energy spectra is the Thue-Morse sequence [27, 72]. The Thue-Morse sequence is generated by the substitution ω_{TM}: A $\rightarrow$ AB, B $\rightarrow$ BA. This binary sequence was first studied by Eugène Prouhet in 1851, who applied it to number theory [73]. Axel Thue in 1906 used it to found the study of combinatorics on words. The sequence was successively brought to worldwide attention by the differential topology work of Marston Morse in 1921, who proved that the complex trajectories of dynamical systems whose phase spaces have negative curvature can be mapped into a discrete binary sequence, the Thue-Morse sequence[7] [74]. More recently, in the context of the algorithmic theory of finite automata, a number of results have been demonstrated that connect the existence of palindromes of arbitrary length in the Thue-Morse and similar binary sequences with singular continuous Fourier spectra [26].

Aperiodic substitutions can also give rise to the third primitive type of spectral measure, the absolutely continuous Fourier spectrum, akin to random processes. The chief example of a deterministic structure with absolutely continuous Fourier spectrum is the Rudin-Shapiro sequence [27, 75, 76]. In a two-letter alphabet, the RS sequence can simply be obtained by the substitution: AA $\rightarrow$ AAAB, AB $\rightarrow$ AABA, BA $\rightarrow$ BBAB, BB $\rightarrow$ BBBA [77]. The Fourier spectra of the three main examples of 1D aperiodic sequences generated by binary substitutions are displayed in Fig. 6. The Fourier spectrum of the Rudin-Shapiro sequence becomes, in the limit of a system with infinite size, a continuous function (i. e., flat spectrum), generating delta-correlated pseudo-random noise (see Figs. 6,7). Rudin-Shapiro structures are expected to share most of their physical properties with disordered random systems, including the presence of

[7] Here is another instance of the deep connection between dynamical systems, number theory, and substitutions.

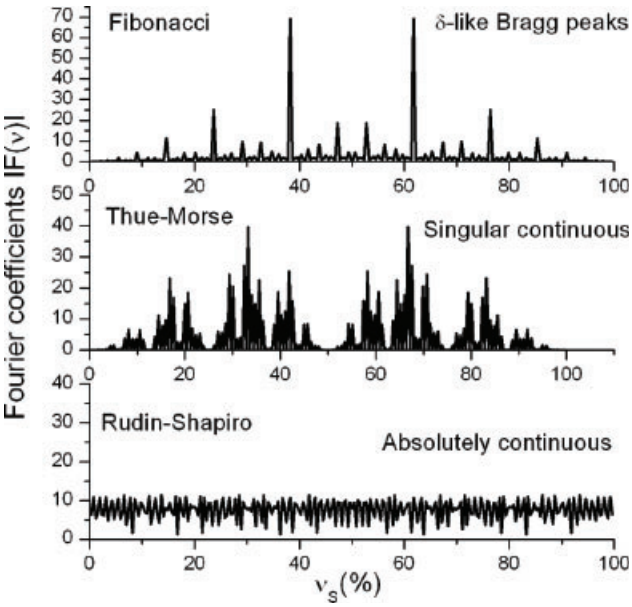

Figure 6 (a) Absolute value of the Fourier coefficients of a quasiperiodic (Fibonacci) structure, (b) of an aperiodic (TM) structure with singular continuous spectrum, (c) of an aperiodic structure with absolutely continuous spectrum (RS structure). From [62].

localized optical states (i. e., Anderson-like states). However, the abundance of short-range correlations, whose main effect is to reduce the degree of disorder and localization, favors the existence of resonant extended states in their energy spectra, and significantly complicates the theoretical analysis of Rudin-Shapiro and other deterministic structures with absolutely continuous Fourier spectra [77, 78]. Optical states in 2D photonic membranes with Rudin-Shapiro morphology have been recently investigated experimentally, and lasing from localized Rudin-Shapiro states has been demonstrated for the first time [79]. These results will be reviewed in Sect. 3.4.

The localization nature of the electronic and optical states of a 1D Rudin-Shapiro system has been theoretically investigated [71]. It was shown that the wavefunctions display a wide range of features ranging from weak to exponential localization. Nevertheless, depending on the values of scattering potential, extended (i. e., delocalized) states have also been discovered in the spectrum of Rudin-Shapiro structures [77, 78]. Another advantage of the substitutional method is that it can be easily generalized to higher dimensions. A quasiperiodic Fibonacci 2D lattice has been recently introduced by applying two complementary Fibonacci substitution rules along the horizontal and the vertical directions, alternatively [62]. This way, a square 2D Fibonacci matrix was obtained. Following this approach, 2D generalizations of both Thue-Morse and Rudin-Shapiro sequences have been recently implemented to design metallic nanoparticle arrays of interest for nanoplasmonics device technology [80]. Figure 7 shows the direct and reciprocal Fourier spaces of Fibonacci, Thue-Morse and Rudin-Shapiro arrays of particles obtained by the 2D substitu-

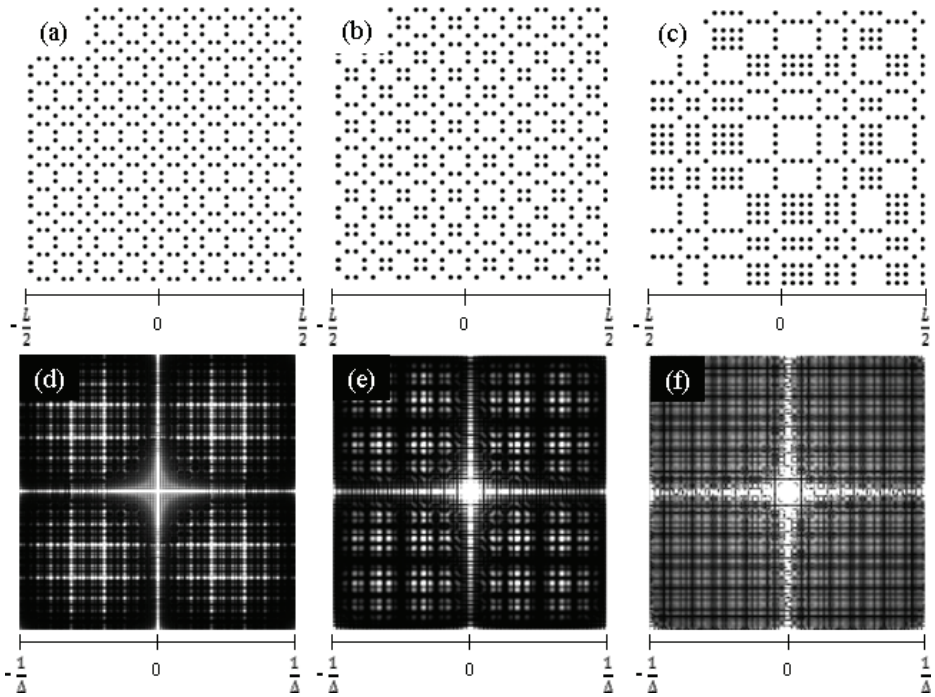

Figure 7 (a) Fibonacci Array, $L = 13.4\,\mu m$, generation 7; (b) Thue-Morse, $L = 12.6\,\mu m$, generation 5; (c) Rudin Shapiro, $L = 12.6\,\mu m$, generation 5; (d) Fibonacci reciprocal space where Δ is the minimum center to center particle distance ($\Delta = 400\,nm$); (e) Thue-Morse reciprocal space where Δ is the minimum center to center particle distance ($\Delta = 400\,nm$); (f) Rudin Shapiro reciprocal space where Δ is the minimum center to center particle distance ($\Delta = 400\,nm$).

tion method. We notice that, despite more sophisticated generation methods have been independently developed to construct 2D aperiodic arrays, the character of the Fourier spectra of the resulting arrays does not depend on the specific generation method [81–83]. E. Maciá [12] has recently proposed a classification scheme of aperiodic systems based on the nature of their diffraction (in abscissas) and energy spectra (in ordinates). According to this classification, *the rigid dichotomy between periodic and amorphous structures is surpassed by a matrix with nine different entries*, corresponding to all the combinations of the possible types of spectral measures, as shown in Fig. 8.

We are now ready to turn the focus of our review towards the implementation of the powerful concept of *aperiodic order* in photonics and plasmonics.

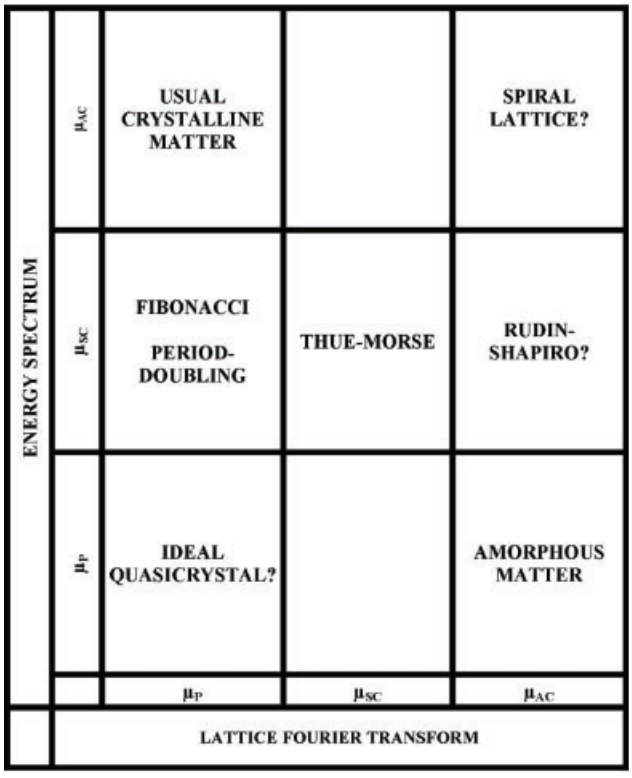

Figure 8 Classification of aperiodic systems according to the spectral measures of their Fourier transform and their Hamiltonian energy spectrum. From [11].

2. One-dimensional aperiodic structures in photonics

The research on 1D quasiperiodic photonic structures started in 1987 with the study of dielectric multilayers arranged in a Fibonacci sequence [16]. Such structures possess a very rich transmission spectrum with a multifractal organization. It has been realized only after the breakthrough discovery of quasicrystals and the fabrication of Fibonacci [19, 20] and Thue-Morse semiconductor heterostructures [84, 85] that physical systems can give rise to a category of energy spectra not previously encountered in natural structures. These energy spectra, named singular-continuous, exhibit a fractal pattern similar to the one of self-similar Cantor sets. In particular, they feature an infinite hierarchy of narrow transmission pseudo-gaps with vanishingly small widths (in the limit of infinite-size systems). Seminal work on the nature of Fibonacci spectra and the corresponding eigenmodes was performed by Kohmoto, who established an exact isomorphism between the 1D Schrödinger equation with arbitrary multiple scattering potentials and the opti-

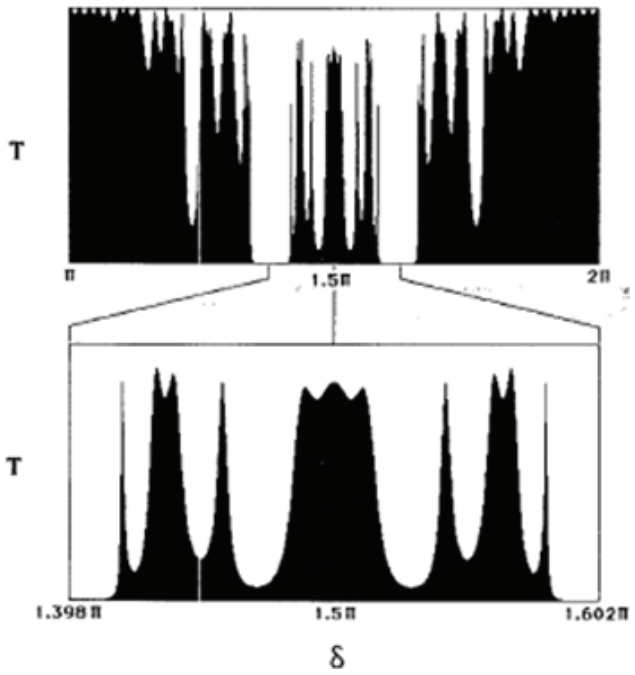

Figure 9 Transmission spectrum versus the optical phase length δ of a layer for a Fibonacci multilayer with 55 layers. The indices of refraction are chosen as $n_A = 2$ and $n_B = 3$. From [16].

cal wave equation [15, 54]. A transfer matrix method was introduced, enabling the analytical treatment of 1D scattering problems for optical and electronic excitations on the same footing.

A powerful approach was subsequently developed by Kohmoto, Kadanoff and Tang [15, 52–54, 86, 87] that made use of recursion relations connecting the Fibonacci transfer matrices (i. e., their traces and anti-traces) of dielectric layers in order to define a *nonlinear dynamical system* (i. e., dynamical map) that governs wave propagation in 1D quasiperiodic structures. From the knowledge of the phase-space trajectories of this dynamical system, complete information on the energy spectra and eigenmodes of optical and electronic quasiperiodic structures can be obtained. This method, known as the *trace map approach*, has been subsequently generalized to more complex 1D aperiodic systems (Thue-Morse, Rudin-Shapiro, arbitrary substitutional sequences) by Kolar and Nori [66], enabling the application of the powerful methods of dynamical system theory to the solution of optical and electronic scattering problems. Following this approach, Kohmoto and Oono [53] discovered the Smale horseshoe mechanism in the dynamical system associated to Fibonacci multilayer stacks, leading to the original prediction of their Cantor-set energy spectrum of nested pseudo-gaps, which was demonstrated experimentally by Gellermann et al [19]. The distinctive scaling of the transmission spectra of optical Fibonacci multilayers is clearly visible in Figs. 9,10. The many pseudo-gaps of Fibonacci optical multilayers are separated by strongly fluctuating wavefunctions with power-law localization scaling, called *critical modes*. The notion of critical wavefunctions is still not rigorously defined in today's literature, leading to somewhat confusing situations. However, general characteristics of critical wavefunctions are their complex oscillatory behavior, which results in self-similar spatial fluctuations best described by multi-fractal scaling and wavelet analysis [12, 88–90]. The spatial oscillations of critical modes originate from the self-similarity of the structures, through a series of tunneling events involving the overlap of different sub-systems, repeating at different length scales. Despite the notion of an envelope function is clearly ill-defined for such

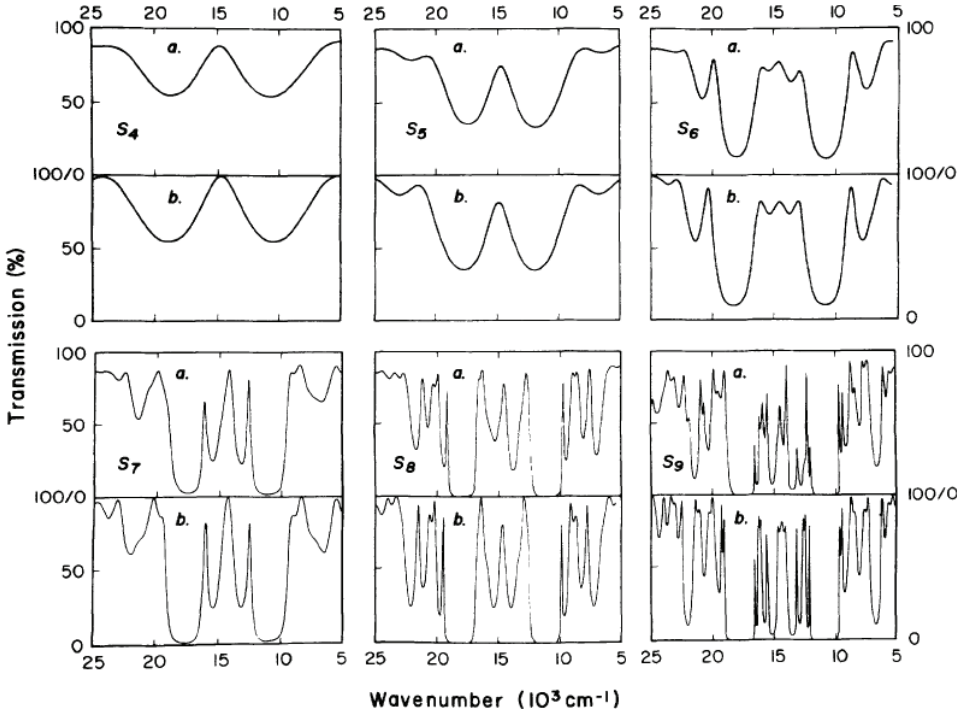

Figure 10 Optical transmission spectra for Fibonacci dielectric multilayers of increasing layer numbers from 5 to 55. Curves (a): experiments. (b): theory. From [19].

strongly fluctuating critical states it is possible, using simple scaling arguments and the Conway's theorem, to show that critical modes decay in space with characteristic power law localization [12, 91]. The rich physical behavior of critical states, including the presence of *extended* fractal wavefunctions at the band-edge energy of the Fibonacci spectrum, and their relation to optical transport are analytically studied by Kohmoto and Maciá using rigorous discrete tight binding method and a transfer matrix renormalization technique, respectively [87, 92]. Critical modes in quasiperiodic Fibonacci systems were observed experimentally by Desideri and co-workers [93] in the propagation of Rayleigh surface acoustic waves on a quasi-periodically corrugated solid. Characteristic spatial patterns with remarkable scaling features were obtained from an optical diffraction experiment. However, to the best of our knowledge, a *direct experimental observation* of multi-fractal critical modes in the optical regime is still missing. The photonic dispersion of photons transmitted through a 1D Fibonacci multilayer structure was investigated experimentally by Hattori and co-workers [94]. In their paper, they deposited 55 layers of SiO_2/TiO_2 to form an optical multilayer stack on a glass substrate, and measured the spectrum of the amplitude and phase of transmitted light using a phase-sensitive Michelson-type interferometer. They experimentally obtained phase and amplitude spectra clearly demonstrating the self-similar fractal nature of the Fibonacci spectra.

The interplay between quasiperiodic order and mirror symmetry has been investigated by Huang et al [95]. They discovered that the addition of internal symmetry greatly enhances the transmission intensity of the many Fibonacci peaks. In particular, the spectral positions and the self-similar scaling of symmetry-induced resonances with perfect unit transmission were discussed for a class of generalized Fibonacci multilayers within the analytical trace map approach. These interesting features were experimentally demonstrated in TiO_2/SiO_2 Fibonacci optical multilayers with internal mirror symmetry by Peng and collaborators [96]. The authors envisioned the use of symmetry-induced perfect transmission states in Fibonacci multilayers for the engineering of multi-wavelength narrowband optical filters, wavelength division multiplexing systems, and photonic integrated circuits, where a high-density of narrow transmission peaks is particularly desired. The light transport properties of Fibonacci band-edge states in porous silicon multilayers have been first investigated by Dal Negro and collaborators by means of ultrashort pulse interferometry [97]. A strongly suppressed group velocity has been observed at the Fibonacci band-edge states with fractal behavior, which resulted in a dramatic stretching in the optical pulses (see Fig. 11). It was also found that the thickness drift naturally occurring during the growth of porous silicon Fibonacci multilayers induces the localization of band-edge modes, without compromising their characteristic self-similar patterns [98].

Non-linear optical phenomena have also been extensively investigated in Fibonacci and other quasiperiodic multilayered systems demonstrating superior performances over periodic structures in terms of optical multi-stability [99]

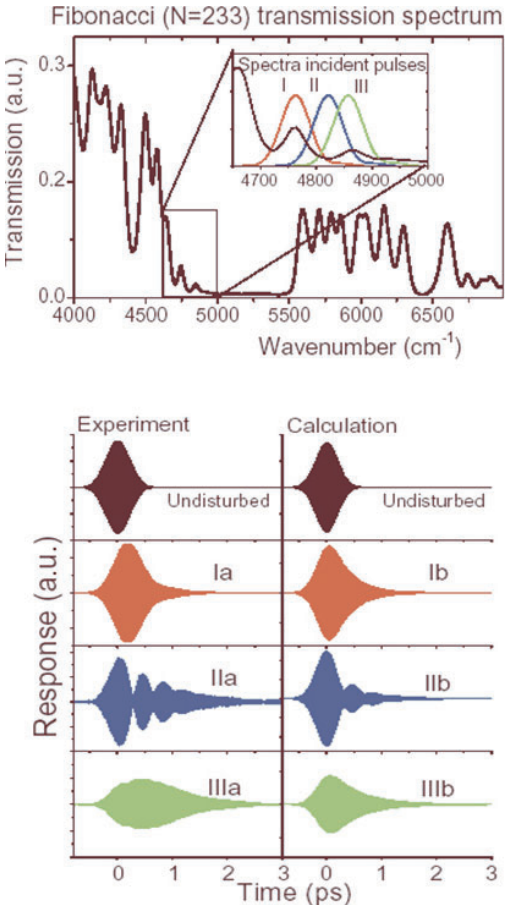

Figure 11 (online color at: www.lpr-journal.org) (top): Measured transmission spectrum of a 12th order Fibonacci quasicrystal. The inset shows three examples of the power spectrum of the incoming laser pulses in the time-resolved experiment reported at the bottom. (bottom): Experimental data and calculation of the transmission through Fibonacci samples at four different frequencies. Also the undisturbed pulse, which has passed through only the substrate and not the Fibonacci sample, is plotted for comparison. When the laser pulse is resonant with one band edge state the transmitted intensity is strongly delayed and stretched. When two band edge states are excited, mode beating is observed. Adapted from [97].

and second/third harmonic generation due to a far richer Fourier spectrum [100, 101]. In particular, the aperiodic nature of quasiperiodic multilayers provides more reciprocal vectors for the simultaneous quasi-phase-matching of different nonlinear processes. Zhu and collaborators [100, 101] showed that this approach leads to a direct third-harmonic generation with high efficiency through a coupled parametric process (Fig. 12). Their results demonstrate that high-order harmonics may be generated in a quadratic nonlinear medium by a number of quasi–phase-matching processes, and therefore, can result in important device applications of quasiperiodic structures in the field of nonlinear optics. Using multiple quasi-phase-matching in aperiodic structures, a 1D photonic quasicrystal which acts as a simultaneous frequency doubler for three independent optical beams has

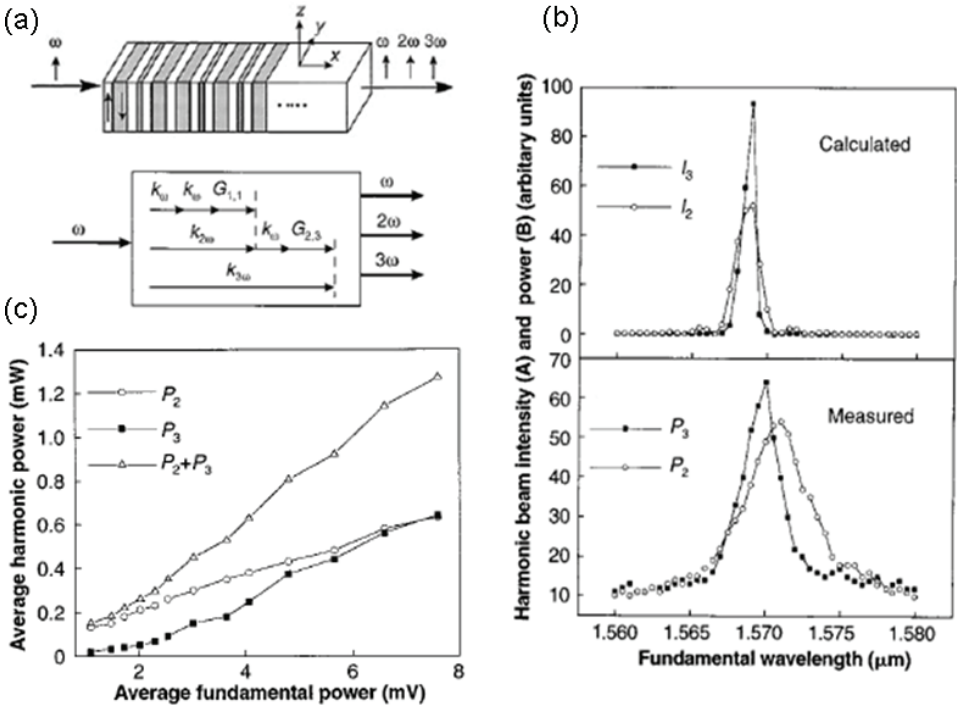

Figure 12 (a) Schematic diagram shows a Quasi Periodic Optical Superlattice (QPOS) composed of two blocks, *A* and *B*, arranged in Fibonacci sequence and the polarization orientation of electric fields in the THG process with respect to the superlattice. Below is shown a schematic diagram of the process of THG in a QPOS material. (b) The SHG and THG tuning curves for the QPOS sample, (top) calculated and (bottom) measured by using an *ns*-optical parametric oscillator. (c) The average powers of second- and third-harmonic fields versus the average power of the fundamental field for the QPOS sample. The light source is an *ns*-optical parametric oscillator with a repetition of 10 Hz. Adapted from [101].

been demonstrated experimentally using electric-field poled $LiTaO_3$ crystals [101]. These devices have been shown experimentally to perform almost a factor of ten better than comparable ones based on quasi-phase-matching in periodically poled structures. Generalized quasiperiodic structures (GQPS) for the simultaneous phase-matching of any two arbitrarily chosen nonlinear interactions have also been recently demonstrated [102]. These quasiperiodic structures, first fabricated in a KTP nonlinear crystal, can efficiently phase-match multiple nonlinear interactions with arbitrary ratio between their wave vector differences.

Recently, the optical properties of multilayered structures based on the Thue-Morse sequence, characterized by a singular continuous Fourier spectrum, have also attracted considerable attention [72, 103]. The first optical Thue-Morse structure was fabricated by Dal Negro et al. using magnetron sputtering of Si/SiO_2 multilayer stacks [84]. In the same paper, optical gaps corresponding to the singularities of the Fourier spectrum have been discovered and explained by the presence of short-range correlations among basic periodic building blocks distributed across the structure [84]. Similar results were reported shortly after by Qiu and collaborators [104]. The presence of a self-similar hierarchy of optical gaps scaling according to a characteristic triplication pattern of symmetry-induced perfect transmission states was also established by Liu and collaborators in Thue-Morse multilayers (Fig. 13) [103]. More recently, Jiang and collaborators demonstrated, both theoretically and experimentally, that the photonic band gaps in Thue–Morse aperiodic systems can be separated into two types, the fractal gaps (FGs) and the traditional gaps (TGs), distinguished by the presence or absence of a fractal structure, respectively [105]. The origin of the two kinds of gaps was explained by the different types of interface correlations and this explanation was confirmed by the gap width behaviors. They also found that the eigenstates near the FGs have a cluster-periodic form with large magnitude fluctuations (i. e. a *critical mode*), while those near the TGs resemble Bloch waves. Spectrally enhanced light emission from SiN_x/SiO_2 Thue-Morse multilayer structures was demonstrated by Dal Negro et al. (Fig. 14) [106]. Significant light-emission enhancement effects at multiple wavelengths corresponding to critically localized states were experimentally observed in a 64 layer thick Thue-Morse structure, yielding a total emission enhancement of almost a factor of 6 in comparison to homogeneous light-emitting SiN_x samples (Fig. 14d) [106]. The self-similar fractal nature of Thue-Morse modes was subsequently investigated by the use of the multi-scale wavelet analysis [107].

The possibility to engineer an all-optical diode using nonlinear Thue-Morse multilayers was recently investigated by Biancalana [108]. In this paper, it was demonstrated that the strong asymmetry of odd-order Thue-Morse lattices, combined with a Kerr nonlinearity, gives rise to a highly nonreciprocal transmission spectrum which is the major feature of an all-optical diode. The proposed Thue-Morse design allows for an unprecedented reduction in device size at relatively low operational optical intensities, a consequence of the intrinsic anti-symmetry of the considered structure, and the localized nature of its transmission states.

Dielectric multilayers consisting of pairs of dielectric materials with different refractive indices arranged according to a fractal structure in the direct physical space have also been investigated, and are referred to as *fractal filters* (Fig. 15). These structures were introduced in optics by Jaggard and Sun in 1990 [109, 110], and their distinctive optical properties have been discussed in detail in [111–114]. Fractal filters generated by *Cantor set* algorithms were found

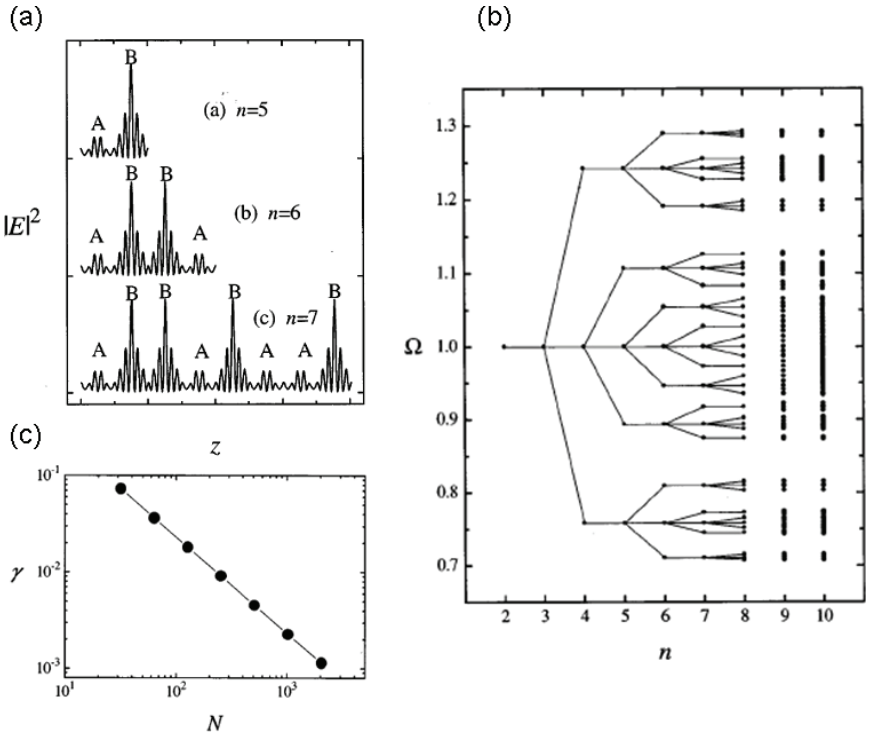

Figure 13 (a) The lattice like electric field distributions in the Thue-Morse multilayers for a completely transparent frequency for structures with 32 ($n = 5$), 64 ($n = 6$), 128 ($n = 7$) layers, respectively. (b) The reduced frequency Ω giving rise to identical matrix vs generation n for $a = b = 0.25$ (quarter-wavelength). Around $\Omega = 1$ is a quasi-continuous band I formed. (c) Localization index γ vs the number of layers N for the lattice like electric field distributions at a completely transparent frequency $\Omega = 0.758$. From [103].

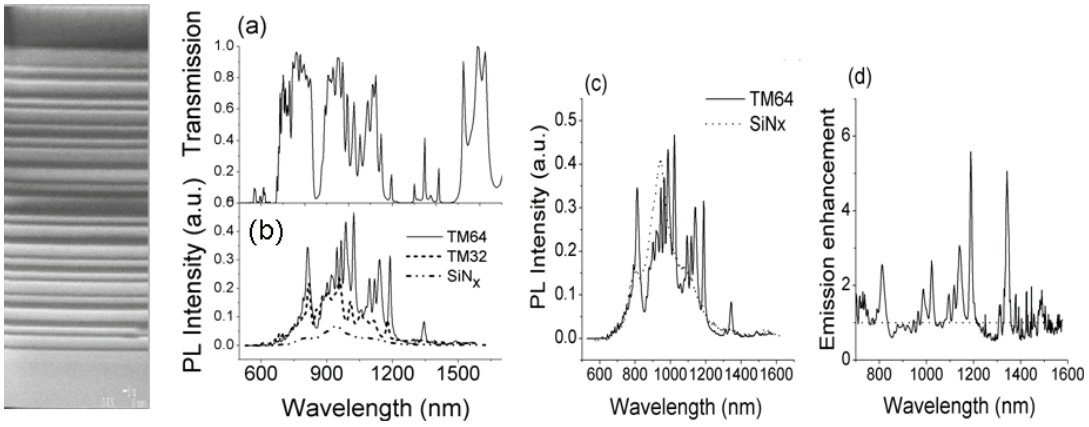

Figure 14 SEM image of light-emitting Thue-Morse (TM) structure with SiN_x and SiO_2 layers. (a) Experimental transmission spectrum for the 64 layer T-M structure. (b) Room temperature PL intensity of TM64 sample (solid line), TM32 sample (dashed line), homogenous SiNx reference sample (dash-dotdot line). The excitation wavelength was 488 nm and the pump power was 10 mW. (c) Comparison of the TM64 transmission spectrum and the homogeneous reference sample emission rescaled according to the SiNx thickness ratio. (d) Experimentally derived wavelength spectrum of the optical emission enhancement in the TM64 sample. Adapted from [106].

to exhibit a distinctive spectral scaling of their transmission spectra resulting from their geometrical self-similarity. Moreover, it was recently demonstrated analytically by Zhukovsky and collaborators that universal *recurrence relations* exist, *valid for every self-similar multilayer structure*, between the intensity reflection and transmission coefficients of generations N and $N+1$ [112, 114].

According to this picture, the transmission/reflection spectrum of every type of optical fractal structure of generation N contains embedded transmission/reflection spectra *of all the preceding generations* squeezed along the frequency axis by a characteristic scaling factor. Finally, the splitting of the transmission bands of *symmetrical* fractal filters has been discovered [111–115], with a multiplicity that grows with the generation number (see Fig. 15). In the case of fractal filters made of layers with refractive indices n_A and n_B, thicknesses d_A and d_B, and satisfying the Bragg condition $n_A d_A = n_B d_B = \lambda_0/4$ at a wavelength λ_0, every period in the transmission spectrum (of amplitude $2\omega_0$, $\omega_0 = 2\pi c/\lambda_0$, c the speed of light) will contain a number of peaks equal to the number of layers in the fractal structure. For example, if N is the generation order of a triadic and pentadic Cantor filter, it can be shown that 3^N and 5^N peaks can be encoded in the periods of the corresponding transmission spectra [112].

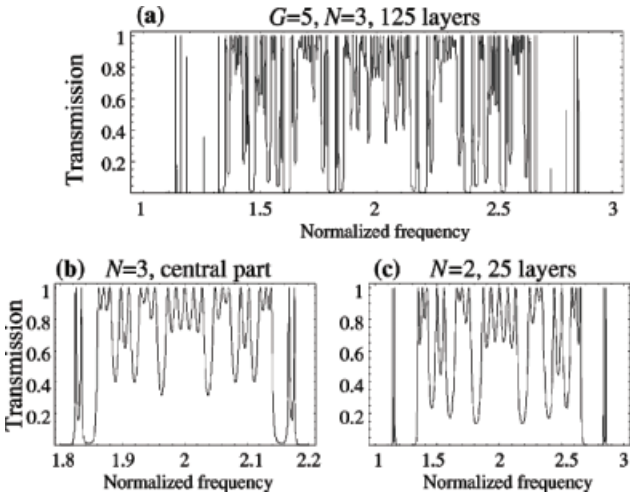

Figure 15 Scalability of optical spectra for Cantor multilayers of order $G = 5$: the full period of a (3,4) spectrum (a) and the central part of it magnified in the frequency scale by 5 (b) versus the full period of a (3,3) spectrum (c). Comparing (b) and (c), one can see that the spectra are scalable with the factor equal to G. From [112].

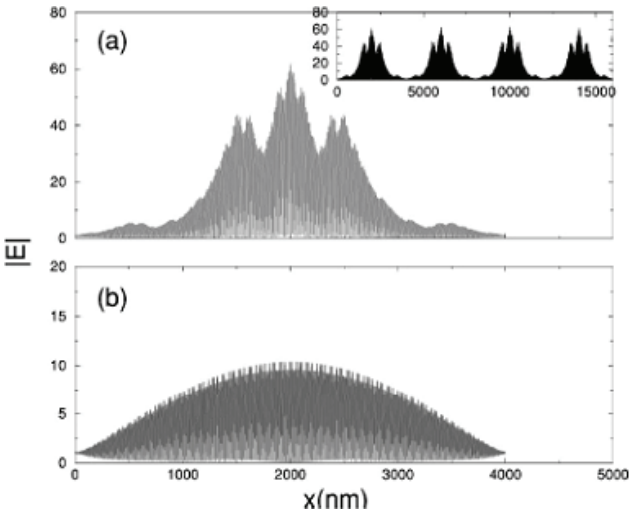

Figure 16 The electric field magnitude vs position x. (a) The gap-edge state near the BFG in an S_{10} TM lattice. The inset shows the state at the same frequency in an S_{12} TM lattice. (b) The gap-edge state near the BTG in an S_{10} TM lattice. From [105].

Finally, the propagation of plasmon-polaritons in 1D metal-dielectric aperiodic superlattices generated by various substitutional sequences was thoroughly investigated by Albuquerque and collaborators [116, 117]. Based on an analytical transfer matrix approach, they investigated polariton spectra and discovered self-similar characteristic patterns with multifractal distributions of polariton bandwidths.

The unique structural and optical properties of deterministic aperiodic nanostructures in one spatial dimension provide unprecedented opportunities for the engineering of novel optical devices that fully leverage on the control of aperiodic order. Specific device applications of 1D aperiodic structures will be discussed in the next section.

2.1. Optical devices based on one-dimensional aperiodic structures

The application of aperiodic order to photonic devices has resulted in the engineering of a number of novel components and functionalities enabled by the unique structural and optical characteristics of aperiodic dielectric multilayers. In what follows, we will discuss the signatures of aperiodic order that are most relevant to device engineering, and review the main achievements.

a) *Critical modes:* these are unique spatial wavefunctions (i. e., optical fields) with strongly fluctuating envelopes and power-law localization properties ideally suited to enhance light-matter interactions (linear and nonlinear) over large areas in defect-free photonic structures. In Fig. 16 we show a calculated band-edge critical mode of a Thue-Morse structure, from [105]. The spatial localization, frequency bandwidth, and intensity enhancement of critical modes can be utilized to engineer multi-frequency light sources and optical sensors. Following this approach, light emission enhancement from Thue-Morse active multilayers [84, 106] and chemical sensing with Thue-Morse porous silicon layers have been recently demonstrated [118]. Moretti et al. have provided a detailed comparison of the sensitivities of resonant optical biochemical sensors based on both periodic and aperiodic structures [118]. The shifts of the reflectivity spectra of these devices upon exposure to several chemical compounds have been measured and Thue-Morse aperiodic multilayers were found more sensitive than periodic ones due to the lower number of interfaces and enhanced mode localization.

b) *Dense reciprocal space*: this feature enables the engineering of multiple light scattering phenomena in the absence of disorder and, for nonlinear materials, it offers the unique possibility of achieving quasi-phase-matching of multiple nonlinear processes simultaneously. Multicolor harmonic generation based on quasiperiodic and aperiodic multilayers has been demonstrated as well as the generation of several harmonics with high efficiency [100–102]. These effects are relevant to the engineering of a novel class of tunable multiwavelength optical parametric oscillators and nonlinear optical devices including multi-frequency bistable elements and adiabatic shapers of quadratic solitons. The high density of reciprocal wave vectors available in quasiperiodic structures has recently been utilized for the demonstration of the first quasi-crystal distributed feedback (DFB) laser by Mahler and co-workers [119]. In particular, they showed that, by engineering a quasi-crystalline structure in an electrically pumped device, several advantages of random lasers, such as the very rich emission spectra, can be combined with the predictability of traditional distributed feedback resonators. Using a Fibonacci sequence, they fabricated a terahertz quantum cascade laser in the one-dimensional grating geometry of a conventional disturbed feedback laser (Fig. 17a,b). This device makes use of

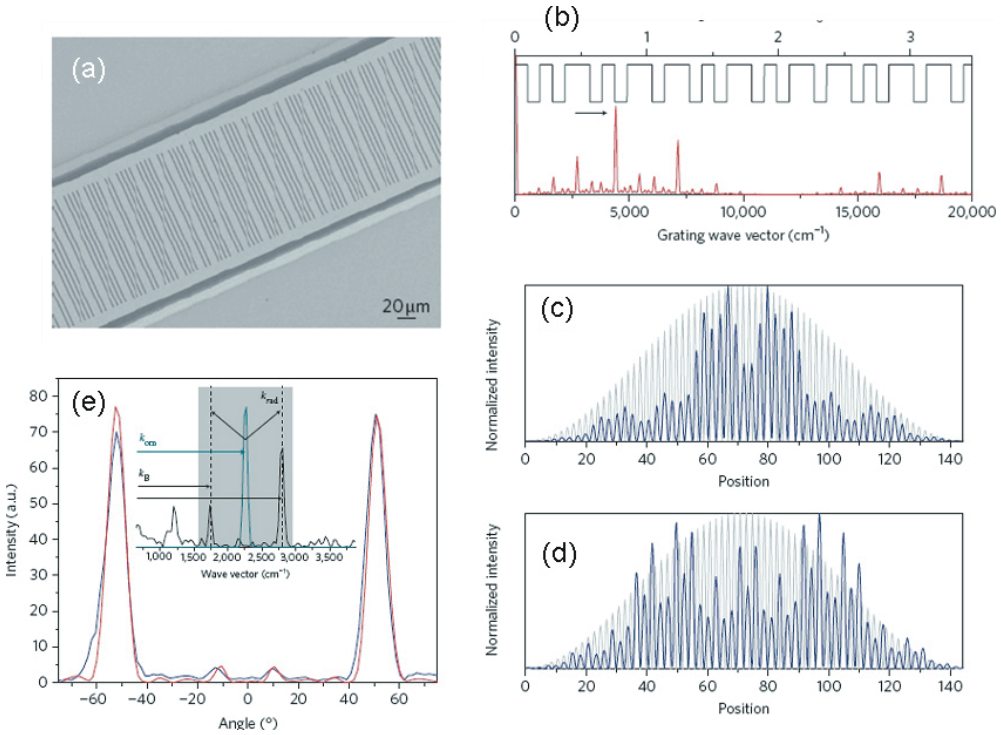

Figure 17 (online color at: www.lpr-journal.org) (a) Top view of the fabricated Fibonacci laser device. (b) Fourier transform of a quasi-periodic grating of the Fibonacci type. The inset shows the corresponding refractive index profile. The Fibonacci sequence features many additional resonances, which can be used to create distributed feedback. The work in [119] considers a DFB with first-order diffraction on the Bragg peak indicated by the arrow. (c–d) Spatial intensity distribution of the modes on the high-energy and low-energy band-edges of the photonic gap that emerges from the Bragg peak highlighted in panel (b). The quasi-crystalline structure (blue) leads to a distribution very different from the periodic case (light grey). The x-axis gives the layer number. (e) Far-field pattern of a device operating on the lower band-edge. The red and blue lines show the computed and measured far-fields, respectively. The inset shows the interaction of the optical mode with the grating, both represented by their Fourier transform in black and cyan respectively. Adapted from [119].

a quantum-cascade active region in the terahertz frequency range, is electrically pumped, and therefore of great interest for realistic applications. Single-mode emission at a specific angle from the device surface was obtained along with dual-wavelength operation. These results demonstrate that the engineering of self-similar spectra of quasiperiodic gratings naturally allows optical functionalities that are hardly possible with traditional periodic resonators, such as directional output independent of the emission frequency and multi-color operation (Fig. 17e). In particular, the dense fractal spectra of quasi-crystals can be easily engineered to control independently the energy spacing and positions of the modes, providing the opportunity of using more than one Bragg resonance for feedback, which leads to a multi-color laser operation at arbitrarily chosen frequencies within the gain bandwidth. Finally, we note that in the weak scattering regime, each Fibonacci Bragg peak leads to a bandgap in the optical transmission spectrum, and therefore the emission properties of quasiperiodic DFB lasers can be entirely designed *a priori* based on the structure of their Fourier space, significantly broadening the engineering possibilities compared to periodic laser devices.

c) *Fractal transmission spectra:* the distinctive fractal scaling and peak splitting behavior of the transmission spectra of quasiperiodic and aperiodic multilayers have profound significance for the engineering of novel devices and the management of group velocity, light dispersion, and energy conversion effects. In relation to dispersion engineering, Gerken et al [120, 121] demonstrated that using a single 66-layer non-periodic thin-film stack enables the separation of four wavelength channels by spatial beam shifting due to strong group velocity dispersion effects, similarly to the superprism effect observed in photonic crystals. However, the use of aperiodic multilayers guarantees larger and more controlled shifts including constant dispersion allowing for equidistant channel spacing. Using this approach, a nearly linear 100 μm shift over a 13 nm wavelength range was achieved, paving the way to the fabrication of thin-film filters that can be utilized to obtain compact, cost-effective wavelength multiplexing and demultiplexing devices.

Using the complex transmission spectra of a fractal multilayer structures, Gaponenko et al [113] have recently suggested the possibility to encode and identify numeric information. This procedure could potentially be used in optical data recording and read-out by coding Fibonacci numbers in the transmission peaks of dielectric multilayers. This approach can open unprecedented scenarios for performing arithmetic operations by the physical process of light

propagation through aperiodic multilayers. The systematic analysis of the splitting behavior of certain transmission peaks in Cantor dielectric multilayers has even revealed fascinating correlations between the numerical values associated to their transmission spectra and the corresponding prime factors [112–115].

Another key application domain where the fragmentation of aperiodic multilayers spectra could play a crucial role is in the field of thermo-photovoltaics. Aperiodic and quasiperiodic dielectric and metal-dielectric multilayers have in fact been utilized to selectively enhance thermal radiation over broad frequency bands [122, 123]. Moreover, it has been shown by Maksimovi and Albuquerque that the spiky thermal emission profiles of the fractal multilayers can be substantially smoothed by incorporating metamaterials in the dielectric layers, thus providing broad spectral ranges of enhanced thermal emission [122, 123]. The highly fragmented nature of the energy spectra of quasiperiodic and aperiodic low-dimensional electronic materials could also play a crucial role in enhancing the generation efficiency of photovoltaic cells by providing an intermediate structure of electronic multi-bands. As discussed by Peng and collaborators in their original design study [124], multiple electronic mini-bands can be engineered below the barriers of semiconductor superlattices thus providing additional channels for efficient photo-induced absorption over broader frequency ranges. Their results are summarized in Fig. 18. By designing the optimal energy band structure through the control of aperiodic order, it appears possible to approach the 93% absolute thermodynamic limit of work production in light converters [125].

d) *Broader design space:* as discussed in Sect. 2, the Fourier space of deterministic aperiodic structures can be flexibly engineered to span across all the possible spectral measures. In addition, the design parameters can further be expanded when following a novel approach pioneered by Maciá [21, 22]. This approach considers the blending of periodically and aperiodically arranged multilayers, thus defining a *hybrid-order* made of different kinds of subunits, with different types of topological order present at different length scales. The introduction of structural subunits with different *periodic/aperiodic order* mimics the mechanisms of structural colors and iridescence phenomena observed in multi-scale natural systems such as biological photonic nanostructures (e. g., butterfly's wings) [126]), and complex biological macromolecules (e. g., DNA). Optical multilayer systems with hybrid-order can be designed to exhibit *complementary optical responses* (i. e., high transmission-high reflection), depending on the choice of the incident angle (see Fig. 19) [21, 22]. These hybrid structures additionally present fundamental questions in the theory of complex optics. In fact, despite it has been shown that hybrid spectra share characteristic features with both their periodic and aperiodic subunits, the mathematical nature of their spectra is still a fascinating open problem [12] that deserves intense work in the near future. Finally, we note that additional parameters can be introduced in the design space of aperiodic structures by: (i) arbitrary structural distortions (e. g., chirped quasiperiodic structures); (ii) suitably combining

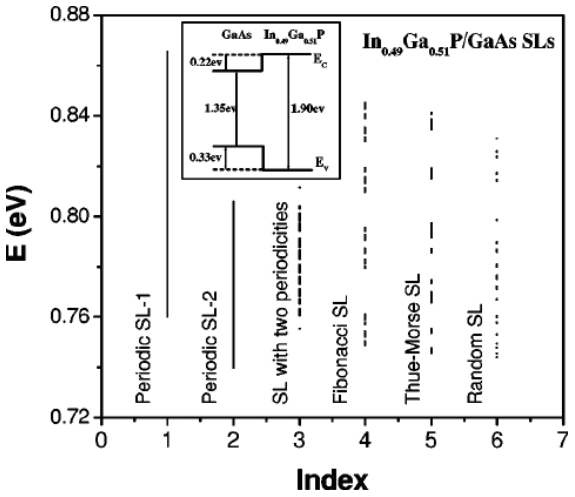

Figure 18 Electronic miniband structures for the several periodic and aperiodic $In_{0.49}Ga_{0.51}P$/GaAs superlattices below the barrier. The origin of the energies is set at the center of the gap of well material GaAs. The index equal to 1–6 stands for the following structure: 1-periodic SL with $N = 21$, $a = b = 2.5$ nm; 2-periodic SL with $N = 21$, $a = b = 3.5$ nm; 3-SL with two parts: the first part with $N = 10$, $a = b = 2.5$ nm, and the second part with $N = 11$, $a = b = 3.5$ nm; 4-Fibonacci SL: $N = 21$, $a = 2.5$ nm, $b = 3.5$ nm; 5-Thue–Morse SL: $N = 16$, $a = 2.5$ nm, $b = 3.5$ nm; 6-one kind of random SL with $N = 21$, $a = 2.5$ nm, $b = 3.5$ nm, where N is the total number of layers, a and b are two thicknesses of the wells (a for block A and b for block B), and the thickness of each barrier of all SLs is the same as $d = 2.0$ nm. The inset is a schematic of the band-edge diagram of the $In_{0.49}Ga_{0.51}P$/GaAs interface. From [124].

different types of aperiodic order within the same structure (aperiodic heterostructures); (iii) abstract symmetry operations such as *symbolic conjugation* (e. g., by interchanging the symbols A and B in binary sequences); *mirror symmetry,* resulting in positional correlations and resonant transmission peaks [12].

3. Two-dimensional aperiodic structures in photonics

In periodic photonic crystals (PhCs), optical bandgaps are formed when coherent multiple scattering of photons induced by periodic variations of the refractive index acts to prevent propagation of electromagnetic waves along certain directions and within certain frequency ranges [127, 128]. On the other hand, random multiple scattering of photons in disordered structures can give rise, for large enough values of refractive index contrast, to a purely interference effect called Anderson localization of light [129]. In turn, multiple light scattering in photonic structures with various degrees of aperiodic order results in a much richer physical picture and leads to the formation of frequency regions of forbidden propagation, known as "pseudo-gaps", and distinctive resonant states with various degrees of spatial confinement, known as critical modes [11]. Although this physical pic-

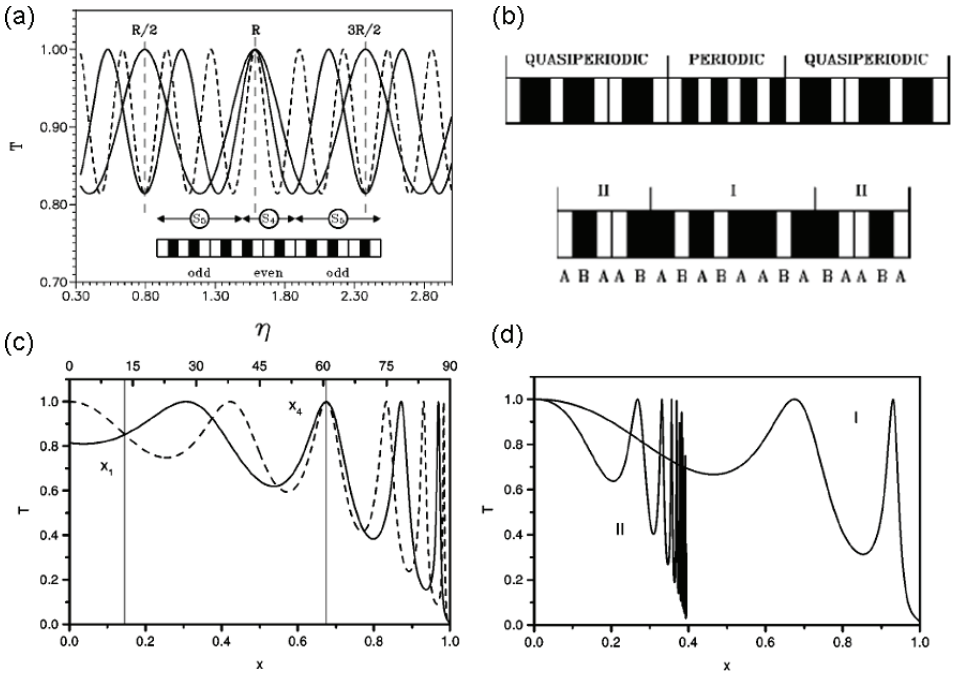

Figure 19 (a) Dependence of the transmission coefficient with the refractive index contrast in hybrid-order dielectric multilayer of different thicknesses. (b) Sketch or hybrid-order structures. (c) Dependence of the transmission coefficient on the angle of incidence for a periodic multilayer and a Fibonacci dielectric multilayer, demonstrating complementary optical responses. (d) Dependence of the transmission coefficient with the incidence angle for the conjugated order device sketched (b), Adapted from [21, 22].

ture is perfectly general, deterministic aperiodic structures in two spatial dimensions are unique at combining long-range structural order with higher order rotational axes (i. e., forbidden symmetries) and more abstract symmetries (e. g., fractal inflations, spiral symmetry, etc.) leading to more isotropic band gaps, omnidirectional reflection spectra, and unusual localization of optical modes.

3.1. Origin of 2D photonic bandgaps and eigenmodes

The frequently-invoked analogy between photonic bandgap materials and condensed matter physics, where electronic bandgaps are present even in the absence of the long-range structural order (e. g. amorphous semiconductors), has inspired the recent study of long-range and short-range spatial correlations in complex photonic structures. The formation of photonic bandgaps in 2D structures with quasiperiodic order has first been demonstrated for octagonal tilings by Chan et al in 1998 [130]. A comparative analysis of the photonic bandgaps evolution in periodically-arranged square supercells of progressively larger sizes led the authors to the conclusion that the gaps formation in quasiperiodic structures is governed exclusively by short-range correlations. The evidence of the major role played by short-range correlations and local symmetry groups has later been observed for photonic quasicrystals with up to 12-fold rotational symmetry [131–134]. However, all the above studies focused on aperiodic structures consisting of high-refractive-index dielectric rods embedded in a low-index host medium (cermet-type structures), which favor formation of bandgaps for transverse-magnetic (TM)-polarized light waves [128]. In this case, usually referred to as the "strongly localized photon picture", short-range coupling of sharp Mie resonances supported by the individual rods is the underlying mechanism that drives the formation of optical bandgaps. Accordingly, cermet-type photonic structures (both periodic and aperiodic) can be described as tight-binding systems of individual Mie resonators with identical resonance frequencies ω_r, analogous to the tight-binding description of electronic gaps by the coupling of atomic orbitals in semiconductors. Interactions of these resonators with each other and with the continuum band of the surrounding medium results in the formation of bandgaps at frequencies distributed around ω_r [13]. Therefore, the spectral positions of bandgaps in cermet-type aperiodic structures with different array morphologies approximately coincide with each other, and also with the positions of bandgaps in periodic crystals with similar geometrical and material parameters [135, 136]. Furthermore, these types of photonic bandgaps are quite robust to positional disorder [137]. In addition to Mie resonance coupling, there is another bandgap formation mechanism, *non-resonant Bragg scattering*, which becomes dominant in the case of low refractive index contrast, sparse or network-like photonic structures [13, 137]. Bragg scattering is a result of the destructive/constructive interference of incident field and the field scattered by the refractive index variations such as dielectric or air rods, lattice planes, etc. In the first-order single-scattering approximation, analogously to nearly-free-electron systems, photonic bandgaps are formed in a one-to-one correspondence with the spectral positions of Bragg peaks in reciprocal space of the structure, and the gap widths scale with the intensities of the corresponding Bragg peaks [138]. Accordingly, the bandgap positions can be adjusted by tuning the nearest-neighbor separation in photonic structures and by designing the Fourier space of the structures. As a result, the Bragg scattering regime is particularly relevant to the engineering of aperiodic systems since simple design rules can be formulated directly by analyzing the Fourier spectral properties of the structures. However,

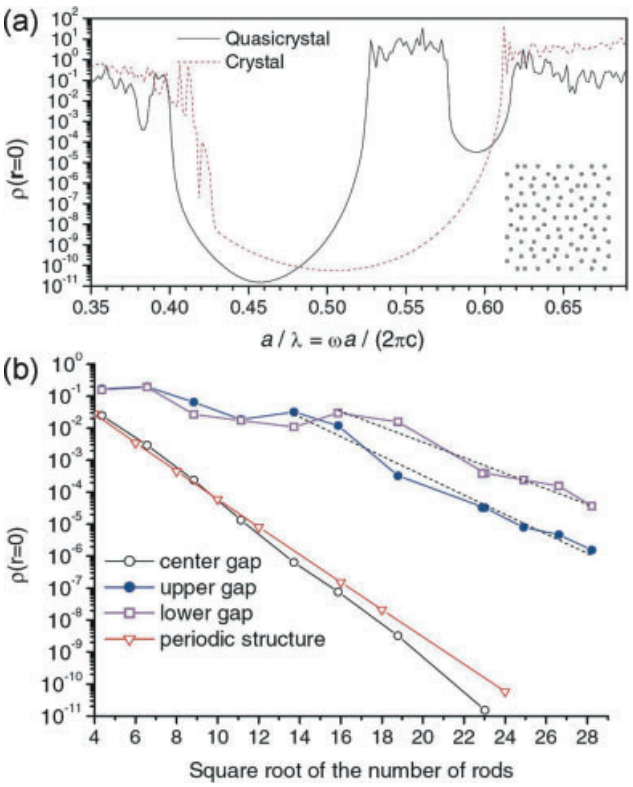

Figure 20 (online color at: www.lpr-journal.org) Bandgaps scaling with the size of the 2D Penrose-type quasicrystal. (a) LDOS spectra of the periodic, and Penrose structures made of 576 and 530 cylinders, respectfully. (b) Minimum LDOS value in the three bandgap scaling with the structure size (adapted with permission from [140].

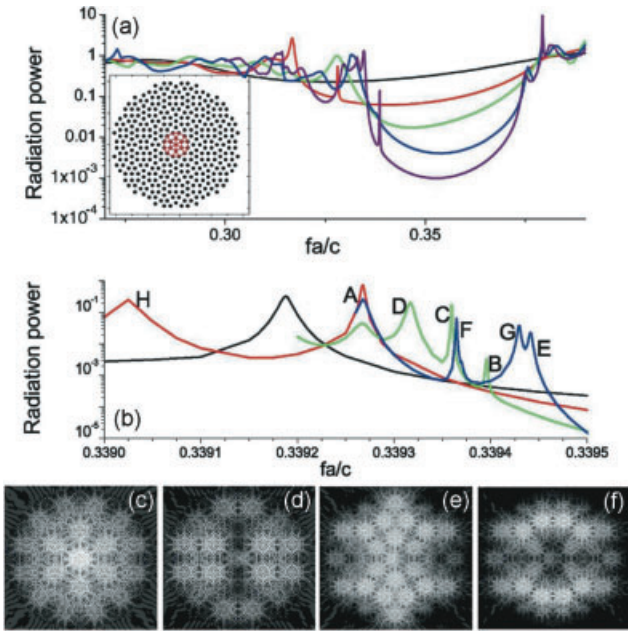

Figure 21 (online color at: www.lpr-journal.org) (a) The radiated power spectra for the 12-fold photonic quasicrystal (shown in the inset) of the lattice radial size $R = 2a$ (black), $4a$ (red), $6a$ (green), $8a$ (blue), and $10a$ (purple); a is the distance between two nearest cylinders. (b) The photonic bandedge evolution in large quasicrystal lattices, $R = 24a$ (black), $36a$ (red), $48a$ (green), and $60a$ (blue). (c–f) The intensity maps at the resonances marked as "A," "H," "B," and "C" in (b). After [143].

photonic structures in the nearly-free-electron regime are more sensitive to structural disorder, which destroys long-range phase coherence of the scattered waves [137]. On the other hand, aperiodic structures in the low index regime have been successfully engineered for optical sensing applications [60], and will be discussed in Sect. 3.4. Finally, Bragg interference effects beyond first-order scattering [139–141] may also play a role in the gap formation, especially in photonic structures with moderate or high index contrast, but are less explored at present. *The Mie-resonance and the Bragg scattering regimes usually co-exist in any given aperiodic photonic structure*, as illustrated in Fig. 20, which shows the structure of photonic bandgaps of a finite-size Penrose array of high-index dielectric cylinders and their evolution with the increase of the structure size [140]. The bandgap formation is revealed via calculation of the local density of states (LDOS) in the center of the quasicrystal. The exponential decay of the LDOS in the central bandgap of the Penrose structure is almost identical to that observed in periodic photonic crystals (see Fig. 20b), which is an indication that it originates from relatively short-range correlations. However, the scaling behavior of the two lateral bandgaps is quite different and shows the existence of a minimum structure size necessary to establish exponential decay, which demonstrates the role of long-range correlations in the formation of these gaps. A similar picture of the bandgaps scaling with the structure size has also been observed in 1D aperiodic multilayer stacks [84, 105, 142].

The complex interplay between short-range and long-range interactions in aperiodic photonic structures is also manifested by the scaling of the band-edge states with the increase of the structural size. As shown in Fig. 21 new states appear at the edges of the bandgaps whose formation is driven by the short-range coupling between Mie resonances of individual scatterers. These new states result from the coupling between resonances of small clusters, which repeat throughout the photonic lattice and act as resonant scatterers [143, 144]. These effects are more pronounced in low-index structures, where coupling between local and global symmetries becomes more dominant, leading to larger deviations of their Mie-scattering-driven bandgap positions/widths from those of periodic photonic crystals [131]. Furthermore, the increase of the structure size of aperiodic structures results in both the appearance of new modes inside the bandgaps and the formation of smaller gaps inside the transmission bands [105, 143, 145, 146], as shown in Fig. 21. Such evolution of the transmission spectra of aperiodic structures originates from the fact that, with the increase of the system's size, larger resonant clusters absent at smaller scales are formed, which can support localized resonances inside the bandgaps. A further increase of the lattice size results in coupling of such cluster resonances and in the formation of new bandgaps. Ac-

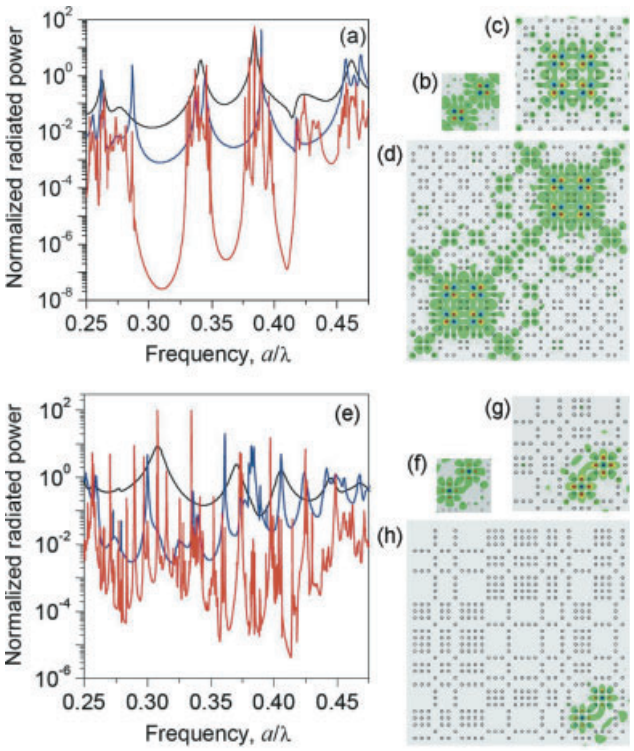

Figure 22 (online color at: www.lpr-journal.org) Evolution of the radiated power frequency spectra (a,e) and the field intensity patterns of selected modes (c–d, g–h) in the Thue-Morse (a–d) and Rudin-Shapiro (e–h) aperiodic structures composed of high-index ($\varepsilon = 10$) dielectric rods (adapted with permission from [146]).

cordingly, resonant modes with extended and self-similar states have been observed in defect-free aperiodic structures [143, 145–150]. Analogously to 1D structures, the modes of 2D aperiodic systems are strongly fluctuating critical modes with a self-similar structure and power-law localization scaling [105, 145, 146, 151]. Localization properties of critical modes in the structures with pure-point (quasiperiodic) or singular continuous Fourier spectra are usually explained by the interplay between the lack of periodicity, which drives for localization, and global scale-invariance (i. e., self-similarity), which drives for the coupling between localized cluster states and thus tends to establish extended wave functions [130]. However, localized modes can form in the structures with sparsely distributed high-symmetry clusters [147, 152, 153] or in aperiodic structures with high degree of disorder (characterized by flat Fourier spectra), which can be viewed as composites of different low-symmetry local clusters with varying resonant characteristics [146, 154, 155]. The effect of the spectral Fourier properties of aperiodic structures on their transmission spectra and modal properties is illustrated in Fig. 22, which compares the Thue-Morse (singular-continuous Fourier spectrum) and Rudin-Shapiro (absolutely-continuous spectrum) arrays of dielectric cylinders. Clearly, coupling of wave functions localized at the clusters that repetitively appear in Thue-Morse arrays of larger size results in the formation of mini-bands inside the bandgap (Fig. 22a) and is reflected in the self-similar scaling of the modes intensity distribution in progressively larger lattices (Fig. 22b–d). To the contrary, increasing the size of the pseudo-random Rudin-Shapiro arrays causes the appearance of new localized states (Fig. 22e), which do not form bands and remain isolated within local clusters of scatterers (Fig. 22f–h).

3.2. Bandgap engineering with aperiodic structures

Traditional 2D photonic crystals have spatial arrangements that correspond to one of the five Bravais lattices. Among these lattices, only the triangular and the honeycomb possess the highest order of rotational symmetry ($n = 6$), and their Brillouin zones are the closest to a circle. As a result, these structures exhibit the widest 2D complete bandgaps (gaps for all polarizations and directions), but their band diagrams are strongly dependent on the light propagation direction.

The study of light propagation in photonic structures with quasiperiodic order [134, 135, 140, 143, 153, 156–165] was initially motivated by the expectation that the higher rotational symmetries of certain classes of quasicrystals would result in more angularly isotropic distributions of scattering peaks in Fourier space, favoring the formation of highly isotropic bandgaps. As discussed in Sect. 1, and in contrast to periodic photonic structures, there is no upper limit to the degree of global rotational symmetry in 2D quasiperiodic and aperiodic crystals. Photonic quasicrystals with 8-, 10-, and 12-fold rotational symmetries were demonstrated, and their optical properties were indeed found to be much less dependent on the propagation direction.

It is worth mentioning that an alternative approach to isotropic photonic dispersion has been recently developed based on the engineering of more complex periodic structures with multi-atom bases, known as Archimedean tilings [25, 166]. These periodic structures can approximate "crystallographically forbidden" rotational symmetries ($n = 5$, $n > 6$) over a finite number of diffraction peaks, and when the number of atoms per cell is increased, their diffraction spots tend to distribute over a circle. A detailed computational analysis of the bandgap and dispersion characteristics of 8-fold and 12-fold quasicrystals in comparison to periodic Archimedean tilings has been carried out in [166] using a standard plane-wave expansion method. Archimedean tilings, in the case of strong refractive index contrast, were found to exhibit the same gap widths and degree of isotropy as 8-fold and 12-fold quasicrystals, reflecting the fact that the light dispersion properties are mostly determined by short-range interactions. The opposite situation was found for structures with moderate or weak refractive index modulation (e. g., silicon nitride in air), where the gap properties of quasicrystals significantly deviate from Archimedean tiling structures due to the presence of very long-range interactions [166]. In this situation, it was concluded that quasiperiodic structures present a decisive advantage for the engineering of isotropic bandgaps compared to their periodic approximants and the Archimedean tilings. It is important to mention

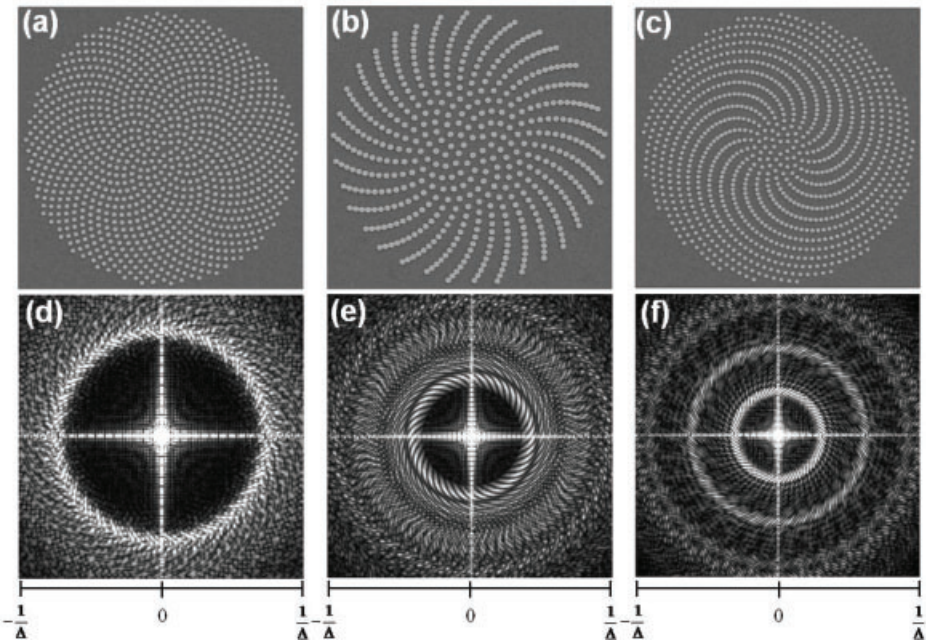

Figure 23 SEM micrographs of (a) Golden spiral array; (b) Vogel's spiral obtained with divergence angle $\theta = 137.6°$; (c) Vogel's spiral obtained with divergence angle $\theta = 137.3°$; the arrays consist of Au particles with 200nm diameters. (d–f) Calculated diffraction patterns (pseudo-Brillouin zone representation) of the spirals shown in panels (a–c). Δ represents the average center to center particle separation. After [172].

that GaN ad GaAs-based light emitting devices incorporating omnidirectional photonic crystals and optimized designs based on the engineering of Archimedean tilings have been successfully demonstrated experimentally [167–170]. Additionally, isotropic photonic structures have been obtained by designing reflection Bragg vectors equispaced in angle [171]. However, it is important to note that this design approach does not allow the investigation of more complex isotropic structures characterized by either continuous (i. e., no well-defined Bragg peaks) or mixed Fourier spectra. More recently, light scattering phenomena in photonic and plasmonic structures with diffuse, rotationally symmetric Fourier spectra were discussed [162, 172]. As mentioned in Sect. 1, the Pinwheel array exhibits a circularly symmetric Fourier space with infinity-fold rotational symmetry, but this feature only develops in the limit of infinite-size arrays. On the other hand, Fourier spaces with circular symmetry are beautifully displayed by *finite-size* aperiodic Vogel's spirals (Fig. 23), which are fascinating structures where *both translational and orientational symmetries are missing* [172]. These structures have been investigated by mathematicians, botanists, and theoretical biologists [63] in relation to the outstanding geometrical problems posed by *phyllotaxis* [173–175], which is concerned with understanding the spatial arrangement of leaves, bracts and florets on plant stems, most notably as in the seeds of a sunflower. Vogel's spiral arrays are obtained by generating spiral curves and subsequently restricting the radial (r) and angular variables (θ) according to the quantization condition [12, 176, 177]: $r = a\sqrt{n}$, $\theta = n\alpha$, where a is a constant scaling factor, $n = 0, 1, 2, \ldots$, $\alpha \approx 137.508°$ is an irrational number known as the "golden angle" that can be expressed as $\alpha = 360/\varphi^2$, $\varphi = (1+\sqrt{5})/2 \approx 1.618$ is the golden number, which can be approximated by the ratio of consecutive Fibonacci numbers. Rational approximations to the golden angle can be obtained by the formula $\alpha° = 360 \times (1 + p/q)^{-1}$ where p and $q < p$ are consecutive Fibonacci numbers. The angle α gives the constant aperture between adjacent position vectors $r(n)$ and $r(n+1)$ of particles in the "sunflower spiral", also called the "golden spiral" (Fig. 23a). Additionally, since the golden angle is an irrational number, the golden spiral lacks both translational and rotational symmetry, as evidenced by its Fourier spectrum (Fig. 23d). Interestingly, Vogel's spirals with remarkably different structures can be obtained by choosing only slightly different values for the aperture angle α, thus providing the opportunity to control and explore distinctively different degrees of aperiodic structural complexity. The structures and the Fourier spectra of the three most investigated types of aperiodic Vogel's spirals [172] (divergence angles $\alpha \approx 137.508°$, $\alpha_1 = 137.3°$, and $\alpha_2 = 137.6°$) are shown in Fig. 23. Only diffuse circular rings are evident in the Fourier spectra of Vogel's spirals (Fig. 23d–f), potentially leading to fascinating new lasing and photon trapping phenomena. To the best of our knowledge, the energy spectrum of elementary excitations propagating through these spiral lattices is still unknown. However, as illustrated in Fig. 24, it was found that the angular dependence of bandgaps (of Bragg scattering origin) in aperiodic structures critically depends on the degree of rotational symmetry of the pseudo-Brillouin zones or their Fourier transforms [162]. Accordingly, structures with higher degree of rotational symmetry, such as the Vogel's spirals, indeed provide wider and more isotropic photonic bandgaps.

Aperiodic photonic structures are also promising candidates for providing not just isotropic but *complete photonic bandgaps controlled by a wider range of parameters* than periodic PhCs. *Complete and isotropic* bandgaps in 2D and 3D photonic periodic structures cannot be easily achieved [128, 178, 179]. In many cases they occur for such values of structural and material parameters that impose stringent fabrication requirements [171, 180–182]. For ex-

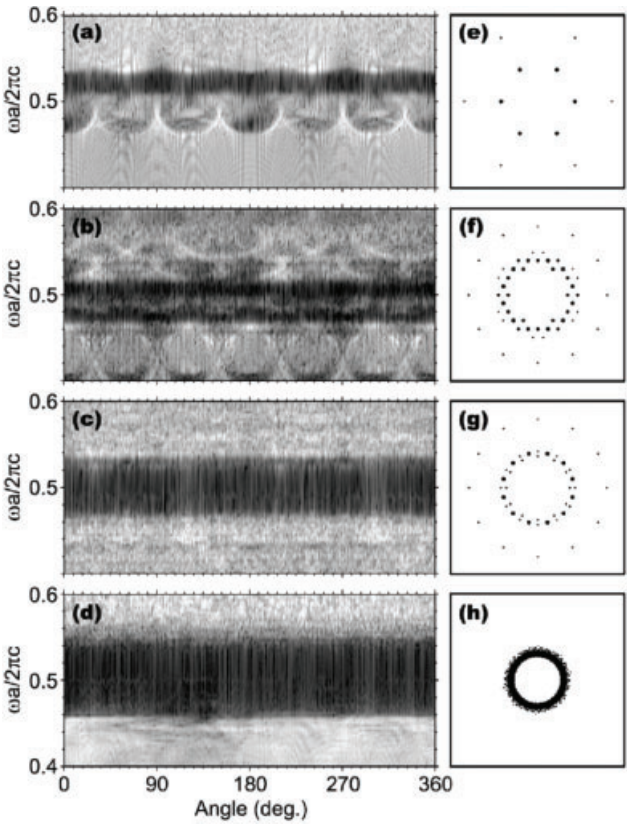

Figure 24 Transmitted electric field intensity (logscale) as a function of the in-plane angle and normalized frequency for (a) hexagonal, (b) dodecagonal, (c) 12-fold Stampfli-inflated, and (d) sunflower lattices of low-index ($\varepsilon = 2$) dielectric rods. Darker color corresponds to lower transmission (bandgap). (e–h) The corresponding diffraction patterns showing only the strongest Bragg peaks (reprinted with permission from [162]).

ample, the 3D face-centered cubic (fcc) lattice does not posses a complete bandgap [178], and complete bandgaps that open up in the spectra of 2D hexagonal lattices require high air filling fractions and a high refractive index contrast, which may be challenging from the fabrication point of view [180, 181]. This limitation of periodic PhCs stems from the degeneracy of the PhC bands at the points of high crystal symmetry, which prevents opening of the bandgaps. It has been shown that by reducing the lattice symmetry (e. g. by adding/removing some of the "building blocks" that form the photonic crystal or by periodically modulating their sizes) it is possible to increase the widths of existing bandgaps, to ease fabrication tolerances, and even to open up new bandgaps where none existed in structures of high-symmetry [178, 179, 183, 184].

The most celebrated examples of reduced-symmetry periodic structures that feature complete bandgaps are the 3D diamond lattice [178] and the 2D honeycomb (also called graphite) lattice [128, 184, 185]. Another example of a 2D periodic lattice with reduced-symmetry is a diatomic square lattice, which consists of two elements (e. g., dielectric rods or air-holes) of different sizes [179, 183]. Complete bandgaps in such a structure can form because the degeneracy of the TE bands at the **M** point of the Brillouin zone is lifted by the introduction of smaller-radii rods at the center of each square unit cell. The ratio of the two radii can be varied to maximize the bandgap width; and the honeycomb lattice is clearly a limit case of the diatomic lattice with $r_2/r_1 = 0$.

Although some controversy exists as to the lowest value of the refractive index contrast necessary for the formation of complete bandgaps in aperiodic lattices [131, 156, 157], there are indications that complete Bragg-scattering induced bandgaps can be realized in large-area aperiodic photonic structures of low refractive index. For example, it has been shown that by increasing the length of aperiodic multilayered stacks, photonic bandgaps can be opened at an arbitrary long wavelength, in the regime where periodic structures behave as homogeneous effective media [186]. Analogously, particle clusters in 2D and 3D aperiodic structures can act as resonant scatterers at lower frequencies than individual scatterers, which drive the formation of low-frequency photonic bandgaps [140, 145]. However, since such effects become dominant only in large-size structures [140, 145, 162], they may not be revealed by performing numerical simulations on finite-size aperiodic systems using periodic-supercell structures, which only retain smaller-size local clusters [130, 131, 157, 187] (see Sect. 5). It is also important to note that, unlike the extended Bloch modes of periodic PhCs, critical band-edge modes of different bandgaps in the same aperiodic photonic structure may feature drastically different spatial electric field distributions [158, 188]. This property of aperiodic lattices opens a way to separately adjust the widths of individual bandgaps (without affecting other gaps) by adding additional structural elements at certain positions within the aperiodic lattice. For example, it was shown that the width of the third bandgap of the 2D 12-fold quasicrystals lattice of dielectric rods can be selectively manipulated by adding metal or dielectric rods at pre-defined locations [158].

An alternative approach to engineer complete photonic bandgaps in aperiodic structures was recently developed by Florescu and collaborators [189]. Building on prior work on the generation of "stealth" and equi-luminous materials [190] with respectively zero and constant scattering intensity over a range of wavelengths, they have designed the first known example of amorphous optical structures of arbitrary size supporting complete photonic bandgaps. In particular, they presented a simple constructive algorithm with only two free parameters for the design of two-dimensional, isotropic, disordered, photonic materials displaying complete photonic band gaps blocking all directions and polarizations (Fig. 25).

The largest photonic band gaps were obtained in the large refractive index contrast, using silicon and air, within an optimization method that starts from a hyperuniform disordered point pattern. The authors observed that there is a strong correlation between the degree of hyperuniformity for a variety of 2D crystal structures and the resulting band gaps. Hyperuniform structures are distinguished by their suppressed density fluctuations on long length scales, and they consist in arrays of points whose number variance

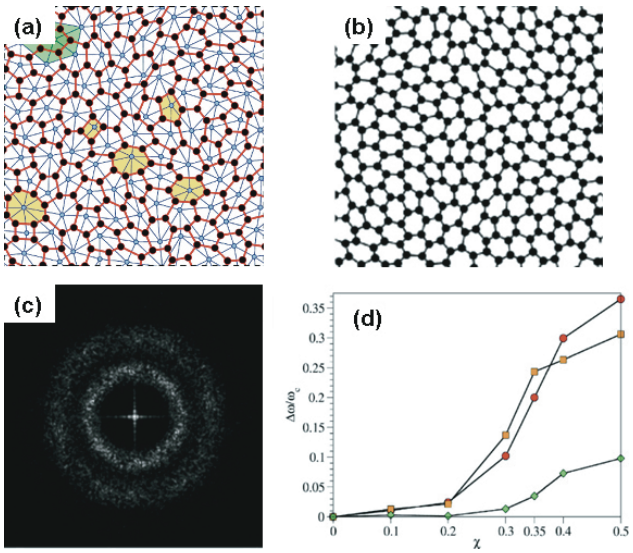

Figure 25 (online color at: www.lpr-journal.org) (a) Protocol for mapping point patterns into tessellations for photonic structure design: a chosen point pattern (open circles) is partitioned by using a Delaunay triangulation (thin lines). Next, the centroids of the neighboring triangles (solid circles) of a given point are connected, generating cells (thick lines) around each point, as shown for the five (green) Delaunay triangles in the upper left corner of the figure. (b) Realization of a stealthy hyperuniform pattern. (c) Structure factor S(k) corresponding to the pattern shown in (b). This structure exhibit a complete photonic bandgap. (d) A plot showing how the PBG increases with the degree of hyperuniformity and short-range geometric order. TM (red circles), TE (orange squares), and complete (green diamonds) photonic band gaps versus order the parameter for disordered, stealthy hyperuniform arrays of Si rods in air. Adapted from [189].

within a spherical sampling window grows more slowly than the volume. In this work, the authors demonstrate that hyperuniformity, combined with uniform local topology and short-range geometric order, result in complete photonic band gaps without long-range translational order, opening novel pathways for the control and manipulation of electronic and photonic band gaps in amorphous materials.

3.3. Structural defects and perturbations of aperiodic structures

It is well-known that localized states can be formed in the bandgaps of periodic PhCs by introducing structural defects [191]. These localized states are classified as either donor or acceptor modes. Donor modes are pulled from the higher-frequency air (conduction) band by introducing extra dielectric material at the defect site. Acceptor modes are pushed into the optical gap from the lower-frequency dielectric (valence) band when dielectric material is removed from one or several unit cells [191,192]. In photonic quasicrystals, each cylinder is located in a different environment, so that removing one cylinder from a different location can produce defect states with different frequencies and mode patterns, thus offering higher degree of flexibility and tunability for defect mode properties [163, 193]. Some studies indicate that for small-size structures, aperiodic geometries exhibit superior defect-mode confinement properties with respect to their periodic counterparts [194]. Waveguides can also be created by introducing channel-type defects in aperiodic lattices that support photonic bandgaps [153, 163, 193, 195], which demonstrate more structured transmission spectra than defect waveguides formed in periodic photonic crystals. Furthermore, finite-size aperiodic structures may support another type of defect modes (surface defect modes), whose frequencies and mode profiles depend on the specific shape of the truncated portion of the photonic lattice [150].

3.4. Device applications

Many of the proposed device applications of 2D aperiodic photonic structures hinge on the characteristic icosahedral group symmetry of quasicrystals, which results in more isotropic photonic gaps. However, multiple light scattering in 2D structures of controlled aperiodic order additionally offers the opportunity to generate unique optical modes with a broad spectrum of localization properties. In this section, we will review photonic devices that rely on the unique localization and spectral properties of critical and localized mode patterns in 2D aperiodic structures, specifically focusing on the engineering of novel light sources, colorimetric biosensors and nonlinear elements for multi-wavelength generation.

A photonic quasicrystal lasers has been recently demonstrated by Notomi and co-workers [196]. In their work, they fabricated Penrose lattices of 150 nm-deep holes in a 1 μm-thick SiO_2 layer on a Si substrate by electron-beam lithography and reactive ion etching. Subsequently, they evaporated a 300 nm-thick active material (DCM-doped Alq_3) layer on the patterned SiO_2 to form a quasiperiodic laser cavity (see Fig. 26). When the samples were optically pumped by a pulsed nitrogen laser at 337 nm pump wavelength, they have observed coherent lasing action above a characteristic pumping threshold ($100\,nJ/mm^2$). This laser action resulted from the optical feedback induced by the quasiperiodicity of the structures, exhibiting a variety of 10-fold-symmetric lasing patterns associated to the *extended critical modes* of the structure. The properties of these lasing modes, including their reciprocal lattice representations and their dependence on the geometrical characteristics of the Penrose lattice, were all explained by diffraction effects induced by the quasiperiodicity. The results of this study show that lasing action due to standing waves coherently extended over the surface of bulk quasicrystals is possible, in contrast to the lasing behavior of traditional photonic crystals lasers, driven by defect-localized states. These results open the way to the engineering of various lasing states and conditions, considering that the wide variety of the reciprocal lattices of quasicrystals can encode an arbitrary order of rotational symmetry and density of spatial frequencies.

Very recently, Yang and co-workers demonstrated laser action from multiple localized modes in deterministic ape-

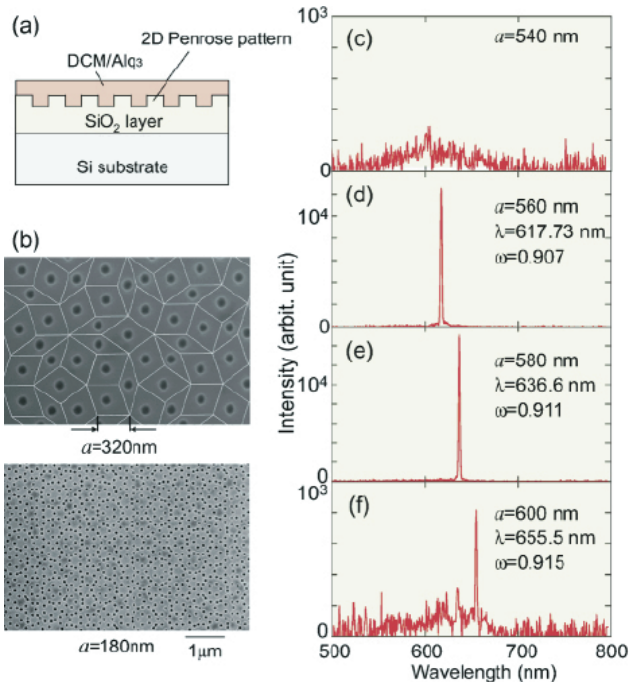

Figure 26 (online color at: www.lpr-journal.org) (a) Schematic view of photonic quasicrystal laser; (b) scanning electron micrographs; (c–f) emission spectra of samples with $a = 540, 560, 580, 600$ nm. From [196].

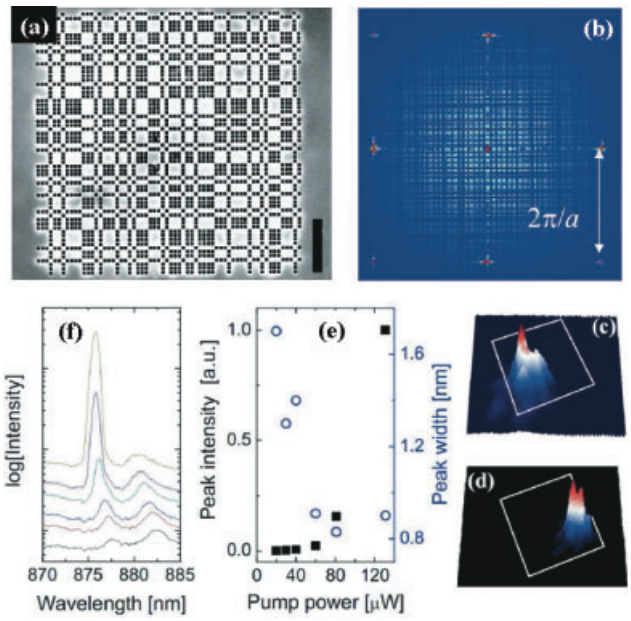

Figure 27 (online color at: www.lpr-journal.org) First demonstration of laser action from pseudo-random DANS in GaAs multi quantum wells. (a) SEM picture of the nanofabricated aperiodic membrane; (b) corresponding Fourier and (c–d) experimentally measured spatial profiles of localized lasing modes and (e–f) lasing characteristics. After [79].

riodic structures with Rudin-Shapiro (RS) pseudo-random morphologies [79] (Fig. 27). As discussed in Sect. 2, RS structures, unlike quasi-periodic systems with discrete Bragg peaks, feature a large density of spatial frequency components which form nearly-continuous bands. As the system size increases, the spectrum approaches the continuous Fourier spectrum of white-noise random processes. These pseudo-random systems are therefore ideally suited to solve the major limitation to device applications of traditional random lasers, namely the lack of control and reproducibility of their lasing modes. Yang and collaborators proposed to solve this problem by engineering lasing modes in deterministic structures with pseudo-random aperiodic order. They fabricated a free-standing GaAs active membrane with an array of air holes arranged in a two-dimensional RS sequence and found that pseudo-random RS arrays of air holes can support spatially localized optical resonances at well-reproducible frequency locations that exhibit clear lasing behavior in the presence of gain.

The air holes were fabricated with a square shape with the side length $d = 330$ nm and an edge-to-edge separation between adjacent holes of 50 nm. The total size of pattern was 25 μm × 25 μm, containing 2048 air holes.

The pump spot, about 2 μm wide, was moved across the sample to excite localized modes at different positions. A numerical study (based on 3D-FDTD calculations) of the resonances performed on passive systems and the direct optical imaging of lasing modes in the active structures enabled the authors to interpret the observed lasing behavior in terms of distinctive localized resonances in the membrane-type RS structures. The reproducibility of these lasing modes, and their robustness against fabrication imperfections, were proved by fabricating and testing three identical RS patterns on the same wafer. The nanofabricated pseudo-random lasers introduced by Yang et al. provide a novel approach, alternative to traditional random media and photonic crystals, for the engineering of multi-frequency coherent light sources and complex cavities amenable to predictive theories and device integration.

The light scattering and localization properties of aperiodic photonic structures may also provide new exciting opportunities for the design of functional elements for bio-chemical sensing applications [60, 61, 154]. In current biosensing technology, 2D periodic lattices, (i. e. 2D optical gratings) provide a well-established approach for biochemical colorimetric detection, which can yield label-free sensing of various molecular analytes and protein dynamics. Standard periodic grating biosensors provide a distinct change either in the intensity of diffracted light or in the frequency of optical resonances in response to changes in the refractive index of the surrounding environment.

The physical mechanism at the base of these optical signatures is the well-known phenomenon of Bragg scattering. While this process provides frequency selective responses that are useful for colorimetric detection, the ability of light waves to interact with adsorbed or chemically bound analytes present on the surface of these sensors is intrinsically limited. In fact, in the small perturbation theory of light scattering from rough surfaces [197], Bragg scattering already appears as a first-order contribution to the complete solu-

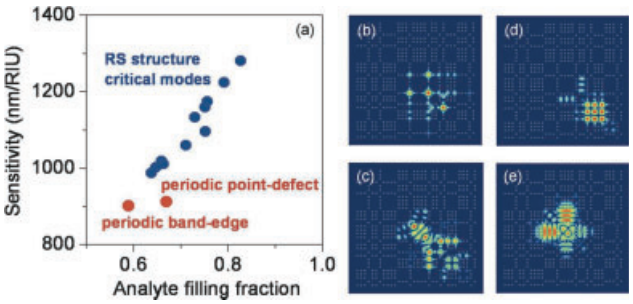

Figure 28 (online color at: www.lpr-journal.org) Calculated sensitivities of the critical modes of the Rudin-Shapiro structure (blue circles) as well as the air band-edge mode and a point-defect monopole mode (red circles) of the periodic PhC as a function of the filling fraction of the mode field energy in the host medium. (b–e) Typical intensity distributions of the high-Q quasi-localized critical modes. Adapted from [146, 154].

tion. Scattered photons easily escape from a periodic surface within well-defined spectral bands and without prolonged interaction with the sensing layer. Development of optical bio(chemical) sensing platforms calls for the design of scattering elements that simultaneously provide high sensitivity to the environmental changes and high spectral resolution, as both factors contribute to the improvement on the sensor detection limit [198].

Detector sensitivity is conventionally defined as the magnitude of the wavelength shift induced by the change of the ambient refractive index $S = \Delta\lambda/\Delta n_h$ (measured in nm/RIU), and can be improved by enhancing the light-matter interaction. In turn, the resolution in measuring wavelength shifts inversely depends on the linewidth of the resonant mode supported by the structure. It has been shown that quasi-localized critical modes of aperiodic photonic structures can simultaneously feature high quality factors and high field intensity distributions over large sensing areas. A combination of these factors results in the improved sensitivity of aperiodic-order-based sensors over their periodic PhC counterparts based either on localized point-defect or extended band-edge modes [154]. This is illustrated in Fig. 28a, where the sensitivity values of quasi-localized critical modes of the Rudin-Shapiro structure are compared to those of point-defect and band-edge modes of the periodic square-lattice PhC. The sensitivity is plotted as a function of the analyte filling fraction, i. e., the fraction of the optical mode energy that overlaps with the analyte [154, 198]:

$$f_a = \frac{\int_{analyte} \varepsilon_a |E(\vec{r})|^2 dV}{\int \varepsilon(\vec{r}) |E(\vec{r})|^2 dV}, \quad 0 \leqslant f_a \leqslant 1, \qquad (1)$$

and the increased overlap of the high-intensity portion of the modal field with the analyte is clearly shown to improve the sensitivity of the device. Typical near-field intensity portraits of four of the high-Q critical modes supported by the Rudin-Shapiro structure are plotted in Fig. 28b–e and feature characteristic quasi-localized intensity fluctuations [146, 154, 155].

A novel approach to label-free optical biosensing has recently been developed by Lee and collaborators based on micro-spectroscopy and spatial correlation imaging of structural color patterns obtained by white light illumination of nanoscale deterministic aperiodic surfaces [61]. In contrast to traditional photonic gratings or photonic crystal sensors (which efficiently trap light in small-volume defect states), aperiodic scattering sensors sustain distinctive resonances localized over larger surface areas. In particular, nanoscale aperiodic structures possess a dense spectrum of critical modes, which result in efficient photon trapping and surface interactions through higher-order multiple scattering processes thereby enhancing the sensitivity to refractive index changes. The complex spatial patterns of critical modes in these structures offer the potential to engineer structural color sensing with spatially localized patterns at multiple wavelengths, which have been called *colorimetric fingerprints* (shown in Fig. 29).

The proposed approach is intrinsically more sensitive to local refractive index modifications compared to traditional ones due to the enhancement of small phase variations, which is typical of the multiple light scattering regime.

Multiple light scattering from nano-patterned deterministic aperiodic surfaces, which occurs over a broad spectral-angular range, leads to the formation of colorimetric fingerprints [60], in their near and far-field zones, which can be captured with conventional dark-field microscopy [60]. These colorimetric fingerprints have been used as transduction signals in a novel type of highly sensitive label-free multiplexed sensors [60, 61]. In particular, both the peak wavelength shifts of the scattered radiation as well as the environment-dependent spatial structure of the colorimetric fingerprints of aperiodic surfaces have already been utilized to detect the presence of nanoscale protein layers [61] (Fig. 30). Lee and collaborators recently proposed to quantify the spatial modifications of the structural color fingerprints induced by small refractive index variations using image autocorrelation analysis performed on scattered radiation (Fig. 30b,c). By engineering the intensity of backscattered radiation from aperiodic surfaces, the refractive index changes induced by the analytes can be detected by shifts in the scattering intensity spectra [60, 61]. Combining Electron Beam Lithography (EBL), dark-field scattering microspectroscopy, autocorrelation analysis and rigorous multiple scattering calculations based on the Generalized Mie Theory (GMT) [199], S. Lee and collaborators have engineered aperiodic arrays of Chromium (Cr) nano-particles on quartz substrates, and showed that the information encoded in *both* spectral and spatial distributions of structural colors can be simultaneously utilized. The potential of the proposed approach for rapid, label-free detection of biomolecular analytes in the visible spectral range was experimentally demonstrated by showing a distinct variation in the spectral and spatial colorimetric fingerprints in response to monolayer increments of protein layers sequentially deposited on the surface of aperiodic arrays of nanoparticles [61].

The unique properties of Fourier spectra of aperiodic structures, which can be designed with any combination of Bragg peaks (wave vectors), have also been successfully

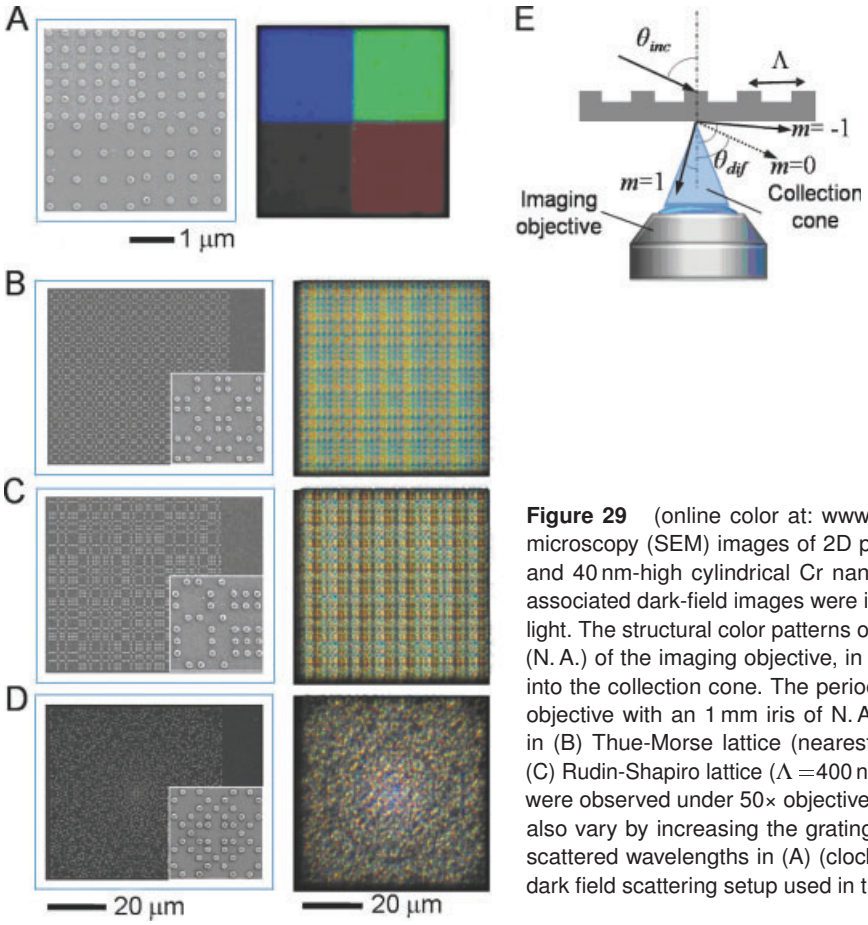

Figure 29 (online color at: www.lpr-journal.org) (A–D) Scanning electron microscopy (SEM) images of 2D periodic and aperiodic arrays of 100-radius and 40 nm-high cylindrical Cr nano-particles on a quartz substrate and the associated dark-field images were illuminated at a grazing incidence with white light. The structural color patterns of the images vary by the numerical aperture (N. A.) of the imaging objective, in which different diffractive order is included into the collection cone. The periodic arrays in (A) were observed under 10× objective with an 1 mm iris of N. A. reduced to 0.1 and the aperiodic arrays in (B) Thue-Morse lattice (nearest center-to-center separation $\Lambda = 400$ nm); (C) Rudin-Shapiro lattice ($\Lambda = 400$ nm); (D) Gaussian prime lattice ($\Lambda = 300$ nm), were observed under 50× objective with N. A. 0.5. The structure color patterns also vary by increasing the grating period with a progressive red-shift of the scattered wavelengths in (A) (clockwise from top-left) (E) A schematic of the dark field scattering setup used in the measurements. From [61].

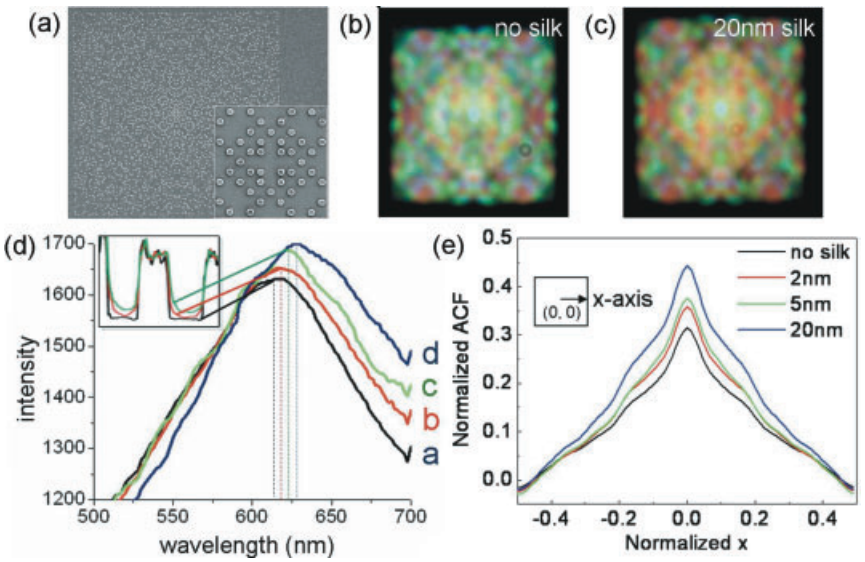

Figure 30 (online color at: www.lpr-journal.org) SEM image of 2D Gaussian Prime aperiodic array of 100 nm-radius and 40 nm-high cylindrical Cr nano-particles on a quartz substrate (a) and the array dark-field images with (c) and without (b) a thin layer of silk polymer on the array surface. The sensitivity to different thicknesses of silk monolayers is quantified by the spectral shift of the scattered radiation peaks (d) and by monitoring the spatial changes of patterns quantified by the variances of their spectral correlation functions (ACFs) (e). From [61].

exploited in the engineering of nonlinear photonic structures for multiple-wavelength or broadband optical frequency conversion. Such structures make use of the three-wave mixing process when two incoming waves $(\omega_1, \vec{k}_1)$ and $(\omega_2, \vec{k}_2)$ can interact via the medium second-order nonlinear susceptibility tensor $\chi^{(2)}$ to produce an outgoing wave $(\omega_3, \vec{k}_3)$ with the frequency $\omega_3 = \omega_1 + \omega_2$ and the wave vector mismatch $\Delta\vec{k} = \vec{k}_1 + \vec{k}_2 - \vec{k}_3$ [200]. The efficiency of the frequency conversion process is proportional to the value of the Fourier transform of the relevant component of $\chi^{(2)}$ at $\Delta\vec{k}$, and thus is maximized if the reciprocal lattice of $\chi^{(2)}$ features a Bragg peak corresponding to the mismatch vector $\Delta\vec{k}$. This approach, known as the "quasi-phase matching" [200] can be implemented in the medium with periodic modulation of

the sign of the nonlinear susceptibility with the period corresponding to the phase mismatch. However, periodically-modulated nonlinear structures are mostly limited to the phase-matching of a single optical process, while simultaneous phase-matching of multiple processes is important for a variety of applications including generation of multicolor optical solitons and creation of multi-frequency optical and THz sources. Multiple-wavelength frequency conversion in nonlinear periodic lattices can only be achieved by using reciprocal wave vectors that are integral multiples of the primary one, thus severely limiting the number of different wavelengths for which the quasi-phase matching can be realized.

To the contrary, nonlinear aperiodic structures provide a large number of reciprocal vectors, which make possible multiple-wavelength frequency conversion [201]. Multiple-wavelength second and third harmonic generation has been successfully demonstrated, both theoretically and experimentally, in a variety of 1D [202–206] and 2D [207–212] aperiodic lattices. An example of the effective generation of red, green and blue light by frequency doubling at three wavelengths in 2D decagonal $LiNbO_3$ nonlinear photonic structure is demonstrated in Fig. 31a–c [207]. The reciprocal space of the decagonal structure shown in Fig. 31a features tenfold rotational symmetry and four concentric sets of most strongly pronounced Bragg peaks. The three reciprocal vectors (labeled in the symbolic five-dimensional vector notation) that provide phase matching of the frequency doubling process at three different wavelengths are shown in Fig. 31b, and the conversion efficiency for the generation of the red, green and blue coherent radiation is plotted in Fig. 31c as a function of the input power of the fundamental beam.

Another example of an aperiodic structure, which is engineered to provide a broadband second harmonic generation, is shown in Fig. 31d. This structure is obtained by arranging randomly-oriented identical unit cells (squares or other polygons) in a 2D periodic lattice. The reciprocal space of this structure features both sharp Bragg peaks reflecting the square-lattice arrangement of unit cells and broad concentric rings related to their random rotations (Fig. 31e). Continuously-distributed reciprocal vectors within the rings provide the phase-matching conditions for the broadband second harmonic generation with the spectrum of the generated light almost covering the whole visible range (Fig. 31f). In general, aperiodic nonlinear structures can be designed to feature any set of wavevectors required

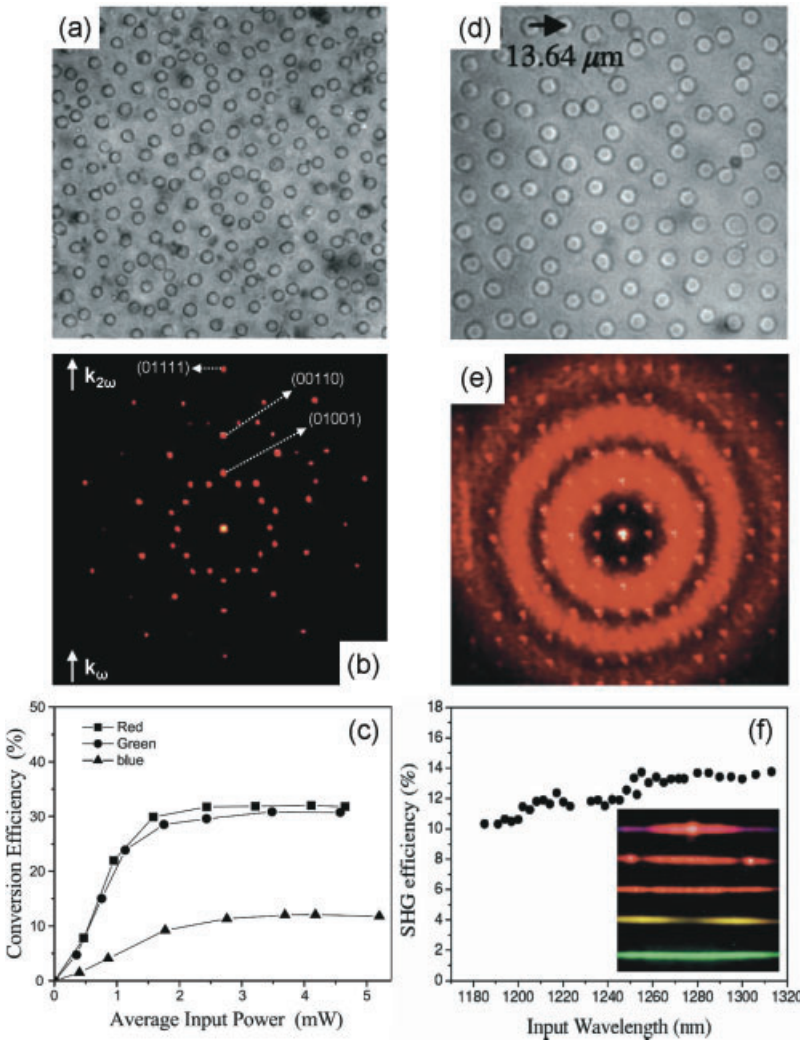

Figure 31 (online color at: www.lpr-journal.org) Multiple-wavelength second harmonic generation in nonlinear aperiodic structures. Decagonal quasiperiodic lattice (a) features a number of sharp Bragg peaks in its reciprocal spectrum (b), and provides phase-matching conditions for several wave-mixing processes (c) (adapted with permission from [207]). Short-range-ordered structure (d) features broad continuous rings in its Fourier space (e), making possible broadband second harmonic generation with nearly constant conversion efficiency (f) (Adapted with permission from [208]).

to provide the condition for quasi-phase matching of several wave mixing processes [206, 210, 211]. However, this is only possible at the costs of lower conversion efficiency and larger structure sizes.

4. Complex Aperiodic Nanoplasmonics (CAN)

Nanoplasmonics is the science of collective oscillations of metal conduction electrons, which occur at metal-dielectric interfaces, metal nanoparticles, or nanoparticles aggregates [213].

These oscillations, called surface plasmons, are mostly electronic oscillations and therefore can be localized on the nanoscale. The nanoscale localization of plasmonic resonances creates high intensity electromagnetic fields called "hot spots", or "giant fields", which are the basis of numerous effects and applications to nanoplasmonics and nanophotonics. Several approaches have been proposed to enhance the field localization and intensity on the nanoscale, including bow-tie nano-antennas, periodic arrays of nanoparticles or nano-holes, and photonic-plasmonic band-gap systems [214–219]. However, today the best approaches to generate strongly enhanced electromagnetic fields rely on "roughening" of metal surfaces by etching or by colloidal synthesis of nanoparticles [220]. This often results in random aggregates of metal nanoparticles or surface corrugations statistically described by fractal morphologies that can lead to a dramatic "structural enhancement" of the local electromagnetic fields sufficient for observing single molecules by Surface Enhanced Raman Spectroscopy (SERS) [221, 222]. Differently from the familiar shapes of Euclidean geometry, such as squares, circles, etc, fractal objects are characterized by a non-integer dimensionality (i. e., *Hausdorff dimension*), which is always smaller than the dimensionality of the space in which fractals are embedded. The fractal dimensionality describes their distinctive scale-invariant symmetry, which is also referred to as *self-similarity*, meaning that the spatial structures observed on one length scale appears identical when observed at successively smaller scales [223]. The physical principles, computational methods, as well as the engineering aspects of *fractal electrodynamics* for the design and implementation of multiband antenna elements and arrays are beautifully reviewed in [224].

4.1. Nanoplasmonics of fractal structures

The optical excitations of small-particle statistical fractal aggregates have been abundantly investigated by Shalaev in relation to surface-enhanced optical nonlinearities [225, 226]. Specific scaling laws and close-form analytical results for enhanced Raman and Rayleigh scattering, four-wave mixing, and Kerr nonlinearities along with important figures of merits are obtained within the quasi-static dipole approximation and beautifully discussed in [225, 226].

Plasmonic nanostructures arranged according to deterministic fractals (i. e., Sierpinski carpet) have also been recently studied in a computational work that demonstrates their sub-diffraction focusing properties [227]. A recent design paper has additionally investigated the potential of Ag nanocylinders arranged in a Pascal triangle for the generation of controllable local field enhancement [228].

Stockman [229] developed a comprehensive theory of the statistical and localization properties of dipole eigenmodes (plasmons) of fractal and random non-fractal clusters. Because of scale-invariance symmetry, the eigenmodes of fractals cannot be extended running waves as for translational invariant (i. e., periodic) structures. On the opposite, fractal clusters of small metallic particles support a variety of dipolar eigenmodes distributed over wide spectral ranges. The vibration eigenmodes of fractals, generally known as *fractons* [91], tend to be spatially localized and are characterized by strong fluctuations of their intensity profiles (see Fig. 32). Differently from the case of random systems, fractons have very inhomogeneous localization patterns and very different coherence length can coexist at the same frequency. As shown by Stockman [229], the plasmon eigenmodes of metal-dielectric fractal structures can even result in a distinctive *chaotic behavior* in the vicinity of the plasmon resonance of individual particles. This chaotic behavior consists of rapid changes of the phase of the amplitude correlation in spatial and frequency domains, and cannot be observed in random clusters with non-fractal geometry [229].

The large fluctuations of the local fields characteristic of self-similar (fractal) structures leads to an efficient transfer of excitations towards progressively smaller length scales of the aggregates where the electromagnetic enhancement reaches the 10^{12} level needed to observe single molecule SERS [222, 230, 231]. Statistical fractal aggregates and rough metal surfaces led to successful applications in single molecule spectroscopy [230], but they lack reproducibility, the hot-spots locations and frequency spectra cannot be known a priori, and they cannot be reliably fabricated using nanolithography approaches. It is in fact important to realize that any physical realization of a self-similar fractal process is necessarily limited by a cut-off length scale associated to the specific fabrication technology, usually electron beam nanolithography (EBL) for plasmonic nanostructures. Therefore, the fascinating physical properties originating from the distinctive scale-invariance symmetry of mathematical fractal objects cannot be entirely displayed by experimental fractal structures, or *pre-fractals*. Moreover, fractal objects obey a power-law scaling of their mass density-density correlation function $\langle \rho(r)\rho(r+R)\rangle \propto R^{D-d}$, where D is the fractal dimension and d the Euclidean dimension of the embedding space (i. e., $D<d$). This defining property constraints the mass density $\rho(r)$ of any fractal object to quickly "rarefy" when increasing its size R, therefore decreasing the density of localized fracton modes [232]. For this reason, fractals cannot display the high density of spatial frequencies associated to the continuous Fourier transforms of pseudo-random structures such as the Rudin-Shapiro sequence. A direct consequence of the power-law density scaling of fractal

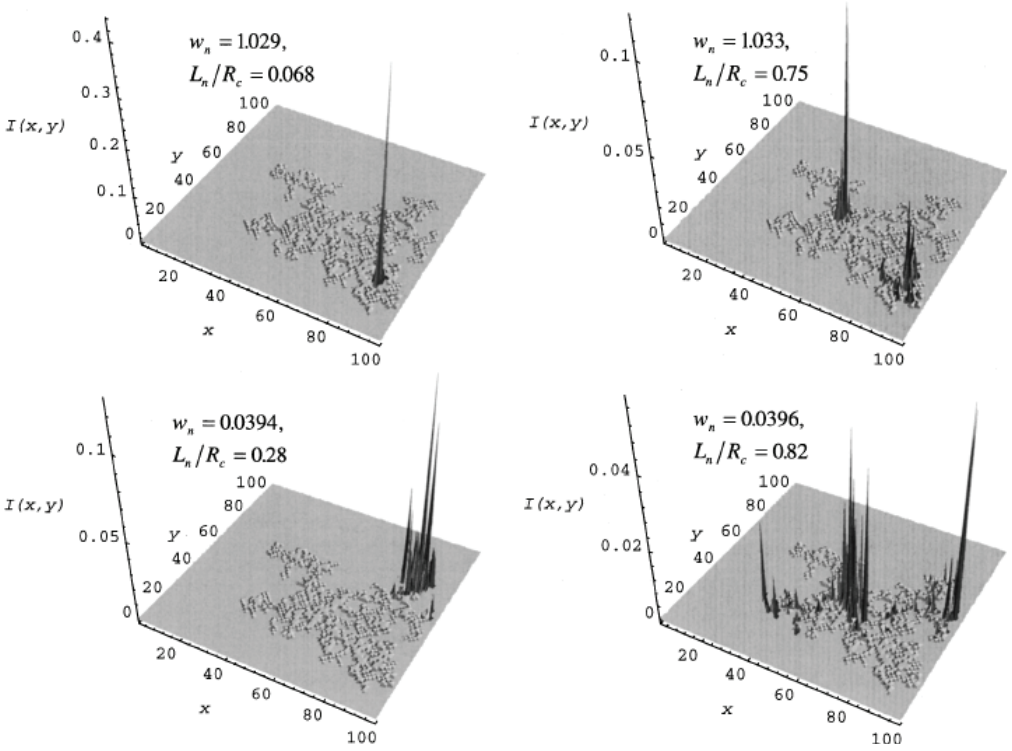

Figure 32 Spatial distribution of the local-field intensities for external excitation of an individual *N*51500 CCA cluster for the values of the frequency parameter X and polarizations of the exciting radiation shown. From [229].

objects is that only a small fraction of the total area of fractal aggregates of metal nanoparticles is covered by localized electromagnetic hot spots. This limits the technological potential of plasmonic fractals for the engineering of planar optical devices such as light-emitters, photo-detectors, optical biosensors that require strong enhancements of electromagnetic fields over large chip areas. On the contrary, engineering aperiodic resonant structures with plasmonic nanoparticles arranged in deterministic patterns with a large density of spatial frequencies could overcome the limitations of both fractals and random media. By generalizing aperiodic substitutions in two spatial dimensions, deterministic aperiodic arrays of metallic nanoparticles with pure-point, continuous and singular continuous diffraction spectra have been recently demonstrated by Dal Negro and collaborators [62, 80] in the context of nanoplasmonics scattering and field localization (Fig. 33). These structures are created by mathematical rules amenable to predictive theories, and provide a novel engineering approach for the control of hot-spot positions, radiation patterns and localized field states in photonic-plasmonic nanoparticle systems between quasiperiodicity and pseudo-randomness.

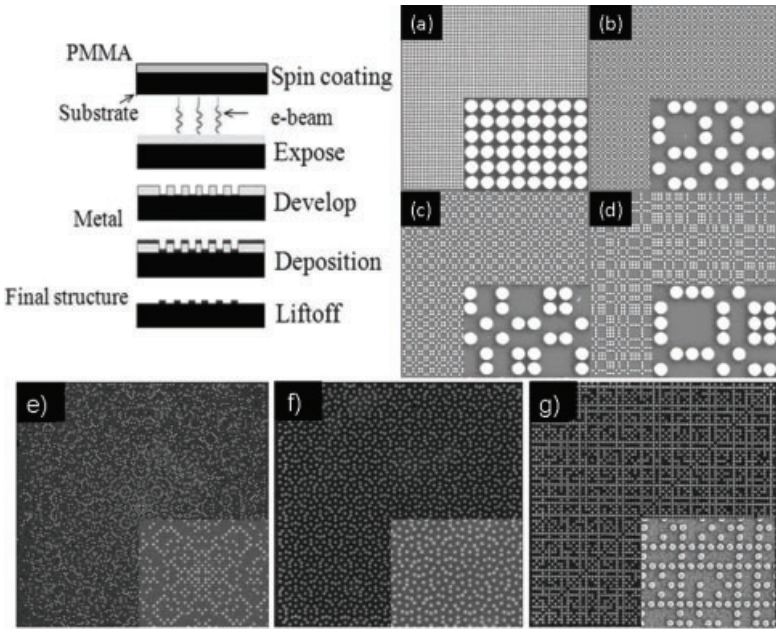

Figure 33 Schematics of the nanofabrication (EBL) process flow developed to fabricate various DANS using metallic nanoparticles and corresponding SEM pictures of arrays of Au nanodisks (200 nm diameter, 20 nm separation, 30 nm thickness) with different deterministic aperiodic geometries: (a) square lattice; (b) Fibonacci array; (c) Thue-Morse; (d) Rudin-Shapiro; (e) Gaussian prime; (f) Penrose lattice; (g) co-prime array.

4.2. Aperiodic nanostructures beyond fractals

New scenarios can emerge by combining deterministic aperiodic geometries with resonant metallic nanostructures supporting surface oscillations of conduction electrons localized on the nanoscale, known as Localized Surface Plasmons (LSPs).

Analogously to the coupling of atomic and molecular orbitals in solid state and quantum chemistry, individual LSPs can strongly couple by near-field quasi-static interactions and by far-field multipolar radiative effects (known in this context as diffractive coupling), giving rise to localized photonic modes in artificial nanoparticle arrays designed on templates with deterministic aperiodic order. The interplay between these two coupling regimes offers a tunable approach to engineer photonic-plasmonic resonances in complex aperiodic media with deterministic order.

The optical properties of surface plasmon-polaritons in localized quasi-crystal arrays of sub-wavelength nanoholes fabricated in metallic thin films have been the subject of intense research efforts in the last few years, leading to the demonstration of novel phenomena such as resonantly enhanced optical transmission, sub-wavelength imaging and super focusing effects [233–236].

Recently, Dal Negro and collaborators explored 1D and 2D deterministic aperiodic arrays of metal nanoparticle arrays as a novel approach to design broadband electromagnetic coupling and sub-wavelength plasmonic field enhancement for on-chip applications. In particular, they initially focused on the spectral, far-field and near-field optical properties of nanoparticle arrays generated according to symbolic substitutions such as Fibonacci, Thue-Morse, and Rudin-Shapiro structures characterized by multifractal and diffuse Fourier spectra [62, 80, 237–240].

This approach offers additional flexibility in the design of the Fourier space of plasmonic devices beyond the limitations of periodic and fractal systems. In particular, this design flexibility enables to better engineer the interplay between short-range quasi-static coupling (i. e., plasmon field localization at the nanoscale) and long-range radiative coupling (e. g., multiple scattering) over broad angular and frequency spectra.

Dal Negro and collaborators showed [62, 237] that the aperiodic sub-wavelength modulation of particle positions in metallic chains and arrays results in a hierarchy of gaps in their energy spectra, and in the formation of localized modes. The full dispersion diagrams of plasmon excitations in quasiperiodic and aperiodic metal nanoparticle arrays are calculated in [237, 240]. In addition, a characteristic power-law scaling in the localization degree of the eigenstates, measured by their participation ratio, was discovered [62], resulting in larger intensity enhancement effects with respect to the case of periodic plasmon arrays. Using accurate multiple scattering calculations (Generalized Mie Theory, T-matrix null-field method approach) the scattering and extinction efficiencies of periodic and deterministic aperiodic arrays of metal nanoparticles were compared [239] for different geometries and lattice parameters, establishing the importance of radiative coupling effects in the plasmonic response of deterministic aperiodic structures. A rigorous analysis was performed by Forestiere and co-workers [240] who developed a theory that enables the quantitative and predictive understanding of the plasmon gap positions, field enhanced states, scattering peaks of metallic quasi-periodic arrays of resonant nanoparticles in terms of the discontinuities of their Fourier spectra. This work extends the reach of the so-called gap-labeling theorem [64] to aperiodic nanoplasmonics.

The role of nanoparticle shape/size and the uniqueness of deterministic aperiodic arrays for the engineering of the spatial localization of plasmonic modes are discussed further in [59, 239, 240]. These works highlight the unique advantages offered by the controllable density of spatial frequencies in aperiodic Fourier space, and show that electromagnetic hot-spots with larger field enhancement values cover a *larger surface areas of aperiodic arrays with respect to periodic structures.*

Gopinath and collaborators have fabricated using Electron Beam Lithography (EBL) 2D arrays of Au nano-disks in various deterministic aperiodic geometries [80], and they demonstrated broad plasmonic resonances spanning across the entire visible spectrum (Fig. 34). It was also discovered in [80] that far-field radiative coupling in deterministic aperiodic structures leads to the formation of distinctive photonic resonances with spatially inhomogeneous profiles, similarly to the case of colorimetric fingerprints of aperiodic surfaces discussed in Sect. 3.4. In addition, the interplay between quasi-static plasmonic localization and photonic localization of morphology-dependent optical modes associated to radiative long-range coupling in aperiodic arrays has been re-

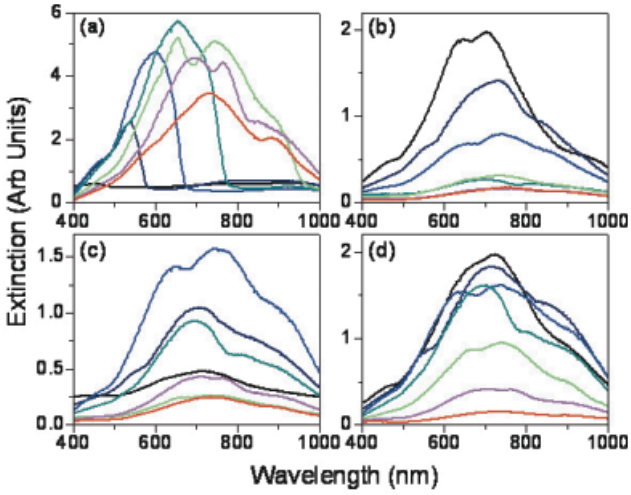

Figure 34 (online color at: www.lpr-journal.org) Measured extinction as a function of the wavelength for 2-D arrays of Au nanoparticles with radii of 100 nm: (a) periodic, (b) Fibonacci, (c) Thue-Morse, and (d) Rudin-Shapiro, and varied minimum separation distances: 50 nm (black), 100 nm (navy), 150 nm (blue), 200 nm (dark cyan), 300 nm (green), 400 nm (magenta) and 500 nm (red). The varying intensity plateaus at around 400 nm arise from different filling fractions of the arrays. Taking into account the collection angle of the objective (40.5°) and the cone of total internal reflection (39.0°), we estimate that we collect 17% of the scattered light. From [80].

cently exploited by the Dal Negro group for the engineering of substrates with large values ($\approx 10^7$–10^8) of reproducible SERS enhancement [241, 242]. Engineered SERS substrates with cylindrical and triangular Au nanoparticles of different diameters, separations and aperiodic morphologies were fabricated by EBL and experimentally characterized by molecular SERS spectroscopy. Large, morphology-dependent values of average SERS enhancement (i. e., averaged over the laser excitation area) in DANS arrays with 25 nm minimum separations [242] were reported (Fig. 35). The fundamental role of long-range radiative coupling in the formation of local hot-spots was discussed [242], along with engineering scaling rules for DANS with different degrees of spectral complexity. Larger values of SERS enhancement were recently obtained by Gopinath and collaborators using a combination of EBL and in-situ chemical reduction giving rise to multi-scale aperiodic structures referred to as "plasmonic nano-galaxies" [241]. Previous studies on the far-field and near-field optical behavior of 2D Fibonacci lattices fabricated by EBL demonstrated the presence of strongly localized plasmon modes whose exact location can be accurately predicted from purely structural considerations [238]. In particular, by performing near-field optical measurements in collection mode and 3D FDTD simulations, Dallapiccola at al [238] showed that plasmonic coupling in a Fibonacci lattice results in deterministic quasi-periodic sub-lattices of localized plasmon modes which follow a Fibonacci sequence. In addition, stronger field enhancement values were experimentally observed in Fibonacci compared to periodic nanoparticle arrays [238], unveiling the potential of quasiperiodic gold nanoparticle arrays for the engineering of novel nanoplasmonic devices. More recently, by engineering the scattering properties of quasiperiodic Fibonacci Au nanoparticle arrays, Gopinath and collaborators [243] fabricated the first plasmonic-coupled quasiperiodic light emitting device using Erbium doping of silicon nitride. In this work [243], by engineering quasi-periodic structures with near-infrared spectral resonances, they demonstrated a 3.6 times enhancement of the photoluminescence intensity of Erbium atoms. In addition, due to the modification of the local density of optical states (LDOS) at the 1.54 μm emission wavelength, a substantial enhancement of the Er emission rate was also observed [243] (see Fig. 36).

In the context of nanoplasmonics, aperiodic arrays of Au nanoparticles with diffuse, circularly symmetric Fourier space were recently investigated by Trevino et al [172]. By studying light scattering from the three main types of Vogel's spirals fabricated by electron-beam lithography on quartz substrates (Figs. 23 and 37 a,c), Trevino et al. showed that plasmonic spirals support distinctive structural resonances with circular symmetry carrying orbital angular momentum (Fig. 37b,d). Moreover, due to the distinctive circular symmetry of the Fourier space, polarization-insensitive planar light diffraction was demonstrated in aperiodic spirals across a broad spectral range, providing a novel strategy for the engineering of diffractive elements that can enhance light-matter coupling on planar surfaces over a broad range of frequencies [172].

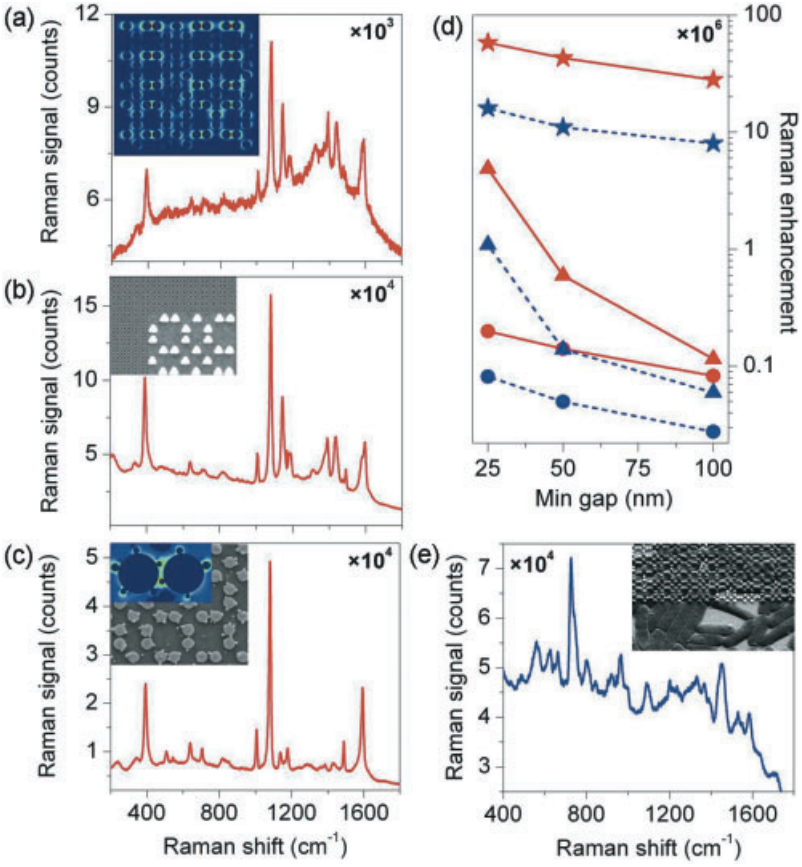

Figure 35 (online color at: www.lpr-journal.org) SERS platforms based on Fibonacci plasmonic nanoparticle arrays. Experimental SERS spectra of pMA on lithographically defined arrays of (a) nanodisks, (b) nanotriangles, and (c) nanodisks decorated by small Au spheres (termed plasmonic nanogalaxy). Au particles are 200 nm in size and are separated by minimum interparticle gaps of 25 nm. The insets show an in-plane electric field pattern in the nanodisk array at the pump wavelength (a), an SEM image of a nanotriangles array (b) and an SEM image of a nanogalaxy array together with a field distribution around one of the electromagnetic hot spots in the structure (c). (d) The scaling behavior of Raman enhancement factor calculated from experimental data in periodic (dash blue) and Fibonacci (solid red) nanoparticle arrays. Circles, triangles and stars correspond to the nanodisk, nanotriangles and nanogalaxy arrays, respectively. (e) Experimental stokes SERS spectrum of E-coli bacteria on the Fibonacci Au nanogalaxy array with 25 nm min interparticle gaps. The inset shows the SEM image of bacteria on the SERS chip. Adapted from [241, 242].

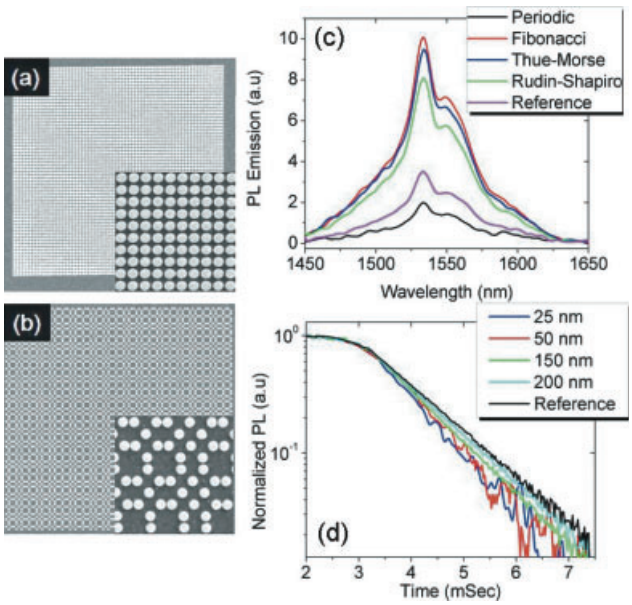

Figure 36 (online color at: www.lpr-journal.org) Demonstration of light emission enhancement from Erbium atoms coupled to quasi-periodic plasmonic arrays of Au nanoparticles (200 nm diameters). SEMs pictures of periodic (a) and quasiperiodic Fibonacci (b) Au nanoparticle arrays fabricated on light emitting Er:SiNx substrates of 80 nm thickness. (c) PL spectra excited at 488 nm through periodic and aperiodic nanoparticle arrays with 50 nm min interparticle separations; (d) PL time decay of Er atoms through unpatterned substrate (black) and Fibonacci arrays with varying interparticle separations indicated in the legend. From [243].

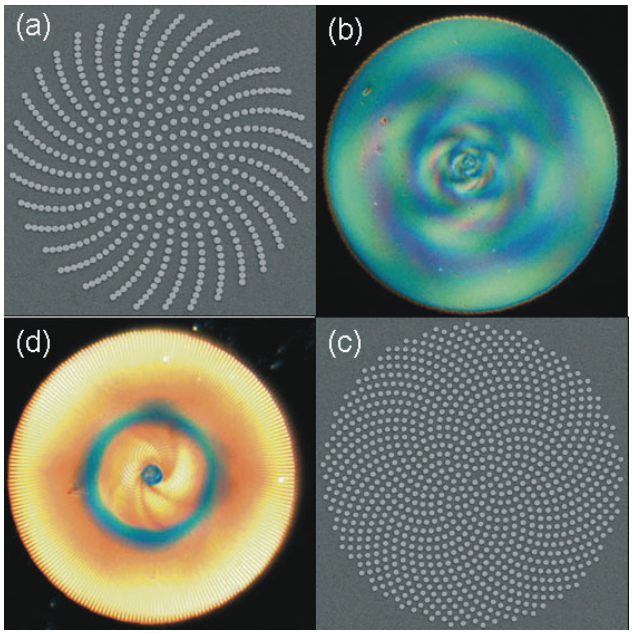

Figure 37 (online color at: www.lpr-journal.org) SEM micrographs of a Au nanoparticle aperiodic α_2-spiral (a) and golden angle (c) spiral arrays. The spirals contain approximately 1,000 particles with a diameter of 200 nm. Dark-field microscopy images of plasmonic golden angle (b) and α_2-spiral (d) spirals on quartz substrates. Adapted from [172].

The importance of non-crystallographic rotational symmetries in quasiperiodic hole arrays for enhancing the absorption of organic solar cells was recently demonstrated experimentally by Ostfeld et al [244]. In this recent work, spectrally broad, polarization-insensitive absorption enhancement of a 24 nm-thick organic layer spin-cast on quasiperiodic hole arrays (fabricated on silver films by Focused Ion Beam) was measured (with 600% peak enhancement at 700 nm) over that of a reference layer deposited on a flat film. Moreover, in correspondence of the absorption enhancement, a significant fluorescence intensity enhancement (up to a factor of 2) was observed as a result of the increased excitation rate in the thin absorbing film [244]. These recent results unveil the potential of engineered nanoplasmonic structures with circularly symmetric Fourier space to enhance the efficiency of thin-film photovoltaic cells. In this section, we have discussed how DANS technology could provide an alternative route for the engineering of novel nanoplasmonic devices with distinctive optical resonances and field localization on the nanoscale. Furthermore, a particularly important advantage of this technological platform is the possibility to enhance simultaneously optical cross sections and nanoscale field intensities across broad frequency spectra and over large device areas. A discussion of these specific aspects will be presented in the next section.

4.3. Broadband enhancement of optical cross sections

An important requirement for device applications of nanoplasmonics, such as solar cells, optical biosensors, nonlinear elements and broadband light sources is the ability to engineer strong enhancement values of optical cross sections and electromagnetic fields over a broad frequency range. Resonant enhancement of nanoscale plasmon fields in *periodic arrays of metal nanoparticles* can be achieved at specific wavelengths when the evanescent diffraction orders spectrally overlap the broad LSP resonances, resulting in strong Fano-type coupling and enhancement of optical cross sections over a relatively narrow frequency range. Under this condition, known as *Rayleigh cut off condition* for periodic gratings, an incoming plane wave at normal incidence is diffracted in the plane of the grating (i. e., at 90 degree angle) and efficiently couples to near-field plasmonic resonances enhancing the strength of local plasmonic fields. For a plane wave incident at an oblique angle θ_0 (in a medium of index n_0) and diffracted by a 1D periodic grating with period a, the Rayleigh cut-off condition yielding strongest plasmonic enhancement is given by:

$$\lambda = \frac{a}{m}(n \pm n_0 \sin\theta_0) \qquad (2)$$

By adjusting the angle of incidence, one can exactly control the wavelength of the strongest coupling to the LSP resonance. This effect has previously been shown to produce extremely narrow LSP resonances, and significant enhancements of the LSP near-fields by Fano-type coupling effects [245].

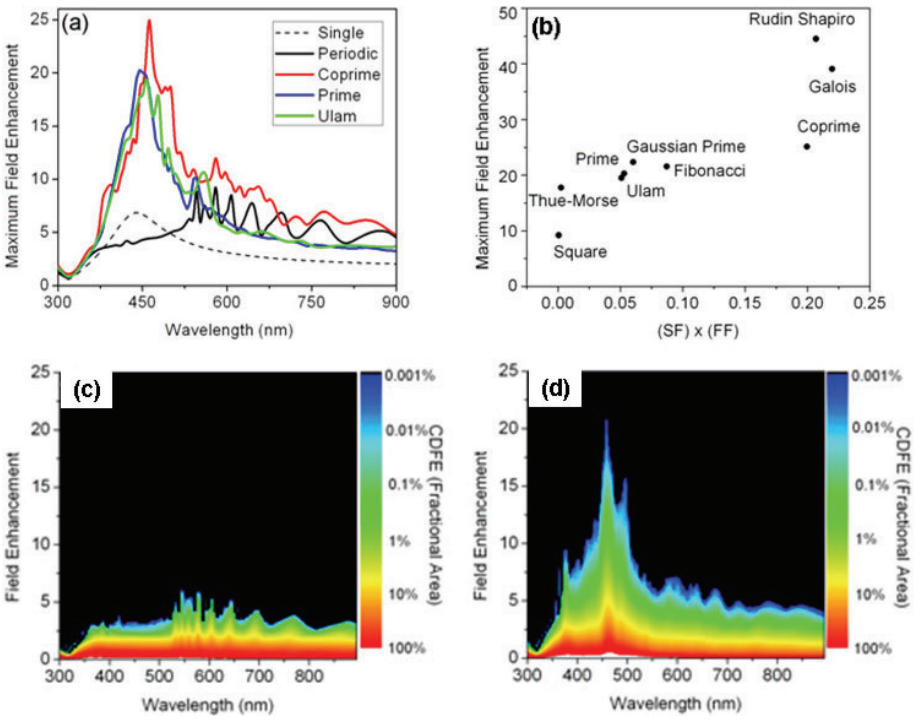

Figure 38 (online color at: www.lpr-journal.org) (a) Calculated spectral dependence of the plasmonic near-field enhancement in different DANS structures of Ag nanospheres with 100 nm diameter and 25 nm separation. (b) Maximum values of plasmonic field enhancement in arrays with different morphologies ranging from periodic to quasi-periodic and pseudo-random. Calculated Cumulative Distribution of Field Enhancement (CDFE) spectra for periodic (c) and RS arrays (d). The color-coded CDFE function measures the geometrical fraction of the arrays that is covered by plasmon fields larger than a fixed value indicated for each frequency by the left vertical axis. Adapted from [59].

The two main ingredients that determine the bandwidth and the strength (i. e., near-field enhancement) of the optical response of plasmonic structures are: a) the linewidth of the LSP near-field resonance, which is mostly broadened by the metallic character (i. e., losses) of nanoparticles coupled in the quasi-static regime; b) the availability of spatial frequencies matching the Rayleigh cut-off condition over the entire bandwidth of the LSP quasi-static response, which is normally very broad (i. e., 50–100 nm).

Deterministic aperiodic arrays of metal nanoparticles offer by construction a high density of spatial frequencies and are ideally suited to feed into multiple LSP resonances distributed across engineerable frequency bandwidths [80]. Moreover, the broadband plasmonic response of DANS can be obtained using arrays of identical particles, differently from random systems, where disorder in particles shapes and sizes is often present. We recall here that the geometry of DANS arrays is described by the spectral Fourier properties of their reciprocal space. This can be engineered to encode large fluctuations in the spatial arrangement of different clusters of identical particles (e. g., dimers, triplets and other local particle configurations, Fig. 39a) which strongly interact in the quasi-static sub-wavelength regime, broadening the overall plasmonic response of the system. The key aspect of aperiodic plasmon arrays is their *ability to further enhance the intensity of these plasmonic near-fields by diffractive effects at multiple wavelengths*, resulting in "multiple Fano-type coupling" for structures with progressively denser Fourier spectra. Moreover, the enhanced density of photonic states available in aperiodic systems results in stronger photonic-plasmonic Fano-type coupling effects compared to traditional periodic gratings (see Fig. 37). These concepts have been recently addressed quantitatively by Forestiere et al. who studied the plasmonic near-field localization and the far-field scattering properties of non-periodic arrays of Ag nanoparticles generated by prime number sequences in two spatial dimensions [59]. In this study, it was demonstrated that the engineering of dense arrays characterized by large values of *spectral flatness* in the Fourier space is necessary to achieve a high density of electromagnetic hot-spots distributed across broader frequency ranges and larger surface areas with respect to both periodic and quasi-periodic structures [59]. The varying degree of structural complexity of the different arrays was quantified by a parameter, called the spectral flatness (SF), associated to their Fourier spectra (see Fig. 38). The SF is a digital signal processing measure of how spectrally diffuse a signal is. In our case, the different arrays are considered as digitized spatial signals and the SF is calculated by dividing the geometric mean and the arithmetic mean of their power spectra, according to the definition [59]:

$$\mathrm{SF} = \frac{\sqrt[N]{\prod_{n=0}^{N-1} |\mathrm{DFT}[s(n)]|}}{\left(\frac{\sum_{n=0}^{N-1} |\mathrm{DFT}[s(n)]|}{N} \right)} \qquad (3)$$

where $s(n)$ is the value of the spatial signal (array) in bin n, N is the total number of bins in the array, DFT is the Discrete Fourier Transform, and $|\ |$ is the magnitude. For a signal with a completely flat power spectrum, the geometric mean will equal the arithmetic mean causing the SF to be equal to one. This indicates that there is equal power in every frequency band. If there are frequencies with zero power, the geometric mean will be zero so SF will also be zero indicating a band limited signal.

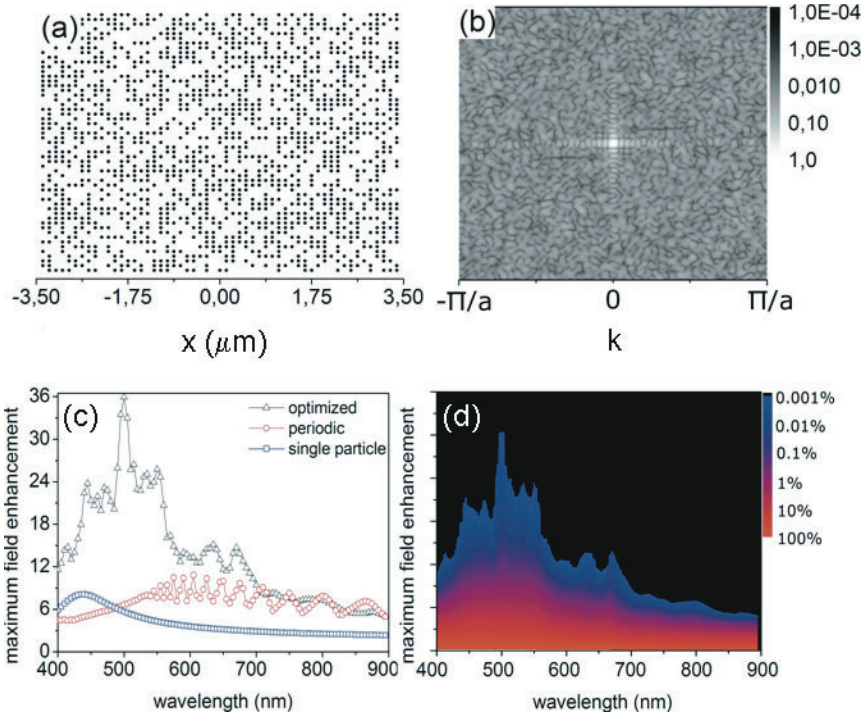

Figure 39 (online color at: www.lpr-journal.org) Geometry of the optimized silver nanoparticle array (a) and its Fourier Transform (b) (log scale). The resulting lattice is made up by 1506 nanoparticle, featuring a particle density of 34 μm^{-2}. In Fig. 1b $a = 125$ nm is the minimum center to center distance. The central peak and the cross in the middle of the Fourier space result from the square symmetry of finite size array. (c) Maximum field enhancement $|E|$ spectra of the optimized arrays (triangles) of silver nanoparticles, illuminated, at normal incidence, by a circularly polarized plane wave of unitary intensity, compared to the performances of periodic array (circles), in which all allowed position are filled by a particle, and with the single particle (squares). The color-map (d) shows the cumulative distribution function of the field enhancement (CDFE) (logarithmic scale) versus wavelength (x-axis) and field-enhancement (y-axis). Adapted from [246].

On a subsequent computational study (Fig. 39) [246], Forestiere et al. demonstrated the role and the importance of aperiodic particle geometries for broadband plasmonic near-field enhancement using an evolutionary computational technique known as "particle swarm" optimization algorithm. In their study, they aimed to find array geometries suitable to achieve high field enhancement values spanning across the 400 nm–900 nm spectral window when the structure was illuminated by a plane wave at normal incidence. Interestingly, the structures "selected" by the optimization algorithm turned out to be aperiodic arrays with almost ideal spectral flatness resulting in many closely packed particle clusters, similarly to the typical geometries of engineered DANS with continuous Fourier spectra [246]. These results demonstrate that significant field-enhancement effects in nanoplasmonics can be obtained *within a specified frequency bandwidth* by engineering deterministic aperiodic order with a large number of spatial frequencies (spectral flatness), enabling the simultaneous coupling of critically localized photonic modes and sub-wavelength plasmonic resonances at multiple frequencies. However, it is clear that aperiodic designs come at the additional cost of a larger system's size compared to narrow-band periodic structures, requiring application-driven engineering trade-offs between intensity enhancement, frequency spectra, and device dimensions in real space.

5. Electromagnetic design of aperiodic systems

The lack of translational invariance in aperiodic photonic structures makes impossible direct application of the analytical tools based on the concepts of the Brillouin zone and the Floquet-Bloch theorem, which are well-established in the design of conventional 2D and 3D periodic Bravais lattices [128, 178, 180, 247]. However, a number of semi-analytical and numerical techniques have been developed to calculate the dispersion diagrams, density of optical states and light transmission characteristics of aperiodic photonic structures. One approach is based on studying finite-size portions of infinite arrays, e. g., obtained by performing only a few iterations of the inflation rule used to define the aperiodic structures [80, 105, 111, 142, 146, 151, 154, 155, 239, 242] or by truncating the size of a quasiperiodic tiling obtained by the cut-and-projection method [135, 144, 150, 158, 165, 248]. Scaling analysis of the bandgap formation and modes localization properties can then be performed by comparing structures of progressively increasing size [105, 140, 142, 143, 145–147]. Alternatively, infinite structures can be constructed by arranging finite-size clusters (supercells) in a periodic arrays, which can then be numerically simulated by imposing periodic boundary conditions at the supercell edges [130–132, 187].

The simplest approximation that can be used to model and design both periodic and aperiodic photonic structures is the first-order Born approximation (also known as the Rayleigh-Gans approximation), which only takes into account single scattering events. In the framework of the Born approximation, the phase shift of a wave propagating inside the particle is considered to be small. In essence, it is equivalent to replacing the total field with the incident field in the calculations of the constructive interference condition and ignoring multiple-scattering effects. Although the validity of the Born approximation is limited to sparse structures and/or structures with low index contrast ($k_0^2(\varepsilon - 1)V \ll 1$, where V is the volume of the scatterer, ε is a relative permittivity and $k_0 = \omega/c$ is the wavenumber in vacuum), it

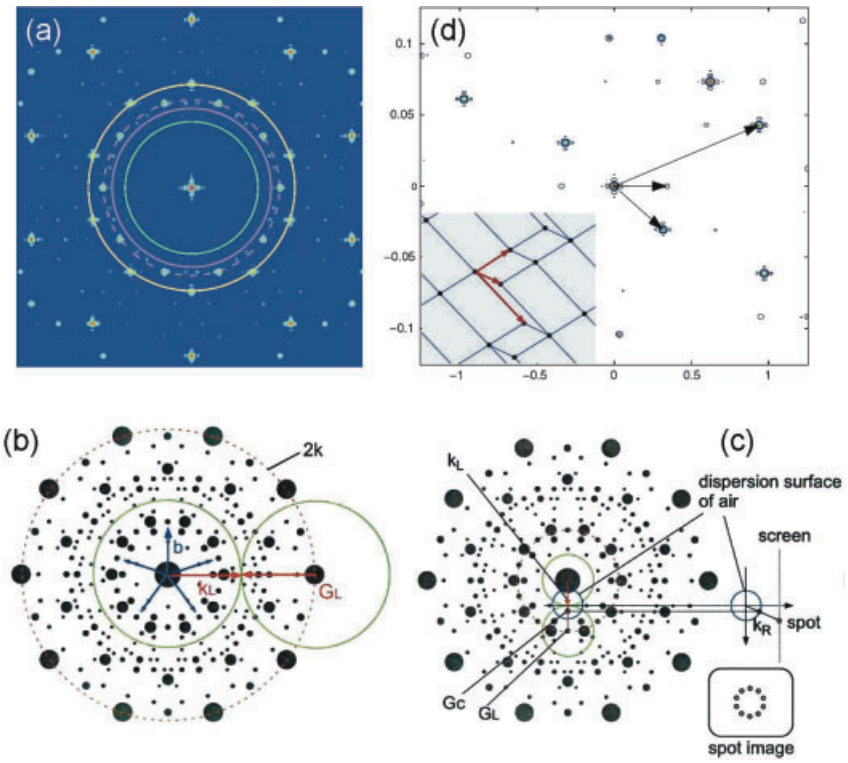

Figure 40 (online color at: www.lpr-journal.org) Fourier-spectrum analysis and design of aperiodic structures. (a) Fourier spectrum of the Penrose quasicrystal with the solid circles corresponding to the Bragg condition for the bandgaps shown in Fig. S1 (reproduced with permission from [140]). Reciprocal lattice representation of lasing conditions (b) and the out-of-plane emission patterns (c) in the photonic structure with Penrose lattice (reproduced with permission from [196]). (d) Fourier transform of an aperiodic structure (shown in the inset) designed to provide strong Bragg peaks required for the phase-matching of multiple nonlinear frequency-conversion processes (adapted with permission from [210]).

provides a useful tool for initial structure design. Indeed, if the influence of the internal resonances of the scattering object is minimized, the correlation between the Fourier spectrum and the optical spectrum of the structure can be very strong [144, 162], as rigorously proved by the gap-labeling theorem in the case of 1D structures [64, 65, 71]. The spectral positions of the low-frequency bandgaps in the optical spectra can be inferred from the locations of the singularities in the lattice Fourier spectrum by using the well-known Bragg law (constructive interference condition):

$$\left\|\vec{G}\right\| = 2k_0, \tag{4}$$

where $\vec{G}$ is a 2D reciprocal space vector of the lattice permittivity profile. This is illustrated in Fig. 40a, where the positions of the lower-frequency bandgaps in the Penrose lattice spectrum are approximately explained by using the Bragg condition (4) [140].

It has also been shown that the lasing modes in low-index aperiodic structures can be analyzed and visualized by using the reciprocal lattice representation as illustrated in Fig. 40b,c [196]. The lasing condition (equivalent to the standing-wave condition for a wave with a wavevector $\vec{k}$) in the simplest two-wave coupling case is $\vec{k} + (\vec{k} - \vec{G}) = 0$, which is satisfied when the circle of radius $2k$ intersects a reciprocal lattice point $\vec{G}$ (see Fig. 40b). In sharp contrast to periodic photonic crystals, for which the standing wave condition can only be satisfied at symmetry points of the first Brillouin zone, a large number of pronounced reciprocal peaks in the Fourier transforms of aperiodic structures translates into a large number of supported lasing modes [196]. Furthermore, the properties of reciprocal lattices of aperiodic structures can be used to visualize the emission patterns of lasing modes as shown in Fig. 40c. The phase-matching condition between the in-plane lasing mode associated with the reciprocal lattice point $\vec{G}_L$ and the out-of-plane radiation modes is satisfied if there are other major reciprocal points $\vec{G}_C$ such that $\|\vec{G}_C\| < \|\vec{G}_L\|$. Out-of-plane emission patterns of the lasing modes can be reconstructed taking into account that the lasing mode energy is emitted in the directions defined by the $\vec{G}_L - \vec{G}_C$ vectors projections on the dispersion surface of air (see Fig. 40c).

Finally, Fourier spectrum design can be used to engineer aperiodic lattices for a specific application. One example of the engineered nonlinear aperiodic structure is shown in Fig. 40d, which features strong Bragg peaks at pre-defined positions and has been used for simultaneous phase matching of several optical frequency-conversion processes. In particular, when illuminated by a single-frequency optical wave this nonlinear structure generates a color fan – the light output that consists of the second, third and fourth harmonics each emitted in a different direction [210].

Photonic bandstructure of both periodic and aperiodic lattices is investigated by solving for the eigenvalues of the wave equation and plotting the resulting dispersion relation $\omega(\mathbf{k})$ [128]. The plane-wave expansion method (PWM) has long been the main workhorse in the simulations of the bandstructures of periodic photonic crystals owing to its simplicity and flexibility [128, 178, 249, 250]. PWM is a spectral method based on the expansion of both the dielectric permittivity and the field amplitudes into Fourier series (plane waves) on the reciprocal lattice and the use of pseudo-periodic conditions to obtain Bloch waves that can propagate in a given direction in an infinite structure. All

possible direction of the wavevector **k** can be considered using crystallographic points. However, the spacing between the basis vectors in the Fourier transforms of quasiperiodic structures is described by irrational numbers, making direct application of the PWM impossible. Yet, it has been shown that a periodic (or rational) approximant to a quasiperiodic structure can be constructed by replacing the basis vectors with approximate vectors whose ratios can be expressed by rational numbers [138, 139, 148, 149], making possible application of PWM to the analysis of quasiperiodic lattices. A complementary approach, which is an analog of the density wave approximation in condensed matter theory [251], relies on identifying a dominant set of Bragg peaks in the reciprocal space of an aperiodic structure and approximating the spatial distribution of the dielectric constant by a Fourier-like series that involve only the reciprocal vectors belonging to the dominant set [142, 160, 252, 253]. Finally, the bandstructure of the photonic quasicrystals that are defined by the cut-and-project construction method can be calculated by solving Maxwell's equations in periodic higher dimensional crystals, to which a generalization of Bloch's theorem applies [254].

Other spectral methods that rely on the expansion of unknown fields into a series of functions that form a complete basis, e. g. "the multiple-scattering technique (MST)" [133, 135, 140, 146, 150, 155, 163, 249, 264] (also known as Generalized multi-particle Mie Theory (GMT) [255]), the Transition Matrix (T-matrix) method [239, 256], and other spectral methods based on surface or volume integral equations 257–261 can be used to study the scattering spectra of aperiodic photonic structures or to probe the local density of states. Multiple-scattering algorithms require inversion of block-form or dense matrices and thus are best suited for simulating finite-size aperiodic structures. For efficient simulations of large-size aperiodic lattices, multiple-scattering formulation can be combined with the sparse-matrix canonical-grid (CMCG) method, which makes possible calculating the interactions between far-away scatterers via a canonical grid by using the Fast Fourier transform algorithms [143, 145]. Finally, the Maxwell equations in both periodic and aperiodic media with the specified boundary conditions can be solved in the frame of the FDTD method [163]. FDTD algorithms can be used to study finite-size aperiodic structures [151, 156], and, by defining a supercell and imposing the periodic boundary conditions at the supercell edges, infinite block-type lattices [130, 163] that combine periodic and aperiodic structural properties.

6. Conclusions and future perspectives

While light transport and localization in periodic and random structures have been investigated for decades, the study of light scattering phenomena in deterministic aperiodic systems is still in its infancy. In this paper, we have reviewed the conceptual foundation, the optical properties and the major device applications of 1D and 2D photonics-plasmonics optical systems with aperiodic index fluctuations generated by algorithmic rules, referred to as Deterministic Aperiodic Nano-Structures (DANS). The study of DANS represents a novel, fascinating, and highly interdisciplinary research field with profound ramifications within different areas of mathematics and physical sciences, such as crystallography and computational geometry, dynamical systems, and number theory. Due to the unprecedented complexity of their Fourier space, which can be designed to span across all possible spectral singularity measures, DANS provide unprecedented opportunities to manipulate light states, diffraction diagrams, and optical cross sections for nanophotonics and nanoplasmonics device technologies. In this paper, we specifically emphasized structural-property relations leading to the formation of photonic pseudo-bandgaps, critically localized optical modes, and multifractal energy spectra in aperiodic structures. The fascinating new regime of isotropic multiple light scattering, or "circular light scattering", and its relevance for the formation of large bandgaps, planar diffraction effects, and omnidirectional gaps in quasi-crystals and amorphous optical structures was also discussed. The main device applications of 1D and 2D photonic DANS in the linear and nonlinear optical regimes, uniquely enabled by their distinctive point-group symmetries, where also reviewed.

In the context of optical biosensing, we have discussed nanoscale aperiodic surfaces and showed that they support a dense spectrum of highly complex structural resonances, i. e., colorimetric fingerprints, giving rise to efficient photon trapping through higher-order multiple scattering processes beyond traditional periodic Bragg scattering. These complex colorimetric structures can be designed by simple Fourier analysis and quantitatively modeled using existing analytical multiple scattering theories, such as Generalized Mie Theory or the T-matrix null-field method theory. In the emerging context of Complex Aperiodic Nanoplasmonics, we have discussed the engineering of structural complexity in aperiodic metal-dielectric nanoparticle arrays and its potential to boost the intensity of nanoscale localized optical fields over large frequency spectra. Specifically, we discussed the phenomenon of broadband photonic-plasmonic coupling, and commented on recent device applications for the enhancement of linear and nonlinear optical processes on chip-scale device structures. In the context of label-free optical biosensing, we showed that the photonic-plasmonic coupled modes of DANS have unique scaling and localization properties that are ideally suited to enhance the sensitivity and reproducibility of SERS substrates. Moreover, current work on the DANS engineering of multi-frequency light sources and lasers with tailored radiation diagrams and angular spectra was also presented. The main numerical and analytical approaches utilized to model aperiodic systems have been briefly reviewed in this paper, with particular attention to simple Fourier space design approaches. In this review, we aimed at significantly broaden the engineering perspective on Fourier space by considering *various types of aperiodic order* and e*ngineering design rules* of aperiodic structures beyond what already present in the mathematical literature (e. g., Thue-Morse, Rudin-Shapiro, etc sequences, etc.) or displayed by natural structures (i. e., quasicrystals). The availability of nanoscale fabrication techniques and of

multi-scale computational methods with increasing predictive power makes possible to take full advantage of aperiodic Fourier spaces by directly engineering *optical functionalities,* without reference to regularity and order in direct space. The paradigm of DANS engineering therefore shifts the traditional engineering perspective from direct to reciprocal space, *enabling to transition flexibly between periodic and aperiodic order uniquely driven by the need of optimizing optical functions and performances* in a much richer parameter space. Interestingly, we note that this engineering approach, which explores the boundary between symmetry and complexity, is often adapted by Nature in its fascinating evolutionary strategies. In fact, more often than it is realized, complex and multi-scale biological systems self-organize according to information-rich, aperiodic patterns that beautifully *optimize specific functions* (i. e., cell networks, tissues and webs geometries, leaves arrangements, etc) *in the absence of directly recognizable symmetry or periodicity*. As amply discussed in this review, the absence of simple symmetries (e. g., translational and rotational symmetry) in complex optical media does not imply recourse to randomness or the associated stochastic optimization methods. On the contrary, given their deterministic character, engineering design rules can still be established for DANS, within clearly defined validity domains. However, the development of a general theory, capable to expand our knowledge of aperiodic deterministic systems beyond what presented in this review paper, is still missing. It is our opinion that this ambitious goal could be achieved by continuing to address the fundamental themes in the optical physics of long-range correlated (deterministic) aperiodic nanostructures, namely:

1) *The relation between topological order and photonic-plasmonic modes*: this effort will provide a better understanding of the relation between the geometrical structure of DANS, determined by spectral measures, and their optical spectra and critical resonances. Only a few classes of aperiodic structures have been considered in the optical literature so far, limiting our ability to conceive novel properties and functions. For instance, DANS structures generated by number-theoretic methods, or possessing combined rotational-translational symmetries (e. g., randomized dot patterns, hyperuniform lattices, aperiodic spirals, etc) exhibit fascinating Fourier properties, often described by an elegant analytical approach, that are yet almost completely unexplored in current device technology. Moreover, the general connection between structural complexity and anomalous optical transport still needs to be properly formalized, despite its potential impact in the engineering of aperiodic inhomogeneous environments for slow-light and solar device applications.
2) *The role of structural perturbations and defects engineering:* very little is currently known on the optical properties of defect-localized modes in DANS environments. This topic is naturally connected to the understanding of hybrid periodic-aperiodic and multi-scale order in nanophotonics, and to the engineering of hierarchical optical structures. For examples, a quantitative phase-space redistribution model for the design of enhanced photonic and plasmonic fields across broad frequency spectra is still missing. Moreover, the fundamental physical and engineering tradeoffs between field concentration, spectral bandwidths, mode localization, and local symmetries in photonic-plasmonic DANS of arbitrary geometries still remain to be adequately addressed beyond the traditional toolsets of Fourier space analysis. More powerful approaches better suited to understand the role of local structural perturbations in aperiodic geometries, possibly requiring the development of local-spectral analysis and time-frequency decomposition tools (e. g., Wavelets, Wigner transforms, phase space optics) still need to find adequate applications in DANS engineering. We expect that further studies will be addressing all these important issues in the near future, leading to a more comprehensive understanding of the complex optical physics of photonic-plasmonic aperiodic nanostructures.
3) *The development of rigorous and predictive multi-scale modeling tools:* while several electromagnetic techniques, both numerical and pseudo-analytical, are currently available to design specific aperiodic structures, a general method capable of dealing with the intrinsic multi-scale character and the large size of DANS is still missing. Moreover, little is known on the solution of multiple light scattering problems in nonlinear and optically active (i. e., lasing, light emitting) DANS, especially in relation to nonlinear-enhanced wave localization phenomena (e. g., aperiodic discrete breathers). The fundamental interplay between aperiodic order and optical nonlinearity still needs to be addressed theoretically and experimentally in photonic-plasmonic DANS, potentially leading to the discovery of novel physical effects. Moreover, novel methods for theoretical and computational research are needed for the efficient solution of inverse scattering problems in aperiodic environments with arbitrary Fourier spectral components. Advances in computational methods capable of dealing with multiple length scales in large aperiodic systems are essential in order to leverage the unique design opportunities enabled by the aperiodic Fourier space.

Finally, we believe that, despite the many challenges still ahead, the engineering of DANS can provide significant advances in both fundamental optical sciences and technological applications, potentially influencing diverse fields such as solid-state lighting, solar cells and photon detection, optical biosensing, and nonlinear nanophotonic devices (i. e., modulators, switchers). Our expectation is that optical DANS could become the platform of choice to elaborate the architecture of the next generation of nanophotonic devices capable to operate over significantly broader frequency and angular spectra by tailoring enhanced light-matter coupling over planar optical chips with controllable degree of structural complexity.

Acknowledgements. This paper is based upon the support of the US Air Force program “Deterministic Aperiodic Structures for on-chip nanophotonic and nanoplasmonic device applications” under the Award FA9550-10-1-0019, the SMART Scholarship Program, and the NSF Career Award No. ECCS-0846651.

Received: 29 December 2010, **Revised:** 16 May 2011, **Accepted:** 17 May 2011

Published online: 8 July 2011

Key words: Photonics, plasmonics, aperiodic structures, light localization.

Luca Dal Negro received both the Laurea in physics, *summa cum laude*, in 1999 and the Ph. D. degree in semiconductor physics from the University of Trento, Italy, in 2003. After his Ph. D. in 2003 he joined MIT as a post-doctoral research associate. Since January 2006 he has been a faculty member in the Department of Electrical and Computer Engineering and in the Material Science Division at Boston University (BU). He is currently an Associate Professor and a member of the Photonics Center at BU. Prof. Dal Negro manages and conducts research projects on light scattering from aperiodic media, nano-optics and nanoplasmonics, silicon-based nanophotonics, and computational electromagnetics of complex structures.

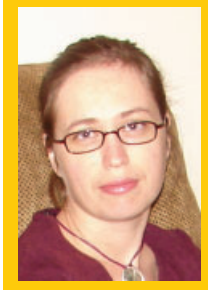

Svetlana V. Boriskina obtained M. Sc. and Ph. D. degrees from Kharkov National University (Ukraine). She is currently a Research Associate at Boston University, with interests in nanophotonics, plasmonics, optoelectronics, metamaterials and biosensing. Dr. Boriskina is a holder of the 2007 Joint Award of the International Commission for Optics and the Abdus Salam International Centre for Theoretical Physics, a senior member of the Institute of Electrical and Electronics Engineers (IEEE), and a member of the Optical Society of America (OSA).

References

[1] P.-E. Wolf and G. Maret, Phys. Rev. Lett. **55**, 2696 (1985).
[2] P. Sheng, Introduction to wave scattering, localization and mesoscopic phenomena (Springer Verlag, Berlin, 2006).
[3] M. P. V. Albada and A. Lagendijk, Phys. Rev. Lett. **55**, 2692 (1985).
[4] D. S. Wiersma, M. P. van Albada, and A. Lagendijk, Phys. Rev. Lett. **75**, 1739 (1995).
[5] A. Lagendijk, B. van Tiggelen, and D. S. Wiersma, Phys. Today **62**, 24–29 (2009).
[6] P. W. Anderson, Phil. Mag. B **52**, 505–509 (1985).
[7] B. A. van Tiggelen, Phys. Rev. Lett. **75**, 422 (1995).
[8] A. Sparenberg, G. L. J. A. Rikken, and B. A. van Tiggelen, Phys. Rev. Lett. **79**, 757 (1997).
[9] F. Scheffold and G. Maret, Phys. Rev. Lett. **81**, 5800 (1998).
[10] D. S. Wiersma, M. Colocci, R. Righini, and F. Aliev, Phys. Rev. B **64**, 144208 (2001).
[11] E. Maciá, Rep. Prog. Phys. **69**, 397–441 (2006).
[12] E. Maciá, Aperiodic structures in condensed matter: Fundamentals and applications (CRC Press Taylor & Francis, Boca Raton, 2009).
[13] W. Steurer and D. Sutter-Widmer, J. Phys. D, Appl. Phys. **40** (2007).
[14] A. N. Poddubny and E. L. Ivchenko, Phys. E **42**, 1871–1895 (2010).
[15] M. Kohmoto, L. P. Kadanoff, and C. Tang, Phys. Rev. Lett. **50**, 1870 (1983).
[16] M. Kohmoto, B. Sutherland, and K. Iguchi, Phys. Rev. Lett. **58**, 2436 (1987).
[17] M. S. Vasconcelos and E. L. Albuquerque, Phys. Rev. B **59**, 11128 (1999).
[18] M. Dulea, M. Severin, and R. Riklund, Phys. Rev. B **42**, 3680 (1990).
[19] W. Gellermann, M. Kohmoto, B. Sutherland, and P. C. Taylor, Phys. Rev. Lett. **72**, 633 (1994).
[20] R. Merlin, K. Bajema, R. Clarke, F. Y. Juang, and P. K. Bhattacharya, Phys. Rev. Lett. **55**, 1768 (1985).
[21] E. Maciá, Appl. Phys. Lett. **73**, 3330–3332 (1998).
[22] E. Maciá, Phys. Rev. B **63**, 205421 (2001).
[23] M. Senechal, Quasicrystals and geometry (Cambridge Univ. Press, Cambridge, 1996).
[24] T. Janssen, G. Chapuis, and M. De Boissieu, Aperiodic crystals: from modulated phases to quasicrystals (Oxford University Press, Oxford, 2007).
[25] M. De Graef, M. E. McHenry, and V. Keppens, J. Acoustical, Soc. Am. **124**, 1385–1386 (2008).
[26] J. P. Allouche and J. O. Shallit, Automatic Sequences: Theory, Applications, Generalizations (Cambridge University Press, New York, 2003).
[27] M. Queffélec, Substitution dynamical systems-spectral analysis (Springer Verlag, Berlin, 2010).
[28] D. A. Lind and B. Marcus, An introduction to symbolic dynamics and coding (Cambridge University Press, Cambridge, 1995).
[29] M. Schroeder, Number theory in science and communication: with applications in cryptography, physics, digital information, computing, and self-similarity (Springer Verlag, Berlin, 2010).
[30] G. H. Hardy, E. M. Wright, D. R. Heath-Brown, and J. H. Silverman, An introduction to the theory of numbers (Clarendon Press, Oxford, 1979).
[31] S. J. Miller and R. Takloo-Bighash, An invitation to modern number theory (Princeton University Press, Princeton, NJ, 2006).
[32] A. N. Whitehead, An Introduction to Mathematics (H. Holt and Company, New York, T. Butterworth, Ltd., London, 1939).
[33] E. Schrödinger and R. Penrose, What is Life? (Cambridge Univ. Press, Cambridge, 1992).
[34] B. Grünbaum and G. C. Shephard, Tilings and patterns (WH Freeman & Co., New York, NY, USA, 1986).
[35] J. Kepler, Harmonices mundi libri V (J. Plank, Linz. Reprinted, Forni, Bologna, 1969).
[36] R. Penrose, Inst. Math. Appl. **7**, 10 (1974).
[37] R. Ammann, B. Grünbaum, and G. Shephard, Discrete Comput. Geom. **8**, 1–25 (1992).
[38] N. G. De Bruijn, Proc. K. Ned. Akad. Wet. A **43**, 84 (1981).
[39] C. Radin, Ann. Math. **139**, 661–702 (1994).
[40] L. Danzer, Discrete Math. **76**, 1–7 (1989).
[41] D. Ruelle, Phys. A **113**, 619–623 (1982).
[42] M. Gardner, Sci. Am. **236**, 110–121 (1977).
[43] D. Shechtman, I. Blech, D. Gratias, and J. W. Cahn, Phys. Rev. Lett. **53**, 1951 (1984).

[44] D. Levine and P. J. Steinhardt, Phys. Rev. Lett. **53**, 2477 (1984).
[45] H. J. Korsch, H. J. Jodl, and T. Hartmann, Chaos: a program collection for the PC (Springer Verlag, Berlin, 2008).
[46] R. C. Hilborn, N. Tufillaro, and T. American Association of Physics, Chaos and nonlinear dynamics (Oxford University Press, Oxford, 2000).
[47] H. Poincaré, Acta Math. **13**, A3–A270 (1890).
[48] F. Diacu and P. Holmes, Celestial encounters: the origins of chaos and stability (Princeton University Press, Princeton, NJ, 1999).
[49] N. Lorenz Edward, J. Atmos. Sci. **20**, 130–141 (1963).
[50] S. Lynch, Dynamical systems with applications using MAPLE (Birkhauser, Boston, 2010).
[51] L. Lam, Introduction to nonlinear physics (Springer Verlag, New York, 2003).
[52] M. Kohmoto, in: Chaos and Statistical Methods, edited by Y. Kuramoto (Springer, Berlin, 1984).
[53] M. Kohmoto and Y. Oono, Phys. Lett. A **102**, 145–148 (1984).
[54] M. Kohmoto, Phys. Rev. B **34**, 5043 (1986).
[55] C. S. Calude, Randomness, and Complexity: from Leibniz to Chaitin (World Scientific, Singapore, 2007).
[56] J. Hoffstein, J. C. Pipher, and J. H. Silverman, An introduction to mathematical cryptography (Springer Verlag, New York, 2008).
[57] Ç. K. Koç, Cryptographic Engineering (Springer US, New York, 2009).
[58] W. Trappe, L. Washington, M. Anshel, and K. D. Boklan, Math. Intell. **29**, 66–69 (2007).
[59] C. Forestiere, G. F. Walsh, G. Miano, and L. Dal Negro, Opt. Express **17**, 24288–24303 (2009).
[60] S. V. Boriskina, S. Y. K. Lee, J. J. Amsden, F. G. Omenetto, and L. Dal Negro, Opt. Express **18**, 14568–14576 (2010).
[61] S. Y. Lee, J. J. S. Amsden, S. V. Boriskina, A. Gopinath, A. Mitropolous, D. L. Kaplan, F. G. Omenetto, and L. Dal Negro, Proc. Natl. Acad. Sci. USA **107**, 12086–12090 (2010).
[62] L. Dal Negro, N. N. Feng, and A. Gopinath, J. Opt. A, Pure Appl. Opt. **10**, 064013 (2008).
[63] P. Prusinkiewicz and A. Lindenmayer, The Algorithmic Beauty of Plants (Springer-Verlag, New York, 1990).
[64] J. M. Luck, Phys. Rev. B **39**, 5834 (1989).
[65] C. Godreche and J. M. Luck, Phys. Rev. B **45**, 176 (1992).
[66] M. Kolar and F. Nori, Phys. Rev. B **42**, 1062 (1990).
[67] G. Gumbs and M. K. Ali, Phys. Rev. Lett. **60**, 1081 (1988).
[68] X. Wang, U. Grimm, and M. Schreiber, Phys. Rev. B **62**, 14020 (2000).
[69] E. Bombieri and J. E. Taylor, Contemp. Math **64**, 241–264 (1987).
[70] E. Bombieri and J. E. Taylor, J. Phys. Colloq. **47**, C3-19–C13-28 (1986).
[71] M. Dulea, M. Johansson, and R. Riklund, Phys. Rev. B **45**, 105 (1992).
[72] M. Kolar, M. K. Ali, and F. Nori, Phys. Rev. B **43**, 1034 (1991).
[73] M. E. Prouhet, CR Acad. Sci. Paris **33**, 225 (1851).
[74] H. M. Morse, J. Math. **42** (1920).
[75] H. S. Shapiro, Extremal problems for polynomials and power series, Sc. M. thesis, Massachusetts Institute of Technology, Boston, MA (1951).
[76] F. Axel and J. Allouche, J. Phys., Cond. Mat. **4**, 8713 (1992).
[77] L. Kroon, E. Lennholm, and R. Riklund, Phys. Rev. B **66**, 094204 (2002).
[78] L. Kroon and R. Riklund, Phys. Rev. B **69**, 094204 (2004).
[79] J.-K. Yang, S. V. Boriskina, H. Noh, M. J. Rooks, G. S. Solomon, L. D. Negro, and H. Cao, Appl. Phys. Lett. **97**, 223101–223103 (2010).
[80] A. Gopinath, S. V. Boriskina, N. N. Feng, B. M. Reinhard, and L. D. Negro, Nano Lett. **8**, 2423–2431 (2008).
[81] A. Barbé and F. Haeseler, J. Phys. A, Math. Gen. **37**, 10879 (2004).
[82] A. Barbé and F. Haeseler, J. Phys. A, Math. Gen. **38**, 2599 (2005).
[83] A. Barbé and F. Von Haeseler, Int. J. Bifurcation Chaos **17**, 1265–1303 (2007).
[84] L. Dal Negro, M. Stolfi, Y. Yi, J. Michel, X. Duan, L. C. Kimerling, J. LeBlanc, and J. Haavisto, Appl. Phys. Lett. **84**, 5186 (2004).
[85] Z. Cheng, R. Savit, and R. Merlin, Phys. Rev. B **37**, 4375 (1988).
[86] C. Tang and M. Kohmoto, Phys. Rev. B **34**, 2041 (1986).
[87] M. Kohmoto, B. Sutherland, and C. Tang, Phys. Rev. B **35**, 1020 (1987).
[88] T. Fujiwara, M. Kohmoto, and T. Tokihiro, Phys. Rev. B **40**, 7413 (1989).
[89] C. S. Ryu, G. Y. Oh, and M. H. Lee, Phys. Rev. B **46**, 5162 (1992).
[90] J. M. L. C. Godreche, J. Phys. A, Math. Gen. **23**, 3769 (1990).
[91] C. Janot, Quasicrystals: A Primer (Oxford University Press, Oxford, 1997).
[92] E. Maciá, and F. Domínguez-Adame, Phys. Rev. Lett. **76**, 2957 (1996).
[93] J.-P. Desideri, L. Macon, and D. Sornette, Phys. Rev. Lett. **63**, 390 (1989).
[94] T. Hattori, N. Tsurumachi, S. Kawato, and H. Nakatsuka, Phys. Rev. B **50**, 4220 (1994).
[95] X. Q. Huang, S. S. Jiang, R. W. Peng, and A. Hu, Phys. Rev. B **63**, 245104 (2001).
[96] R. W. Peng, X. Q. Huang, F. Qiu, M. Wang, A. Hu, S. S. Jiang, and M. Mazzer, Appl. Phys. Lett. **80**, 3063–3065 (2002).
[97] L. Dal Negro, C. J. Oton, Z. Gaburro, L. Pavesi, P. Johnson, A. Lagendijk, R. Righini, M. Colocci, and D. S. Wiersma, Phys. Rev. Lett. **90**, 055501 (2003).
[98] M. Ghulinyan, C. J. Oton, L. Dal Negro, L. Pavesi, R. Sapienza, M. Colocci, and D. S. Wiersma, Phys. Rev. B **71**, 094204 (2005).
[99] S. D. Gupta and D. S. Ray, Phys. Rev. B **38**, 3628 (1988).
[100] S.-n. Zhu, Y.-Y. Zhu, Y.-Q. Qin, H.-F. Wang, C.-Z. Ge, and N.-b. Ming, Phys. Rev. Lett. **78**, 2752 (1997).
[101] S.-n. Zhu, Y.-Y. Zhu, and N.-B. Ming, Science **278**, 843–846 (1997).
[102] K. Fradkin-Kashi, A. Arie, P. Urenski, and G. Rosenman, Phys. Rev. Lett. **88**, 023903 (2001).
[103] N.-h. Liu, Phys. Rev. B **55**, 3543 (1997).
[104] F. Qiu, R. W. Peng, X. Q. Huang, X. F. Hu, M. Wang, A. Hu, S. S. Jiang, and D. Feng, Europhys. Lett. **68**, 658 (2004).
[105] X. Jiang, Y. Zhang, S. Feng, K. C. Huang, Y. Yi, and J. D. Joannopoulos, Appl. Phys. Lett. **86**, 201110 (2005).
[106] L. Dal Negro, J. H. Yi, V. Nguyen, Y. Yi, J. Michel, and L. C. Kimerling, Appl. Phys. Lett. **86**, 261905 (2005).

[107] L. Dal Negro, M. Stolfi, Y. Yi, J. Michel, X. Duan, L. C. Kimerling, J. LeBlanc, and J. Haavisto, New Mater. Microphotonics **871**, 75–81 (2004).
[108] F. Biancalana, J. Appl. Phys. **104**, 093113 (2009).
[109] D. L. Jaggard and X. Sun, Opt. Lett. **15**, 1428–1430 (1990).
[110] X. Sun and D. L. Jaggard, J. Appl. Phys. **70**, 2500–2507 (1991).
[111] C. Sibilia, I. S. Nefedov, M. Scalora, and M. Bertolotti, J. Opt. Soc. Am. B **15**, 1947–1952 (1998).
[112] A. V. Lavrinenko, S. V. Zhukovsky, K. S. Sandomirski, and S. V. Gaponenko, Phys. Rev. E **65**, 036621 (2002).
[113] S. V. Gaponenko, S. V. Zhukovsky, A. V. Lavrinenko, and K. S. Sandomirskii, Opt. Commun. **205**, 49–57 (2002).
[114] S. V. Zhukovsky, A. V. Lavrinenko, and S. V. Gaponenko, Europhys. Lett. **66**, 455 (2004).
[115] S. V. Zhukovsky, S. V. Gaponenko, and A. V. Lavrinenko, Nonlinear Phenom. Complex Syst. **4**, 383–389 (2001).
[116] E. L. Albuquerque and M. G. Cottam, Phys. Rep. **376**, 225–337 (2003).
[117] M. S. Vasconcelos and E. L. Albuquerque, Phys. Rev. B **57**, 2826 (1998).
[118] L. Moretti, I. Rea, L. Rotiroti, I. Rendina, G. Abbate, A. Marino, and L. De Stefano, Opt. Express **14**, 6264–6272 (2006).
[119] L. Mahler, A. Tredicucci, F. Beltram, C. Walther, J. Faist, H. E. Beere, D. A. Ritchie, and D. S. Wiersma, Nat. Photon. **4**, 165–169 (2010).
[120] M. Gerken and D. A. B. Miller, IEEE Photon. Technol. Lett. **15**, 1097–1099 (2003).
[121] M. Gerken and D. A. B. Miller, Appl. Opt. **42**, 1330–1345 (2003).
[122] F. F. Medeiros, E. L. Albuquerque, M. S. Vasconcelos, and P. W. Mauriz, J. Phys., Cond. Mat. **19**, 496212 (2007).
[123] M. Maksimovi and Z. Jakš,i, J. Opt. A, Pure Appl. Opt. **8**, 355 (2006).
[124] R. W. Peng, M. Mazzer, and K. W. J. Barnham, Appl. Phys. Lett. **83**, 770–772 (2003).
[125] A. Luque and A. Marti, Phys. Rev. B **55**, 6994 (1997).
[126] S. Y. S. Kinoshita, J. Miyazaki, Rep. Prog. Phys. **71**, 1–30 (2008).
[127] E. Yablonovitch, Phys. Rev. Lett. **58**, 2059 (1987).
[128] J. D. Joannopoulos, S. G. Johnson, J. N. Winn, and R. D. Meade, Photonic crystals: molding the flow of light (Princeton University Press, Princeton, NJ, 2008).
[129] S. John, Phys. Rev. Lett. **58**, 2486 (1987).
[130] Y. S. Chan, C. T. Chan, and Z. Y. Liu, Phys. Rev. Lett. **80**, 956 (1998).
[131] S.-C. Cheng, X. Zhu, and S. Yang, Opt. Express **17**, 16710–16715 (2009).
[132] Y. Yang and G. P. Wang, Opt. Express **15**, 5991–5996 (2007).
[133] E. Di Gennaro, C. Miletto, S. Savo, A. Andreone, D. Morello, V. Galdi, G. Castaldi, and V. Pierro, Phys. Rev. B **77**, 193104 (2008).
[134] Y. Wang, Y. Wang, S. Feng, and Z.-Y. Li, Europhys. Lett. **74**, 49–54 (2006).
[135] C. Rockstuhl, U. Peschel, and F. Lederer, Opt. Lett. **31**, 1741–1743 (2006).
[136] D. Sutter-Widmer and W. Steurer, Phys. Rev. B **75**, 134303 (2007).
[137] E. Lidorikis, M. M. Sigalas, E. N. Economou, and C. M. Soukoulis, Phys. Rev. B **61**, 13458 (2000).
[138] K. Wang, S. David, A. Chelnokov, and J. M. Lourtioz, J. Mod. Opt. **50**, 2095–2105 (2003).
[139] A. Ledermann, D. S. Wiersma, M. Wegener, and G. von Freymann, Opt. Express **17**, 1844–1853 (2009).
[140] A. Della Villa, S. Enoch, G. Tayeb, V. Pierro, V. Galdi, and F. Capolino, Phys. Rev. Lett. **94**, 183903 (2005).
[141] A. Ledermann, L. Cademartiri, M. Hermatschweiler, C. Toninelli, G. A. Ozin, D. S. Wiersma, M. Wegener, and G. von Freymann, Nat. Mater. **5**, 942–945 (2006).
[142] M. Kaliteevski, V. Nikolaev, R. Abram, and S. Brand, Opt. Spectrosc. **91**, 109–118 (2001).
[143] Y. Lai, Z.-Q. Zhang, C.-H. Chan, and L. Tsang, Phys. Rev. B **76**, 165132 (2007).
[144] D. Sutter-Widmer, S. Deloudi, and W. Steurer, Phys. Rev. B **75**, 094304 (2007).
[145] Y. Lai, Z. Q. Zhang, C. H. Chan, and L. Tsang, Phys. Rev. B **74** 54305 (2006).
[146] S. V. Boriskina, A. Gopinath, and L. Dal Negro, Opt. Express **16**, 18813–18826 (2008).
[147] A. Della Villa, S. Enoch, G. Tayeb, F. Capolino, V. Pierro, and V. Galdi, Opt. Express **14**, 10021–10027 (2006).
[148] K. Wang, Phys. Rev. B **76**, 085107 (2007).
[149] K. Wang, Phys. Rev. B **73**, 235122 (2006).
[150] C. Rockstuhl and F. Lederer, J. Lightwave Technol. **25**, 2299–2305 (2007).
[151] L. Moretti and V. Mocella, Opt. Express **15**, 15314–15323 (2007).
[152] Y. Wang, X. Hu, X. Xu, B. Cheng, and D. Zhang, Phys. Rev. B **68**, 165106 (2003).
[153] K. Mnaymneh and R. C. Gauthier, Opt. Express **15**, 5089–5099 (2007).
[154] S. V. Boriskina and L. Dal Negro, Opt. Express **16**, 12511–12522 (2008).
[155] S. V. Boriskina, A. Gopinath, and L. D. Negro, Phys. E **41**, 1102–1106 (2009).
[156] M. E. Zoorob, M. D. B. Charlton, G. J. Parker, J. J. Baumberg, and M. C. Netti, Nature **404**, 740–743 (2000).
[157] X. Zhang, Z.-Q. Zhang, and C. T. Chan, Phys. Rev. B **63**, 081105 (2001).
[158] Y. Wang, S. Jian, S. Han, S. Feng, Z. Feng, B. Cheng, and D. Zhang, J. Appl. Phys. **97**, 106112–106113 (2005).
[159] M. A. Kaliteevski, S. Brand, R. A. Abram, T. F. Krauss, R. D. L. Rue, and P. Millar, Nanotech. **11**, 274–280 (2000).
[160] M. A. Kaliteevski, S. Brand, R. A. Abram, T. F. Krauss, P. Millar, and R. M. De La Rue, J. Phys., Cond. Mat. **13**, 10459–10470 (2001).
[161] R. Gauthier and K. Mnaymneh, Opt. Express **13**, 1985–1998 (2005).
[162] M. E. Pollard and G. J. Parker, Opt. Lett. **34**, 2805–2807 (2009).
[163] S. S. M. Cheng, L.-M. Li, C. T. Chan, and Z. Q. Zhang, Phys. Rev. B **59**, 4091 (1999).
[164] M. C. Rechtsman, H.-C. Jeong, P. M. Chaikin, S. Torquato, and P. J. Steinhardt, Phys. Rev. Lett. **101**, 073902–073904 (2008).
[165] J. Yin, X. Huang, S. Liu, and S. Hu, Opt. Commun. **269**, 385–388 (2007).
[166] S. David, A. Chelnokov, and J. M. Lourtioz, IEEE J. Quantum Electron. **37**, 1427–1434 (2001).
[167] A. David, T. Fujii, E. Matioli, R. Sharma, S. Nakamura, S. P. DenBaars, C. Weisbuch, and H. Benisty, Appl. Phys. Lett. **88**, 073510–073513 (2006).

[168] H. B. M. Rattier, E. Schwoob, C. Weisbuch, T. F. Krauss, J. M. Smith, R. Houdre, U. Oesterle, Appl. Phys. Lett. **83**, 1283 (2003).
[169] J. D. H. Benisty, A. Telneau, S. Enoch, J. M. Pottage, A. David, IEEE J. Quantum Electron. **44**, 777 (2008).
[170] K. B. C. Weismann, N. Linder, U. T. Schwartz, Laser Photonics Rev. **3**, 262 (2009).
[171] D. R. D. P. L. Hagelstein, Opt. Letters **24**, 708 (1999).
[172] H. C. J. Trevino and L. Dal Negro, Nano Lett., DOI: 10.1021/nl2003736 (2011).
[173] P. Ball, Shapes (Oxford University Press, New York, 2009).
[174] R. V. Jean, Phyllotaxis (Cambridge University Press, New York, 1995).
[175] D. A. W. Thompson, On Growth, and Form (Dover, New York, 1992).
[176] M. Naylor, Math. Mag. **75**, 163–172 (2002).
[177] G. J. Mitchison, Science **196**, 270–275 (1977).
[178] K. M. Ho, C. T. Chan, and C. M. Soukoulis, Phys. Rev. Lett. **65**, 3152 (1990).
[179] C. M. Anderson and K. P. Giapis, Phys. Rev. Lett. **77**, 2949 (1996).
[180] M. Plihal and A. A. Maradudin, Phys. Rev. B **44**, 8565 (1991).
[181] A. Barra, D. Cassagne, and C. Jouanin, Appl. Phys. Lett. **72**, 627–629 (1998).
[182] H. Benisty and C. Weisbuch, Photonic crystals, in: Progress in Optics, Vol. 49, edited by E. Wolf (Elsevier, Amsterdam, 2006), pp. 177–313.
[183] C. M. Anderson and K. P. Giapis, Phys. Rev. B **56**, 7313 (1997).
[184] D. Cassagne, C. Jouanin, and D. Bertho, Phys. Rev. B **52**, R2217 (1995).
[185] D. Cassagne, C. Jouanin, and D. Bertho, Phys. Rev. B **53**, 7134 (1996).
[186] F. Zolla, D. Felbacq, and B. Guizal, Opt. Commun. **148**, 6–10 (1998).
[187] H. Zhao, R. P. Zaccaria, J.-F. Song, S. Kawata, and H.-B. Sun, Phys. Rev. B **79**, 115118 (2009).
[188] M. Florescu, S. Torquato, and P. J. Steinhardt, Phys. Rev. B **80**, 155112–155117 (2009).
[189] M. Florescu, S. Torquato, and P. J. Steinhardt, Proc. Natl. Acad. Sci. USA **106**, 20658 (2009).
[190] R. D. Batten, F. H. Stillinger, and S. Torquato, J. Appl. Phys. **104**, 033504–033512 (2008).
[191] R. D. Meade, K. D. Brommer, A. M. Rappe, and J. D. Joannopoulos, Phys. Rev. B **44**, 13772 (1991).
[192] E. Yablonovitch, T. J. Gmitter, R. D. Meade, A. M. Rappe, K. D. Brommer, and J. D. Joannopoulos, Phys. Rev. Lett. **67**, 3380 (1991).
[193] M. Bayindir, E. Cubukcu, I. Bulu, and E. Ozbay, Phys. Rev. B **63**, 161104 (2001).
[194] E. Di Gennaro, S. Savo, A. Andreone, V. Galdi, G. Castaldi, V. Pierro, and M. R. Masullo, Appl. Phys. Lett. **93**, 164102–164103 (2008).
[195] J. Romero-Vivas, D. Chigrin, A. Lavrinenko, and C. Sotomayor Torres, Opt. Express **13**, 826–835 (2005).
[196] M. Notomi, H. Suzuki, T. Tamamura, and K. Edagawa, Phys. Rev. Lett. **92**, 123906 (2004).
[197] J. A. K. L. Tsang, K. Ding, Scattering of electromagnetic waves: Theories, and Applications (John Wiley & Sons, Inc., New York, 2000).
[198] I. M. White and X. Fan, Opt. Express **16**, 1020–1028 (2008).
[199] Y. Xu, Appl. Opt. **34**, 4573–4588 (1995).
[200] J. A. Armstrong, N. Bloembergen, J. Ducuing, and P. S. Pershan, Phys. Rev. **127**, 1918 (1962).
[201] R. Lifshitz, Nanotechnology and quasicrystals: from self-assembly to photonic applications, in: Silicon Versus Carbon (Springer Verlag, Dordrecht, 2009), pp. 119–136.
[202] B.-Y. Gu, Y. Zhang, and B.-Z. Dong, J. Appl. Phys. **87**, 7629–7637 (2000).
[203] Y. Qin, C. Zhang, D. Zhu, Y. Zhu, H. Guo, G. You, and S. Tang, Opt. Express **17**, 11558–11564 (2009).
[204] Y. W. Lee, F. C. Fan, Y. C. Huang, B. Y. Gu, B. Z. Dong, and M. H. Chou, Opt. Lett. **27**, 2191–2193 (2002).
[205] H. Liu, S. N. Zhu, Y. Y. Zhu, N. B. Ming, X. C. Lin, W. J. Ling, A. Y. Yao, and Z. Y. Xu, Appl. Phys. Lett. **81**, 3326–3328 (2002).
[206] A. Bahabad, N. Voloch, A. Arie, and R. Lifshitz, J. Opt. Soc. Am. B **24**, 1916–1921 (2007).
[207] Y. Sheng, J. Dou, B. Cheng, and D. Zhang, Appl. Phys. B, Lasers Opt. **87**, 603–606 (2007).
[208] Y. Sheng, J. Dou, B. Ma, B. Cheng, and D. Zhang, Appl. Phys. Lett. **91**, 011101–011103 (2007).
[209] Y. Sheng, S. M. Saltiel, and K. Koynov, Opt. Lett. **34**, 656–658 (2009).
[210] R. Lifshitz, A. Arie, and A. Bahabad, Phys. Rev. Lett. **95**, 133901 (2005).
[211] A. Bahabad, A. Ganany-Padowicz, and A. Arie, Opt. Lett. **33**, 1386–1388 (2008).
[212] V. Berger, Phys. Rev. Lett. **81**, 4136 (1998).
[213] S. A. Maier, Plasmonics: fundamentals and applications (Springer Verlag, New York, 2007).
[214] J. Dai, F. Ccaronajko, I. Tsukerman, and M. I. Stockman, Phys. Rev. B **77**, 115419 (2008).
[215] S. Enoch, R. Quidant, and G. Badenes, Opt. Express **12**, 3422–3427 (2004).
[216] N. Felidj, J. Aubard, G. Levi, J. R. Krenn, M. Salerno, G. Schider, B. Lamprecht, A. Leitner, and F. R. Aussenegg, Phys. Rev. B **65**, 075419 (2002).
[217] D. A. Genov, A. K. Sarychev, V. M. Shalaev, and A. Wei, Nano Lett. **4**, 153–158 (2003).
[218] B. Khlebtsov, A. Melnikov, V. Zharov, and N. Khlebtsov, Nanotechnology **17**, 1437 (2006).
[219] K. Li, M. I. Stockman, and D. J. Bergman, Phys. Rev. Lett. **91**, 227402 (2003).
[220] K. Kneipp, M. Moskovits, and H. Kneipp, Surface-enhanced Raman scattering (Springer, Berlin, 2006).
[221] K. Kneipp, H. Kneipp, V. B. Kartha, R. Manoharan, G. Deinum, I. Itzkan, R. R. Dasari, and M. S. Feld, Phys. Rev. E **57**, R6281 (1998).
[222] K. Kneipp, Y. Wang, H. Kneipp, L. T. Perelman, I. Itzkan, R. R. Dasari, and M. S. Feld, Phys. Rev. Lett. **78**, 1667 (1997).
[223] K. J. Falconer and J. Wiley, Fractal geometry: mathematical foundations and applications (Wiley, New York, 2003).
[224] D. H. Werner and R. Mittra, Frontiers in Electromagnetics, IEEE Press Series on RF and Microwave Technology (IEEE Press, New York, 2000).
[225] V. M. Shalaev, Nonlinear optics of random media: fractal composites and metal-dielectric films (Springer, Berlin, 1999).
[226] V. M. Shalaev, Optical properties of nanostructured random media (Springer Verlag, Berlin, 2002).
[227] G. V. G. Volpe, R. Quidant, Opt. Express **19**, 3612 (2011).

[228] G. V. P. Kumar, Appl. Opt. **49**, 6872 (2010).
[229] M. I. Stockman, Phys. Rev. E **56**, 6494 (1997).
[230] M. Moskovits, L. L. Tay, J. Yang, and T. Haslett, SERS and the single molecule, in: Optical Properties of Nanostructured Random Media (Springer, Berlin, 2002), pp. 215–227.
[231] S. Nie and S. R. Emory, Science **275**, 1102–1106 (1997).
[232] A. Bunde and S. Havlin, Fractals and disordered systems (Springer-Verlag, New York, 1991).
[233] T. Matsui, A. Agrawal, A. Nahata, and Z. V. Vardeny, Nature **446**, 517–521 (2007).
[234] H. Fu Min, Z. Nikolay, C. Yifang, and F. J. G. d'Abajo, Appl. Phys. Lett. **90**, 091119 (2007).
[235] T. S. K. Fu Min Huang, V. A. Fedotov, Y. Chen, N. I. Zheludev, Nano Lett. **8**, 2469 (2008).
[236] H. J. L. D. Pacifici, L. A. Sweatlock, R. J. Walters, H. A. Atwater, Opt. Express **16**, 9222 (2008).
[237] L. Dal Negro and N.-N. Feng, Opt. Express **15**, 14396–14403 (2007).
[238] R. Dallapiccola, A. Gopinath, F. Stellacci, and L. Dal Negro, Opt. Express **16**, 5544–5555 (2008).
[239] C. Forestiere, G. Miano, S. V. Boriskina, and L. Dal Negro, Opt. Express **17**, 9648–9661 (2009).
[240] C. Forestiere, G. Miano, G. Rubinacci, and L. Dal Negro, Phys. Rev. B **79**, 085404 (2009).
[241] A. Gopinath, S. V. Boriskina, W. R. Premasiri, L. Ziegler, B. R. M. Reinhard, and L. Dal Negro, Nano Lett. **9**, 3922–3929 (2009).
[242] A. Gopinath, S. V. Boriskina, B. M. Reinhard, and L. Dal Negro, Opt. Express **17**, 3741–3753 (2009).
[243] A. Gopinath, S. V. Boriskina, S. Yerci, R. Li, and L. Dal Negro, Appl. Phys. Lett. **96**, 071113–071113 (2010).
[244] A. E. Ostfeld and D. Pacifici, Appl. Phys. Lett. **98**, 113112 (2011).
[245] E. S. Y. Chu, T. Yang, K. B. Crozier, Appl. Phys. Lett. **93**, 181108 (2008).
[246] C. Forestiere, M. Donelli, G. F. Walsh, E. Zeni, G. Miano, and L. Dal Negro, Opt. Lett. **35**, 133–135 (2009).
[247] R. D. Meade, A. M. Rappe, K. D. Brommer, J. D. Joannopoulos, and O. L. Alerhand, Phys. Rev. B **48**, 8434 (1993).
[248] S.-W. Daniel and S. Walter, Phys. Rev. B **75**, 134303 (2007).
[249] K. Busch, C. R. Phys. **3**, 53–66 (2002).
[250] R. D. Meade, A. M. Rappe, K. D. Brommer, and J. D. Joannopoulos, J. Opt. Soc. Am. B **10**, 328–332 (1993).
[251] D. Levine and P. J. Steinhardt, Phys. Rev. B **34**, 596 (1986).
[252] M. A. Kaliteevski, S. Brand, R. A. Abram, T. F. Krauss, R. De La Rue, and P. Millar, J. Mod. Opt. **48**, 9–14 (2001).
[253] M. A. Kaliteevski, S. Brand, R. A. Abram, T. F. Krauss, R. M. De La Rue, and P. Millar, J. Mod. Opt. **47**, 1771–1778 (2000).
[254] A. W. Rodriguez, A. P. McCauley, Y. Avniel, and S. G. Johnson, Phys. Rev. B **77**, 104201 (2008).
[255] Y.-l. Xu, Appl. Opt. **34**, 4573–4588 (1995).
[256] T. W. A. Doicu, Y. Eremin, Light scattering by systems of particles, null-field method with discrete sources: theory and programs (Springer, Berlin, 2006).
[257] D. Felbacq, G. Tayeb, and D. Maystre, J. Opt. Soc. Am. A **11**, 2526–2538 (1994).
[258] S. V. Pishko, P. D. Sewell, T. M. Benson, and S. V. Boriskina, J. Lightwave Technol. **25**, 2487–2494 (2007).
[259] S. V. Boriskina, P. Sewell, T. M. Benson, and A. I. Nosich, J. Opt. Soc. Am. A **21**, 393–402 (2004).
[260] I. Chremmos and N. Uzunoglu, IEEE Photon. Technol. Lett. **18**, 1173 (2006).
[261] A. Asatryan, S. Fabre, K. Busch, R. McPhedran, L. Botten, M. de Sterke, and N. A. Nicorovici, Opt. Express **8**, 191–196 (2001).
[262] A. Gopinath, S. V. Boriskina, W. R. Premasiri, L. Ziegler, B. M. Reinhard, and L. Dal Negro, Nano Lett. **9**, 3922–3929 (2009).
[263] A. Della Villa, V. Galdi, F. Capolino, V. Pierro, S. Enoch, and G. Tayeb, IEEE Antennas Wirel. Propag. Lett. **5**, 331–334 (2006).
[264] C. Rockstuhl and F. Lederer, New J. Phys. **8**, 206–206 (2006).